Numerical modelling of the electrokinetic remediation of heavy metal contaminated soil

by

by John D. McKinley[1] & Chrysanthi Savvidou[2]

CUED / D - SOILS / TR.292 (1997)

[1] Assistant Lecturer, Geotechnical Group, Department of Engineering, University of Cambridge.
[2] formerly Lecturer, Geotechnical Group, Department of Engineering, University of Cambridge.

Numerical modelling of the electrokinetic remediation of heavy metal contaminated soil

by

by John D. McKinley & Chrysanthi Savvidou

INTRODUCTION

Electrokinetic remediation is a developing technology for the extraction of contaminants from saturated fine-grained soils, suitable for the *in-situ* removal of ionic inorganic compounds, particularly heavy metals. Electrokinetic remediation imposes DC currents of the order mA / cm^2 [Alshawabkeh and Acar, 1992] to remove the contaminants. The dominant removal mechanisms are electro-osmosis, in which the electric field induces movement of the pore fluid, and ionic migration, in which the electric field induces movement of ions. Other physicochemical interactions also occur, such as acid-base reactions, aqueous complexation and precipitation [Datla and Yeung, 1994]. In this paper an attempt is made understand and model the complex transport, electrochemical and physical chemistry processes involved.

This paper does not present a separate overview of previous work on electrokinetic remediation of contaminated soil. The interested reader is refered to the articles of Gray and Mitchell [1967], Groenevelt and Elrick [1976], Lageman *et* al. [1989], Alshawabkeh and Acar [1992], Yeung and Mitchell [1993], and Yeung and Datla [1995]. The literature to 1994 is reviewed in Hellawell [1994].

BACKGROUND AND ANALYSIS

Electrical conductivity of electrolytes

The electrical conductivity of a aqueous solution is a function of the nature and amount of the electrolytes present. For simple changes such as dilution it is generally sufficient to generate a calibration curve for electrical conductivity against concentration, but for complicated changes such as those expected during electrokinetic remediation a more sophisticated approach is needed. The model for electrical conductivity needs to be robust in the face of changes in the concentration of individual chemical species and in the relative proportions of different species, and for this some basic electrochemistry results are necessary.

Consider first the electrical conductivity of an electrolyte solution. The ionic strength I_s is given by:

$$I_s = \tfrac{1}{2}\sum m_i z_i^2 \qquad (1)$$

where m_i is the molality and z_i is the charge valency for species i [Crow, 1994]. Molality indicates the concentration in moles per kg of solution, and for dilute solutions at laboratory temperatures may be taken equal to the concentration in moles per litre.

The properties of an ion species in solution are affected by the presence of other ions with which it interacts electrostatically, except at infinite dilution, and the activity a_i expresses the availability of the species to determine properties, to take part in a chemical reaction or to influence the position of an equilibrium [Crow, 1994]. Activity is related to concentration c_i:

$$a_i = \gamma_i c_i \tag{2}$$

where γ_i is the ion activity coefficient.

A number of expressions exist for predicting γ_i, but based on the results of a series of measurements by the first author of the conductivity of pure solutions for the solutes and range of concentrations of interest, the most applicable is that due to Davies [1962]:

$$\log y; = -0.5092;\left(\frac{\sqrt{I_s}}{1+\sqrt{I_s}} - 0\cdot 3I_s\right) \tag{3}$$

Using Kohlrausch's Law of Independent Migration of Ions [Crow, 1994] the electrical conductivity κ of the solution is:

$$\kappa = \sum a_i\lambda_i^0 = \sum \gamma_i c_i \lambda_i^0 = \sum c_i \lambda_i \tag{4}$$

where λ_i^0 is the limiting ionic conductivity in water and $\lambda_i = \gamma_i \lambda_i^0$ is the ionic conductivity in water.

Transport properties of ions in soil

The transport properties of ions in soil are related to their transport properties in solution. The mobility u_i of an ion in an electric field and the conductivity of a solution are intimately connected, since it is the movement of the ions which effects the charge transfer. Relating the current density to the rate of charge transfer gives:

$$u_i = \frac{\lambda_i}{z_i|F} \tag{5}$$

where F is the Faraday constant and the absolute value of the charge valency is used because ionic mobility is defined as a speed [Hibbert, 1993].

Imagining a situation where the migration of ions induced by an electric field exactly balances their diffusion and using a Boltzmann distribution to relate the concentration of ion species i to the applied potential yields for the free diffusion coefficient D_i:

$$D_i = \frac{\lambda_i RT}{z_i^2 F^2} \tag{6}$$

which is the Nernst-Einstein equation [Hibbert, 1993], where R is the gas constant and T is the absolute temperature.

Tabulated values for λ_i, u_i and D_i generally indicate the values at 25°C and infinite dilution. Typically, all three increase by 2–3% per °C relative to the value at 25°C. Strictly, the above relationships apply at infinite dilution only, but should be applicable where the activity coefficients are close to unity.

In a soil the transport will be characterised by an effective diffusion coefficient D_i^*, an effective mobility u_i^* and an effective molar conductivity λ_i^*. If the soil particles are inert with regards to ionic transport, such that the effects of surface charge and interface diffusion can be ignored, then relationships between these effective coefficients can also be developed. The relationships presented by Yeung and Mitchell [1993] can be written:

$$\lambda_i^* = \omega_i \lambda_i \tag{7}$$

$$u_i^* = \omega_i u_i \tag{8}$$

and

$$D_i^* = \omega_i D_i \tag{9}$$

where ω_i is the tortuosity for the ion species and is a measure of how much more difficult it is for the ion to move because of the need to travel around the soil grains. It is usual to regard ω_i as a function of the soil type and porosity and not of the ion species, and it is typically in the range 0·5–0·01 for non-adsorbed ions in porous geologic materials [Freeze and Cherry, 1979].

The equivalent bulk conductivity κ^* of the soil will be:

$$\kappa^* = n\omega\kappa \tag{10}$$

where n is the porosity and ω is the tortuosity of the soil. This is effectively an average of the tortuosities for the individual ion species. The term $n\omega$ in equation (10) is clearly the reciprocal of the formation factor [Bear, 1969], which is typically in the range 1·5–4 for uncemented soils [Campanella et *al.*, 1994].

Ionic equilibrium within the pore water

Within the pore water, the chemical species present interact according to the laws of physical chemistry. For transport of ionic metal contaminants three significant reversible reactions are considered: the autoprotolysis of water molecules, the association of the metal into its uncharged aqueous hydroxide form, and the formation of the solid metal hydroxide.

Water molecules undergo autoprotolysis according to the reaction:

$$2H_2O(l) \leftrightarrow H_3O^+(aq) + OH^-(aq)$$

for which the equilibrium constant at standard state is:

$$K_w = [H_3O^+][OH^-] = 10^{-14} \tag{11}$$

where the terms in square brackets are activities [Atkins, 1994].

Regarding the aqueous metal hydroxide, consider the hydroxide of a metal Me of valency $+z$ dissociating according to the reversible reaction:

$$Me(OH)_z(aq) \leftrightarrow Me^{z+}(aq) + zOH^-(aq)$$

for which the equilibrium constant is:

$$K_c = \frac{[Me^{z+}][OH^-]}{[Me(OH)_z]} \tag{12}$$

where the hydroxide is in aqueous form. Note that K_c is the reciprocal of the stability constant for the metal hydroxide. Martell and Smith [1974] list stability constant for a great number of reactions, including the precipitation of crystalline metal hydroxides and oxides from solution.

If the concentration of aqueous metal hydroxide exceeds the solubility limit then the solid metal hydroxide will form according to the reversible reaction:

$$Me(OH)_z(s) \leftrightarrow Me^{z+}(aq) + zOH^-(aq)$$

for which the equilibrium constant is:

$$K_{sp} = [Me^{z+}][OH^-]^z \tag{13}$$

where K_{sp} is the solubility product of the metal hydroxide. Equation (13) also applies to the various dehydrated forms of the solid hydroxide, such as:

$$MeO(OH)_{z-2}(s) + H_2O \leftrightarrow Me^{z+}(aq) + zOH^-(aq)$$

so that, for example, for a divalent metal the solid precipitate might be interpreted as the metal oxide instead of the hydroxide, using the solubility product for the oxide. This would not change the analysis, and might be appropriate because for many metals the precipitated solid hydroxide would turn into the more stable solid oxide given sufficient time.

The reversible reactions are commonly assumed to reach equilibrium conditions instantaneously, so that the pore water passes through a series of states each at chemical equilibrium. This is the chemical quasi-equilibrium assumption, and should hold if the rates of the reversible reactions are significantly higher than the rates of chemical transport.

Given concentrations of metal, aqueous metal hydroxide, solid metal hydroxide, hydronium and hydroxy not in chemical equilibrium, it is possible to calculate the equilibrium state such that equations (1 1), (12) and (13) are satisfied. This is very difficult if allowance for the variation in the activity coefficients is made, so the simplifying assumption that activities and concentrations are equal is made for the calculation of chemical equilibrium here. The transport properties are calculated from the activities, however.

Simple relaxation techniques applied to the chemical equilibrium equations converged too slowly to be practical. Instead a technique similar to that of Compos and Rollett [1995] is used. The equations are recast using pH as the governing variable and a search for the equilibrium pH is then made. Use of pH as the governing variable significantly compresses the search space and means that the relative error in the calculation of the equilibrium concentrations can be easily controlled.

First, it is assumed that the solid metal hydroxide is present. The total amount of metal Me, must stay constant during the equilibration process, so:

$$\mathrm{Me}, = \left[\mathrm{Me}^{z+}\right] + \left[\mathrm{Me(OH)}_z\right] + \left[\mathrm{Me(OH)}_z(s)\right]$$

$$= \left[\mathrm{Me}^{z+}\right]_{ne} + \left[\mathrm{Me(OH)}_z\right]_{ne} + \left[\mathrm{Me(OH)}_z(s)\right]_{ne} \qquad (14)$$

where $\left[\mathrm{Me(OH)}_z(s)\right]$ is the number of moles per litre of pore fluid of the solid hydroxide, and $\left[\mathrm{Me}^{z+}\right]_{ne}$, $\left[\mathrm{Me(OH)}_z\right]_{ne}$ and $\left[\mathrm{Me(OH)}_z(s)\right]_{ne}$ are the out-of-equilibrium values.

Now, by definition the pH is given by:

$$\left[\mathrm{H_3O^+}\right] = 10^{-\mathrm{pH}} \qquad (15)$$

so combining equations (15) and (11) gives:

$$\left[\mathrm{OH^-}\right] = \frac{K_w}{\left[\mathrm{H^+}\right]} = K_w 10^{\mathrm{pH}} \qquad (16)$$

and substitution of equation (16) into equation (13) leads to:

$$\left[\mathrm{Me}^{z+}\right] = \frac{K_{sp}}{\left(K_w 10^{\mathrm{pH}}\right)^z} \qquad (17)$$

while combining equations (12) and (13) gives:

$$\left[\mathrm{Me(OH)}_z\right] = \frac{K_{sp}}{K_c} \qquad (18)$$

and substitution of equations (17) and (18) into equation (14) gives:

$$\left[\mathrm{Me(OH)}_z(s)\right] = \mathrm{Me}, - \frac{K_{sp}}{\left(K_w 10^{\mathrm{pH}}\right)^z} - \frac{K_{sp}}{K_c} \qquad (19)$$

Since every term in equations (15)–(19) are known except the pH the speciation calculation then reduces to the calculation of the equilibrium pH. Once this is determined, the amounts of the different species can be calculated directly. Stoichiometry requires that there be no net change in electrical charge as a result of the speciation reactions so:

$$z\left[\mathrm{Me}^{z+}\right] + \left[\mathrm{H_3O^+}\right] - [\mathrm{OH}-] = z\left[\mathrm{Me}^{z+}\right]_{ne} + \left[\mathrm{H_3O^+}\right]_{ne} - \left[\mathrm{OH^-}\right]_{ne} \qquad (20)$$

during equilibration.

The only way to produce a hydronium concentration and therefore a pH which is different from the equilibrium value without changing the amounts of any other component is to add or remove $\mathrm{H_3O^+}$ ions, which would produce a change in electrical charge. The terms on the right hand side of equation (20) are fixed, while the terms on the left hand side can be calculated for any estimated pH, so the difference between these is the charge balance error arising because the estimated pH differs from the equilibrium pH. If this error is $f(\mathrm{pH})$ then:

$$f(\mathrm{pH}) = \left(\left[\mathrm{H^+}\right]_{ne} - \left[\mathrm{OH^-}\right]_{ne} + z\left[\mathrm{Me}^{z+}\right]_{ne}\right) - \left(10^{-\mathrm{pH}} - K_w 10^{\mathrm{pH}} + \frac{zK_{sp}}{\left(K_w 10^{\mathrm{pH}}\right)^z}\right) \qquad (21)$$

by substitution.

If, at a given pH the amount of solid hydroxide calculated from equation (19) is negative then no solid hydroxide has been formed. Repeating the analysis ignoring the precipitation reaction leads to:

$$f(\mathrm{pH}) = \left([\mathrm{H}^+]_{ne} - [\mathrm{OH}^-]_{ne} + z[\mathrm{Me}^{z+}]_{ne}\right) - \left(10^{-\mathrm{pH}} - K_w 10^{\mathrm{pH}} + \frac{z\mathrm{Me}_T K_c}{\left(K_w 10^{\mathrm{pH}}\right)^z + K_c}\right) \tag{22}$$

Equation (21) will apply at high pH where solid hydroxide is present and equation (22) at low pH where it is not.

Analysis of equations (21) and (22) shows that $f(\mathrm{pH})$ is a continuous function which increases monotonically as the estimated pH increases and is smooth except at the point where the hydroxide would first form. The problem reduces to the calculation of the roots of $f(\mathrm{pH})$, of which there is only one, the equilibrium pH. Since the derivative of $f(\mathrm{pH})$ is analytical the root can be found using the Newton-Raphson method, although the change in gradient at the the point where the hydroxide would first form may cause problems. Using this method in combination with bisection search where the Newton-Raphson method converges slowly, according to the algorithm in Press et al. [1989], meant that the equilibrium state could be found reasonably quickly. For more complicated pore water chemistry sophisticated techniques for calculating the equilibrium state are available which allow for a large number of species and for the variation in activity coefficient with concentration [de Stefano *et* al., 1989; Compos and Rollett, 1995], but the computational demands rapidly become very great, as can be seen in Datla and Yeung [1994].

Electrokinetic transport in soils

Figure 1 illustrates the basic transport processes taking place during electrokinesis due to the electric field: ionic migration, electro-osmosis and electrophoresis. Electrophoresis, the movement of (generally negatively) charged colloidal particles in soil, is inconsequential for most natural soils [Esrig, 1968]. Models for one-dimensional ionic transport in soils due to applied electric fields have been presented by Acar and co-workers [Alshawabkeh and Acar, 1992; Acar et al., 1994], while a similar but more fundamental formulation was presented by Groenevelt and Elrick [1976] and more fully by Yeung and Mitchell [1993]. Differences in the expressions for the transport properties arise because the former cast the equations in terms of concentration per unit volume of soil, while the latter use the more conventional concentration per unit volume of pore fluid. Using the conventional variables in the formulation due to Yeung and Mitchell and including the effects of mechanical dispersion and constant retardation gives the transport equation for species i of valency z_i at concentration c_i moving in a rigid soil of constant porosity:

$$R_i \frac{\partial c_i}{\partial t} = \frac{\partial}{\partial x}\left\{D_L \frac{\partial c_i}{\partial x}\right\} - \frac{\partial}{\partial x}\left\{\left[\bar{v} - u_i^* \frac{z_i}{|z_i|}\frac{\partial \Phi}{\partial x}\right]c_i\right\} + G_i \tag{23}$$

where R_i is the retardation factor, D_L is the coefficient of longitudinal hydrodynamic dispersion, $\bar{v}$ is the mean pore fluid velocity, Φ is the electrical potential and G_i represents addition or removal of the ion. The governing equation is identical in form to the advection-dispersion equation for contaminant transport [see Freeze and Cherry, 1979, for example], with the electrokinetic component providing an additional advective term. For constant transport properties and electrical potential gradient equation (23) reduces to the classic form of the advection-dispersion equation.

The dispersion coefficient is given by:

$$D_L = D_i^* + \alpha_L \bar{v} \tag{24}$$

where a, is the dispersivity of the medium. The mean pore fluid velocity is given by:

$$\bar{v} = \frac{v}{n} = -\frac{1}{n}\left(k_e \frac{\partial \Phi}{ax} + k_h \frac{\partial h}{\partial x}\right) \tag{25}$$

where v is the specific discharge, n is the porosity, k_e is the electro-osmotic permeability, k_h is the hydraulic conductivity and h is the pore water head, noting that the pore water tends to flow down the hydraulic potential gradient and, in most soils, down the electrical potential gradient.

In the theoretical Hemholtz-Smoluchowski model, derived for capillary pores whose radius is large in relation to the thickness of the diffuse double layer of charge on the pore walls [Gray and Mitchell, 1967], k_e is related to the surface charge by:

$$k_e = \frac{\varepsilon \zeta}{\eta} n \tag{26}$$

where ε is the permittivity of the pore fluid, ζ is the zeta potential and η is the viscosity of the pore fluid [Alshawabkeh and Acar, 1992].

If the electrokinetic component of the equation equation were constant, then existing analytical solutions to the advection-dispersion equation could be applied, for suitable boundary conditions. In general, however, the transport will change the electrical conductivity and the electrical potential gradient will vary with distance and time, so no general solution is possible.

Solving the electrokinetic transport equation

The transport equations and the chemical reaction equations are directly linked, and an exact model of ekectrokinetic remediation would have to solve both sets of equations simultaneously. This is generally very difficult, and the usual approach is to use a time marching, operator splitting quasi-equilibrium numerical method: the physical system is assumed to pass from one state to another in a series of steps without undergoing chemical changes during the steps, but

the chemical equilibrium condition is enforced at the end of each step. That is, the transport and chemical reaction operators are split so that over the time increment there is only transport, and the state at the end of the increment is brought into local chemical equilibrium instantaneously.

The electrokinetic transport equation has the same form as the advection-dispersion equation, and consideration of the electrokinetic component indicates that the term equivalent to the advection velocity will be variable and large. Significant work on techniques for solving the advection-dispersion equation for highly advective transport has been and continues to be done in the areas of water resources research and environmental geotechnics, and it is from this work that robust methods for solving equation (23) must be drawn. Three solutions to the electrokinetic transport equation are developed: a numerical solution using the predictor-corrector finite difference scheme of Tagamets and Sternberg [1974]; a numerical solution using the random walk particle method of Tompson and Gelhar [1990]; and an approximate simple analytical solution ignoring the dispersive and pore fluid velocity terms.

Tagamets and Sternberg [1974] presented a predictor-corrector time-marching finite difference solution to the one-dimensional advection-dispersion equation for a Langmuir adsorption isotherm. Two finite difference approximations are used, each advancing the solution by half an increment in the time domain, resulting in an improved approximate solution at high grid Peclet and Courant numbers. Tagamets and Sternberg's result also indicate that their method avoids much of the phase shift error apparent in the classic Crank-Nicolson method [Noorishad et *al.*, 1992]. Such errors become important where several interacting species are being transported.

The governing equation without adsorption can be written as:

$$\frac{\partial c}{at} = D_L \frac{\partial^2 c}{\partial x^2} - \bar{v}\frac{\partial c}{ax} \tag{27}$$

for constant coefficients. The predictor equation advances from time t_j to time $t_{j+½}$ with an implicit approximation to the dispersion term and an explicit approximation to the advection term:

$$\frac{2}{\mathrm{At}}\left(w_{i,j+½} - w_{i,j}\right) = \frac{D_L}{(\Delta x)^2}\left(w_{i+1,j+½} - 2w_{i,j+½} + w_{i-1,j+½}\right) - \frac{\bar{v}}{2\Delta x}\left(w_{i+1,j} - w_{i-1,j}\right) \tag{28}$$

where A is the increment, w is the approximation to c, i is the subscript for the space increment and j is the subscript for the time increment. The corrector equation advances from time t_j to time t_{j+1} using the predicted values at time $t_{j+½}$ in the advection term and a Crank-Nicolson approximation to the dispersive term:

$$\frac{1}{\mathrm{At}}\left(w_{i,j+1} - w_{i,j}\right) = \frac{D_L}{2(\Delta x)^2}\left(w_{i+1,j+1} - 2w_{i,j+1} + w_{i-1,j+1}\right)$$

$$- \frac{D_L}{2(\Delta x)^2}\left(w_{i+1,j} - 2w_{i,j} + w_{i-1,j}\right)$$

$$- \frac{\bar{v}}{2\Delta x}\left(w_{i+1,j+\frac{1}{2}} - w_{i-1,j+\frac{1}{2}}\right) \tag{29}$$

and the effect of a linear adsorption isotherm can clearly be incorporated in equations (28) and (29) without difficulty. Comparison with analytical and approximate solutions for transport with no adsorption [Tagamets and Sternberg, 1974] showed good agreement.

Tompson and Gelhar [1990] and Tompson [1993] argued that the storage and processing time demands needed to refine a finite difference grid or a finite element mesh to reduce the grid Peclet number to order one for realistic, heterogeneous porous media rapidly make such an approach impractical. At large grid Peclet numbers ($v\Delta x/D$) spurious oscillatory behaviour may occur near sharp concentration fronts using conventional finite element or finite difference techniques. Tompson and Gelhar presented a random walk particle method solution to the complete form of the advection-dispersion equation for conservative transport.

The one-dimensional form of the equations are used. The governing equation is:

$$\frac{\partial\{nc\}}{at} = \frac{13}{ax}\left\{nD_L\frac{\partial c}{\partial x}\right\} - \frac{\partial\{n\bar{v}c\}}{ax} \tag{30}$$

and for constant n, D_L and $\bar{v}$ equation (30) reduces to equation (27). The random walk particle method represents the spatial distribution of some extensive quantity, such as concentration of a particular chemical constituent, by a large collection of particles transported under the influence of spatially varying fluid velocities and dispersion processes. The particles are point masses, and the model is based upon analogies between mass transport equations and stochastic differential equations. A particle is displaced according to the simple relationship:

$$X_{j+1} = X_j + A(X_j)\Delta t + B(X_j)Z\sqrt{\Delta t} \tag{31}$$

where X_{j+1} is the position at time t_{j+1}, X_j that at time t_j, $A(X)$ is a deterministic forcing term, B(X) is a deterministic scaling term and Z is a random number with mean zero and unit variance. The motion of one particle is statistically independent from that of another, and if a large number of identical particles are moved simultaneously, with forcing and scaling terms given by their initial position, their number density $f(x,t)$ will approximately satisfy the Ito-Fokker-Planck equation [Kinzelbach, 1988; Uffink, 1988]:

$$\frac{\partial f}{at} = \frac{\partial^2\left\{\frac{1}{2}B^2 f\right\}}{ax} \frac{\partial\{Af\}}{\partial x} \tag{32}$$

Comparison of equations (30) and (32) shows that if the number density is taken as an approximation to nc and $A(X)$ and $B(X)$ are defined by:

$$A = \bar{v} + \frac{\partial D_L}{\partial x} + \frac{D_L}{n}\frac{\partial n}{\partial x} \tag{33}$$

$$B^2 = 2D_L \tag{34}$$

the cathode end. Consideration of the electrical charge flows in and out of a control volume around each electrode, shown dotted in figure 1, indicates that this implements Faraday's laws [Hibbert, 1993], since the number of charge carriers created in the control volume will be equal to the net transfer of charge out of the control volume, and that water electrolysis is the only significant electrode reaction. Across the central section of the sample the concentrations are unchanged.

Let the bulk electrical conductivity of the three zones be κ_c^*, κ_0^* and κ_a^*, starting from the cathode end. The total electrical resistance R_s of the sample is:

$$R_s = \frac{1}{A}\left(\frac{l_c}{\kappa_c^*} + \frac{L - l_c - l_a}{\kappa_0^*} + \frac{l_a}{\kappa_a^* 1}\right. \tag{35}$$

and the current I is:

$$I = \frac{\Delta\Phi}{R_s} \tag{36}$$

Combining equations (35) and (36) gives the voltage gradient over the middle section:

$$\left.\frac{\partial\Phi}{\partial x}\right|_{centre} = \left(\frac{I}{L - l_c - l_a}\right)\left(\frac{L - l_c - l_a}{A\kappa_0^*}\right) = \frac{\Delta\Phi}{\kappa_0^*}\left(\frac{l_c}{\kappa_c^*} + \frac{L - l_c - l_a}{\kappa_0^*} + \frac{l_a}{\kappa_a^*}\right)^{-1} \tag{37}$$

It is this potential gradient which drives the electrokinetic movement in the central section.

For a non-sorbing soil the rate at which the cation-depleted zone at the anode end grows is given by:

$$\frac{dl_a}{dt} = \bar{v} + u_+^* \left.\frac{\partial\Phi}{\partial x}\right|_{centre} \tag{38}$$

where u_+^* is the effective ionic mobility of the cation, while the rate at which the anion-depleted zone at the cathode end grows is given by:

$$\frac{dl_c}{dt} = -\bar{v} + u_-^* \left.\frac{\partial\Phi}{\partial x}\right|_{centre} \tag{39}$$

where u_-^* is the effective ionic mobility of the anion if the cations in the anion depleted zone move at the same velocity as the cations in the central zone, and the anions in the cation depleted zone move at the same velocity as the anions in the central zone. If this latter condition does not hold then the ion distribution in the end zones would not be uniform and the analysis breaks down. The condition will hold if the voltage gradients are approximately uniform. Note that electro-osmosis and ionic migration produce ion movement in the same direction for cations but oppose each other for anions.

The result is a pair of coupled equations. Further simplification is possible since the ionic mobilities of most simple ions other than hydronium and hydroxy are roughly equal, so ignoring the contribution of $\bar{v}$ and setting both ionic mobilities equal to their mean value u^* results in a symmetric system in which $l_c = l_a$ and:

$$\left(\frac{L}{\kappa_0^*}+l_c\left(\frac{1}{\kappa_c^*}-\frac{2}{\kappa_0^*}+\frac{1}{\kappa_a^*}\right)\right)\frac{dl_c}{dt}=\frac{u^*}{\kappa_0^*}\Delta\Phi \tag{40}$$

The solution of equation (40) is:

$$l_c=\frac{-\frac{L}{\kappa_0^*}+\sqrt{\left(\frac{L}{\kappa_0^*}\right)^2+2\left(\frac{1}{\kappa_c^*}-\frac{2}{\kappa_0^*}+\frac{1}{\kappa_a^*}\right)\frac{u^*}{\kappa_0^*}t\Delta\Phi}}{\left(\frac{1}{\kappa_c^*}-\frac{2}{\kappa_0^*}+\frac{1}{\kappa_a^*}\right)} \tag{41}$$

as $l_c = 0$ when $t = 0$. Note that if the denominator in this expression is negative, which it will be if the conductivity in the two end zones is higher than that in the central section, then the numerator will also be negative.

The limiting value for l_c is $l_c = 0 \cdot 5\, L$, which will occur at time T:

$$T=\frac{L^2\kappa_0^*}{8u^*\Delta\Phi}\left(\frac{1}{\kappa_c^*}+\frac{2}{\kappa_0^*}+\frac{1}{\kappa_a^*}\right) \tag{42}$$

at which time the acid front and the basic front meet. Thereafter a new, central zone will have developed in which no contaminant is present. This zone will have a very low electrical conductivity, as the pore fluid is clean water, and the electric potential gradient will be large in this zone and small in the remaining soil.

If the electrical conductivity of either end zone becomes very small, possibly due to a precipitation reaction, then T will be very large and l_c will grow very slowly prior to that. However, reducing the electrical conductivity of all sections by the same factor, by reducing the initial concentration of solute say, does not affect the variation in l_c with time. This is to be expected, since the rate of clean up due to electrokinesis is determined by the speed of the ions not their flux, and their speed is given by their ionic mobility times the local electrical potential gradient. In fact, the rate of clean up may be slightly less at higher concentrations, since the ionic mobility decreases as concentration increases due to the electrostatic interactions, the activity coefficient decreases and the electrical conductivity increases less rapidly than the concentration. This is apparent from equations (3) and (4). For a divalent-divalent solute the mean activity coefficient at a concentration of $0 \cdot 1$mol L^{-1} is 0.285 while that at $0 \cdot 001$mol L^{-1} is 0.76 1; that is, for the same electrical potential gradient the ions in the more dilute solution will be moving almost three time faster than those in the more concentrated solution.

MODELLING ELECTROKINETIC TRANSPORT -THE ELK COMPUTER PROGRAM

General features

The ELK program solves the one-dimensional electrokinetic transport problem for a rigid saturated soil containing a dissolved ionic contaminant, using either the predictor-corrector method or the random walk method. It uses a two-step operator splitting procedure to separately solve the transport and chemical equilibrium equations, using the local equilibrium assumption. As noted above, this method is less rigorous than solving both sets of equations

together and can lead to erroneous mass distributions where there is material addition or removal [Valocchi and Malmstead, 1992], but it is a much more practical computational method [Datla and Yeung, 1994]. The input data format for both versions is the same, and is detailed in appendix B .

The geometry of the ELK models is shown in figure 2: a soil sample of cross-sectional area A is constrained between two filters with a water filled well at each end. A mesh electrode is placed against the outer face of each filter, and the distance between the electrodes is L. A voltage is applied between the two electrodes, and a hydraulic gradient can also be imposed across the sample. The length of each well is set to $0 \cdot 1L$. Within the wells the electrical potential gradient is zero, the fluid velocity is $n\bar{v}$ by continuity with the volumetric flow rate within the soil, and the dispersivity is set arbitrarily to ten times that within the soil. The higher dispersivity within the wells is an attempt to account for mixing effects and flushing flow.

These modelling assumptions lead to discontinuities in the transport velocities at the electrodes, as the electric potential gradient in the wells is set to zero and water velocity in the wells is less than that in the soil by volumetric flow rate continuity. This means that there is a tendency for cations to be swept to the cathode and accumulate there, as the advective and ion migration forces sweeping them away from the cathode into the well are weaker than those sweeping them out of the soil towards the cathode. Similar-y, the ion migration force sweeps anions out of the soil towards the anode but there is no such force in the well and the advective force is from the anode well into the soil, so there is a tendency for anions to accumulate at the anode. This tendency for material to accumulate at the electrodes is counter-balanced by higher diffusion rates in the wells, and by the higher rate of dispersion which results from assuming that the dispersivity in the wells is an order of magnitude greater than that in the soil. Accumulation will occur if the effects of the discontinuities in transport velocities at the electrodes dominate, and will be absent if the effects of greater dispersion in the wells dominate.

The Debye relaxation time for ionic rearrangement due to charge imbalances is $\leq 1\mu s$ [Hibbert, 1993], and the recombination rate of water is very rapid, so the rate at which charge imbalances will dissipate is very large. Assuming electroneutrality locally is equivalent to saying that the soil has zero capacitance. The strength of the tendency for electroneutrality to be maintained because of ionic rearrangement is dealt with in appendix A. Although that analysis shows that nature of the rearrangement depends on the relative concentrations of the various species present the relaxation analysis is too unwieldy to perform after every time increment. Electroneutrality is therefore enforced at the end of each transport step and prior to the calculation of the chemical equilibrium state by adjusting the concentration of hydronium and hydroxy ions at each node, as in Datla and Yeung [1994]. This was the result of the relaxation analysis when the concentration of other ions was low in relation to the concentration of either the hydroxy or hydronium ions, because water autoprotolysis supplies enough ions to dissipate

the local charge imbalance. For high ionic strengths this approach to electroneutrality may not be satisfactory, since the hydroxy and hydronium ions are no longer the dominant species in solution. Although it may be possible to crudely represent the relaxation by some kind of mechanism in which ions are "poached" from adjacent nodes in order to satisfy electroneutrality at nodes within the simulation domain away from the electrodes, which like assuming water autoprotolysis supplies sufficient ions would not violate mass conservation, the details of how this should be done are unclear. Also,, as noted above, the enforcement of electroneutrality in this way satisfies Faraday's laws at the electrodes, assuming that water electrolysis is the only significant electrode reaction.

This should result in the cathode end of the sample becoming alkali and the anode end becoming acidic, with the further possibility of formation of the aqueous and solid metal hydroxides at the cathode end. If the metal hydroxide is relatively insoluble, then the ionic strength of the pore water at the cathode end will fall and the electrical resistance rise at that end. This would reduce the total electrical current flowing for a given voltage difference, and increase the electrical potential gradient at the cathode end relative to that in the rest of the sample.

The two versions of the program are identical except for the transport step calculation method. Both calculate the concentrations and activity coefficients on a fixed grid at the end of each time step and the resulting distribution is used as the starting position for the next time step. In the predictor-corrector version the local values of dispersivity and transport velocity are used even though Tagamets and Sternberg [1974] developed equations (28) and (29) strictly for the constant coefficients case. If the coefficients vary smoothly the error should not be great. This problem does not arise in the random walk particle method of Tompson and Gelhar [1990] because that formulation is based on varying coefficients.

The program allows for eight species: a cation and an anion representing the dissolved contaminant, hydronium and hydroxy ions, an aqueous-phase uncharged complex of the contaminant cation and hydroxy ions, a solid precipitate of the contaminant cation hydroxide, and a cation and an anion from a background electrolyte. These eight species must be distinct. The background electrolyte is assumed to be completely dissolved. The background electrolyte concentration is taken as constant in space and time, so that transport of the background electrolyte ions is not modelled; this implies that the background electrolyte ions are continuously replenished from the wells as they are swept way from the electrodes into the soil. Their effect on ionic strength, electrical conductivity and the transport properties of the other ions is allowed for. The limiting ionic conductivity of each ionic species must be specified, and the other transport properties are calculated from equations (5), (6), (7), (8) and (9). The diffusion coefficient for the aqueous contaminant hydroxide complex and that for the solid contaminant cation hydroxide precipitate must also be specified.

Electra-osmosis and hydrodynamic dispersion

Water will flow through the soil pores under the action of a hydraulic pressure at a rate given by Darcy's Law, and under the action of the electrical field at a rate equal to the electro-osmotic permeability times the electrical potential gradient. For a rigid matrix with constant hydraulic conductivity and constant electro-osmotic permeability it is easy to show that it is the overall gradients which determine $\bar{v}$, not the local gradients, as described in appendix C. Variations in the gradient of Φ will generate variations in pore pressure such that the net flux of water is the same through all sections. In practice, the pore pressure variation will cause consolidation or swelling of the soil, and the pore pressure variation within the sample can have a significant effect on the pore fluid flow behaviour [Thevanayagam and Wang, 1994].

The electrokinetic process will change the ionic composition and concentration of the pore fluid, and this will in turn change the electro-osmotic permeability. There is theoretical and experimental evidence that the electro-osmotic permeability increases as the pore water concentration decreases [Gray and Mitchell, 1967], with the ionic strength of the pore water being a probable factor. Gray and Mitchell [1967] showed that the increase is greater in low exchange capacity materials. Hamed et *al.* [1991] found that in kaolinite k_e decreases as the acid front generated at the anode during electrokinetic remediation sweeps across the specimen, a phenomenon which Alshawabkeh and Acar [1992] ascribed to a decrease in the zeta potential evolving from the decrease in pH. This affect may be more marked in kaolinite, whose apparent surface charge is particularly sensitive to pH and to the pore water composition [McBride, 1978; Herrington et al., 1992; Shackelford and Redmond, 1995].

If the dependence of surface charge on pore chemistry were known, the consequent effect on k_e could be calculated from equation (26). However, for practical purposes k_e lies in the range $10^{-9} - 10^{-8}$ $m^2s^{-1}V^{-1}$ [Mitchell, 1991] while effective ionic mobilities are typically about 3×10^{-8} $m^2s^{-1}V^{-1}$ for simple ions except for H_3O^+ and OH^-, which have mobilities nearly an order of magnitude larger. As a result, the ionic mobility component will generally dominate over the electro-osmotic component in equation (23) and spatial and temporal variations in k_e should have little effect on the ionic transport. This may not be the case where there are large variations in pore water chemistry within a soil body, both because of changes in surface charge and because large variations in local electrical potential gradient may exist. Such behaviour can be important [Eykholt and Daniel, 1994] but is too complex for this study and so the electro-osmotic permeability is assumed constant here.

The question also arises as to whether the electro-osmotic flow cause mechanical dispersion in the same manner as flow under hydraulic gradients, that is, whether equation (25) is valid. The relationship between hydrodynamic dispersion and pore water velocity is well established for flow due to hydraulic gradients [see Bear, 1969 and Bear, 1988 for example]. The same is not true for the relationship between hydrodynamic dispersion and pore water flow due to electrical gradients. The conventional model for electro-osmosis derives from consideration of

flow in cylindrical capillaries with shearing across the diffuse double layer [Casagrande, 1949; Gray and Mitchell, 1967; Crow, 1994] which indicates that the velocity distribution across the moving plug will be more uniform than that in Darcian flow. Incidentally, it also implies a moving charge independent of the ionic mobility. Furthermore, the velocity of water flow is independent of the width of the capillaries, whereas in Darcian flow the velocity decreases as the channels become narrower. The variation in flow rate will also depend on the extent to which the electrical field is channeled within the pore space, since static electric fields modify the diffused double layer around charged solid particles [Grosse and Foster, 1987] and would cause the electric equipotentials to deform around the soil grains. It therefore seems reasonable to expect less dispersion during electro-osmotic flow than during Darcian flow at the same flow rates. However, this has not yet been quantified, and in general electro-osmosis and electrokinetic remediation techniques are used in fine-grained soils in which mechanical dispersion should not be a significant factor. With that caveat, the best approximation to make at this time is to assume that mechanical dispersion due to electro-osmotic flow varies with flow velocity in the same way as that due to Darcian flow.

SIMULATIONS

The first simulation, ELK01 , was for a column of length $L = 0 \cdot 2\text{m}$, cross-sectional area $A = 4 \cdot 418 \times 10^{-3}\text{m}^2$, filter length 0·002m, initially spiked with a $0 \cdot 1\text{mol L}^{-1}$ copper sulphate solution at pH = 4, subject to an electrical potential difference of 40V for 8 hours at a temperature of 25°C. The soil properties were electro-osmotic permeability $k_e = 1 \times 10^{-9}\text{m}^2\text{s}^{-1}\text{V}^{-1}$, porosity $n = 0 \cdot 5$, tortuosity $\omega = 0 \cdot 5$ and dispersivity a, $= 1 \times 10^{-6}$ m . The configuration and properties correspond to a series of laboratory tests on E-grade Kaolin done by the first author to examine initial electrokinetic behaviour; these tests are the subject of a report in preparation. The properties used are similar to those in Datla and Yeung [1994] and are in the range quoted by Hellawell [1994]. Limiting ionic conductivities were taken from Atkins [1994]. The stability constant for aqueous copper hydroxide was taken from Martell and Smith [1974] and its free diffusion coefficient set equal to $1 \times 10^{-9}\text{m}^2\text{s}^{-1}$, which is approximately the same as the free diffusion coefficient for Cu^{2+}. The solubility product of the copper oxide was used, since this is more stable than the solid copper hydroxide and the black precipitate observed at the cathode end in the laboratory tests is believed to be copper oxide. For CuO K_{sp} was taken from Martell and Smith [1974] and the free diffusion coefficient also set equal to $1 \times 10^{-9}\text{m}^2\text{s}^{-1}$. No background electrolyte was present and no hydraulic gradient was imposed on the sample. Copper hydroxide is relatively insoluble, so variations in the electrical potential gradient because of reduction in ionic strength at the cathode should be significant.

Simulations ELK02 and ELK03 were identical to ELK01 except that $k_e = 3 \times 10^{-9}$ and $1 \times 10^{-8}\text{m}^2\text{s}^{-1}\text{V}^{-1}$ respectively, illustrating the effect of increased electro-osmosis on the initial

electrokinetic behaviour. Simulations ELK04 and ELK05 were identical to ELK01 except that the initial copper sulphate concentration was 0·01 and 0·001mol L^{-1} respectively, illustrating the effect of decreased contaminant concentration. Simulations ELK06, ELK07 and ELK08 were identical to ELK01 except that the temperature was set at 5°C, 45°C and 65°C respectively, with the limiting ionic conductivities and the free diffusion coefficients being increased by 2% per °C relative to the value at 25°C; no adjustment was made to the equilibrium constants. Simulations ELK09, ELK10 and ELK1 1 were identical to ELK01 except that a sodium chloride background electrolyte was added at a concentration of 0.001, 0·01 and 0·lmol L^{-1} respectively. Simulations ELK12 and ELK1 3 were identical to ELK01 except that the voltage was applied for longer, 80 and 800 hours respectively.

Simulation ELK14 was identical to ELK01 except that a sodium chloride contaminant was modelled at an initial concentration of 0· lmol L^{-1}. The stability constant for aqueous sodium hydroxide was taken from Mat-tell and Smith [1974] and its free diffusion coefficient set equal to 1 x 10^{-9} m^2s^{-1}, as before. No solubility product for NaOH is listed in Mat-tell and Smith, nor in any any of the other reference books consulted, which suggested that the solid form is effectively completely soluble, and K_{sp} was therefore set to a sufficiently large value that no solid NaOH would form for the feasible range of pH. Sodium hydroxide is highly soluble, so the effect of hydroxide formation at the cathode should not be significant. ELK15 was identical to ELK14 except that the simulated test duration was 16 hours instead of 8.

Simulations ELK16 and ELK17 were for a copper sulphate contaminant, and were identical to ELK12 except that the simulated test duration was 160 hours and 320 hours respectively, with the electrical potential difference being 20V and 10V respectively. That is, half the voltage is applied for twice as long in ELK16 compared to ELK12, and similarly for ELK17 compared to ELK16. Simulation ELK18 was identical to ELK12 except that the coefficient of electo-osmotic permeability was set equal to zero, to eliminate pore water movement in the simulation.

Simulation ELK19 was for a column of length L = 0·12m, filter thickness 0·002m, cross-sectional area A = 1 · 134 x 10^{-3} m^2, initially spiked with a 0 · lmol L^{-1} sodium chloride solution at pH = 7, subject to an electrical potential difference of 5·5V for 12 hours at a temperature of 25°C. The soil properties were k_e = 1 · 6 x 10^{-9} $m^2s^{-1}V^{-1}$, n = 0 · 45, ω = 0·52 and α_L = 1 x 10^{-6} m. The configuration and properties correspond to laboratory test E-K-2 on 180-grade silica flour reported by Hellawell [1994].

Simulation ELK20 was a repeat of ELK01 except that the electrical potential was assumed to vary linearly between the two electrodes. This is not a physically correct simulation, since the variation in electrical conductivity as a result of the changing pore water chemistry was not modelled. The effect on ionic strength and the other transport properties was modelled, however. The purpose of this simulation was to illustrate the effect of assuming a constant

electrical conductivity, since this is an assumption made in several previous works such as Alshawabkeh and Acar [19921, Datla and Yeung [1994], and Hellawell [1994].

Simulations ELK2 1 and ELK22 were for a sodium chloride contaminant. Simulation ELK2 1 was identical to ELK14 except that the temperature was set to 65°C instead of 25°C, to examine the effect of temperature on the electrokinetic transport where the metal hydroxide is highly soluble; the limiting ionic conductivities and the aqueous sodium hydroxide free diffusion coefficient were increased by 2% per °C relative to the value at 25°C. Simulation ELK22 was identical to ELK14 except that a potassium bromide background electrolyte was added at a concentration of $0 \cdot 1 mol\ L^{-1}$, to examine the effect of a background electrolyte where the metal hydroxide is highly soluble.

Simulations ELK23, ELK24 and ELK25 were for a copper sulphate contaminant, and were identical to simulations ELK06, ELK07 and ELK08 respectively except that the limiting ionic conductivities and the free diffusion coefficients were increased by 3% per °C relative to the value at 25°C instead of 2% per °C; again, no adjustment was made to the equilibrium constants.

RESULTS

Figures 3-13 show the results for simulation ELKOl. Figure 3 shows the variation in electrical current with time predicted using all three methods. Also shown is the variation measured in laboratory test JMEK07, an experiment on E-grade Kaolin clay spiked with copper sulphate subject to the same conditions as simulation ELK0 1, except that JMEK07 was performed at a slightly lower temperature, 18°C instead of 25°C. Figure 4 shows the variation in specific discharge over time. Figures 5, 6 and 7 show the variation over time of the amount of dissolved copper, sulphate and total copper, respectively, in the soil as a percentage of the initial amount. Figures 8, 9, 10 and 11 show the final distribution of dissolved copper, sulphate, total copper and pH, respectively, through the soil and the wells. The difference between figure 5 and 7, and between figure 8 and 10, is the copper present as the aqueous hydroxide. Figure 12 shows the final distribution of electric potential, with the variation measured in laboratory test JMEK07 superimposed. In figure 13 the final distributions of both dissolved and total copper for ELK01 are plotted normalised with respect to the initial concentration, with the corresponding values from laboratory test JMEK07 also plotted.

Figures 14, 15 and 16 show for ELK02 the variation in specific discharge over time, the final distribution of total copper and the final distribution of sulphate respectively, while figures 17, 18 and 19 show the corresponding plots for ELK03. ELKOl, ELK02 and ELK03 represent increasing electro-osmotic permeability. Figures 20, 21 and 22 show for ELK04 the electrical current variation over time, the variation in percentage total copper with time and the final distribution of total copper respectively, while figures 23, 24 and 25 show the corresponding plots for ELK05. ELK01 , ELK04 and ELK05 represent decreasing contaminant concentration.

Figures 27, 29 and 31 show the variation in percentage total copper with time for ELK06, ELK07 and ELK08 respectively, while figures 26, 28 and 30 show the corresponding variation in current with time. ELK06, ELK01, ELK07 and ELK08 represent increasing temperature.

For ELK09 figure 32 shows the variation in current with time, figure 33 the final distribution of total copper and figure 34 the final distribution of sulphate, while figures 35, 36 and 37 and figures 38, 39 and 40 are the corresponding plots for ELK10 and ELK1 1 respectively. Figure 41 shows the final distribution of electric potential for ELK1 1. ELK01, ELK09, ELK10 and ELK1 1 represent increasing sodium chloride background electrolyte concentration.

For ELK12 figure 42 shows the variation in current with time, figure 43 the variation in percentage total copper with time and figure 44 the variation in percentage sulphate with time, while figures 45, 46, 47 and 48 show the final distribution of total copper, sulphate, pH and electric potential respectively. Figures 49, 50 and 51 show the variation with time in current, percentage total copper and percentage sulphate respectively, while figure 52 shows the final distribution of pH, for ELK1 3. Simulations ELK01 , ELK12 and ELK1 3 represent increasing duration of the application of voltage.

Simulations ELK14 and ELK15 were for a sodium chloride contaminant, with ELK15 representing a longer duration of voltage application than ELK14. Figures 53, 54, 55 and 56 show the variation with time in current, specific discharge, percentage dissolved sodium and percentage chloride respectively for ELK14, while figures 57, 58, 59, 60 and 61 show that simulation's final distribution of dissolved sodium, chloride, total sodium, pH and electric potential respectively. Figures 62 and 63 show the final distribution of dissolved sodium and of chloride respectively for ELK 15.

Simulations ELK16 and ELK17 were for a copper sulphate contaminant. ELK12, ELK16 and ELK17 represent progressively smaller voltages applied for progressively longer times such that the product of voltage and duration is constant. Figures 64 and 65 show the variation in percentage total copper with time and the final distribution of total copper respectively for ELK 16, while figures 66 and 67 show the corresponding plots for ELK17. In ELK1 8 the electro-osmotic permeability was zero with the other conditions the same as for ELK12, and figures 68 and 69 show the variation with time in percentage total copper and percentage sulphate respectively, while figures 70 and 71 show the final distribution of total copper and sulphate respectively, for ELK 18.

ELK19 represents Hellawell's [1994] laboratory test E-K-2 for sodium chloride in 180-grade silica flour. Figures 72, 73 and 74 show the final distribution of dissolved sodium, chloride and electric potential respectively for ELK19, with the corresponding data points from Hellawell [1994] superimposed.

Figures 75, 76 and 77 show the variation with time in percentage dissolved copper, percentage sulphate and percentage total copper respectively for ELK20. Figures 78, 79, 80

and 81 show the final distribution of dissolved copper, sulphate, total copper and pH for ELK20. The test conditions for ELK20 were the same as those for ELK01 but in the analysis a linear electrical potential distribution was assumed.

Figures 82, 83 and 84 show the variation with time in current, percentage dissolved sodium and percentage chloride respectively for ELK2 1, which was for a sodium chloride contaminant and was identical to ELK14 except for being at a higher temperature. Figure 85 show the final distribution of electric potential for ELK21.

ELK22 was also for a sodium chloride contaminant, and was identical to ELK14 except that a potassium bromide background electrolyte was added at a concentration of 0 · lmol L^{-1}. Figures 86 and 87 show for ELK22 the variation with time in current and percentage dissolved sodium respectively, while figure 88 shows the final distribution of dissolved sodium.

A general feature of the simulations for copper sulphate contaminant is that the current is initially constant for a short time and then starts to fall rapidly, finally tending towards a stable value. The time at which the current starts to fall and the time at which it starts to stabilise were calculated from the results for simulations ELKOl, ELK06, ELK07, ELK08, ELK23, ELK24 and ELK25, which were identical except for temperature and the magnitude of the temperature correction, with the time at which the current starts to stabilise being taken as the time when the drop in current equals 90% of the total drop for the simulation. This was done for simulations using the random walk version of ELK only. Figure 89 shows the variation in these two times with temperature for the two temperature correction factors, and the stabilisaton time found in the laboratory experiments.

DISCUSSION

It is necessary to examine the results from the first simulation, ELKOl, in some detail. In this simulation of a short duration electrokinetic test on copper sulphate contaminated soil both numerical models predict a small initial rise in the current followed by a large decrease over the first one to four hours to an approximately constant value of about a third of the initial current for the predictor-corrector model and about a tenth of the initial current for the random walk model. This corresponds to a decrease in the apparent electrical conductivity of the whole sample. Acar and Gale [1992] report a fourfold decrease in the apparent electrical conductivity over the first one hundred hours or so for their constant-current experiments on lead contaminated kaolinite, in which the electrical current density was one hundredth of the initial value for ELK0 1, although it must be pointed out that the lead concentrations were sufficiently low for the majority to be adsorbed on to the clay.

There is basic agreement with the experimental results from JMEK07, with the initial rate of decrease of the measurements lying between the two numerical predictions and the variation from the random walk model being particularly close to the measured one. The random walk model predicts a more rapid decrease than the predictor-corrector model and lower currents

throughout, with the electric current decreasing rapidly at about nine minutes and stabilising at a low value at about 25 minutes. The simple analysis gives an even more rapid decrease and lower currents again. Arbitrarily increasing κ_c^*, the electrical conductivity of the cathode zone, by a factor of ten causes the simple model to predict a variation very close to that measured except that the initial rate of decrease is still much higher in the simple model, indicating that this model over-predicts the reduction in electrical conductivity due to copper hydroxide formation at the cathode. The specific discharge is roughly constant in the predictor-corrector model, but decreases nearly to zero in the random walk model with a variation similar to that of the electrical current.

The predictor-corrector model gives an approximately 30% reduction in the percentage of dissolved copper and an approximately 20% reduction in the percentage of sulphate over the eight hour period, while the random walk gives approximately 5% for dissolved copper and no sulphate reduction. The difference in the variation of the total amount of copper present predicted by the two numerical models is striking: while the random walk model gives a very slight reduction the predictor-corrector model gives an increase of about 10%. This unphysical behaviour must be a consequence of the lack of mass conservative behaviour in the finite difference based predictor-corrector model, and it appears from figure 7 that the predictor-corrector model erroneously adds copper at the cathode end.

The final distributions of dissolved copper and total copper are similar in the two numerical predictions except at the alkaline end, where the predictor-corrector model gives high concentrations of copper hydroxide and almost no dissolved copper in the first 50mm of soil, while the random walk model gives significant copper hydroxide concentrations close to the cathode only. Both models predict a very slight movement of copper away from the anode and accummulation of copper at the cathode, although the movement is greater in the predictor-corrector model. However, the predictor-corrector model gives a much larger movement of anions away from the cathode than the random walk model, which predicts a small degree of accumulation of sulphate at the anode but little overall movement.

The random walk method gives some accumulation of copper at the cathode and of sulphate at the anode, while the predictor-corrector method gives no accumulation at either electrode. It is not known whether accumulation should occur, that is whether the effects of the discontinuity in the transport velocities at the electrodes dominates over the effects of increased dispersion in the wells. It may be that the stochastic nature of the random walk model leads to an erroneous concentration peak where the transport parameters change, since fluctuations in the concentration distribution are a feature of this model [Tompson and Dougherty, 1988]. Alternatively, it may be that the predictor-corrector method has sufficient numerical dispersion to suppress this peak, since numerical dispersion is a feature of finite difference models not based on upwind formulations [McBride, 1985; Noorishad et *al.*, 1992].

The stochastic nature of the random walk model shows up clearly in the plots of final concentrations, as there are small peaks in the distributions, but this effect is very marked in the final pH distribution: the small peaks in the anion distribution predicted by the random walk method correspond to the narrow troughs in the pH distribution. This is a consequence of the enforcement of electroneutrahty by adjustment of the hydronium ion concentrations and the logarithmic dependence of pH on hydronium concentration. Electroneutrality enforcement also explains the lack of dissolved copper at the cathode in the predictor-corrector solution, as hydroxy ions must be added to balance the copper ions "created" there in the model, raising the pH and encouraging copper hydroxide formation.

The random walk model and the predictor-corrector model both give a zone of higher pH at the cathode. This zone is very narrow in the random walk model. Within this alkaline zone copper complexes into the hydroxide and the electrical conductivity is very low, which shows up clearly in figure 12: in both models most of the electric potential is dropped over this narrow zone, the difference being that the random walk model gives a much sharper break in the distribution while the predictor-corrector model gives a wider zone with a smaller gradient of electric potential. The point where the electric potential becomes almost constant in the predictor-corrector solution corresponds to the edge of the alkaline zone. Since this is also the point where there will be a sudden change in the transport velocity it seems likely that the unphysical results of the predictor-corrector model arise from an inability to cope with this velocity change and the large grid Peclet number that results, an inability compounded by the lack of mass conservative behaviour in that model. This suggests that the predictor-corrector model is unsuitable for problems where a zone of much lower electrical conductivity is expected to form, problems for which the analysis in appendix D indicates that the grid Peclet number will become large and independent of the grid spacing. This will be examined further in the discussion of simulation ELK20.

The electric potential distribution measured experimentally in JMEK07 indicates that almost all of the potential is dropped across a very thin zone at the cathode with a smaller amount being dropped across a thin zone at the anode, and more closely resembles that given by the random walk model. A consequence of the electric potential gradient being almost zero across most of the soil is that ionic migration becomes negligible in comparison with electro-osmosis and diffusion, an effect which is more marked in the random walk model than in the predictor-corrector model and explains why the former gives less sulphate movement. That is, the formation of a low conductivity alkaline zone close to cathode dominates the process and has dramatically reduced the effectiveness of the electrokinetic remediation. Moreover, in the random walk model this zone is sufficiently narrow that it falls almost entirely within the cathode filter, so that the total electric potential difference across the soil is much reduced and the specific discharge due to electro-osmosis becomes greatly reduced. While both models predict that ion migration becomes suppressed because of the formation of a zone of low

electrical conductivity at the cathode end, the random walk model predicts that electro-osmosis also becomes suppressed, in which case the rate of remediation becomes negligible. This accounts for the much smaller distance by which the contaminants have moved in the random walk model than in the predictor-corrector model, and also for the fact that the random walk model gives an electrical current variation similar to that for the simple analytical model, since that model ignores the effect of electro-osmosis.

Although there is considerable scatter in the experimental data on final copper distribution, the results in figure 13 do indicate some copper accumulating at the cathode even in this short duration test and very little copper movement, with the measured values lying between those from the two numerical models. It appears that the stochastic random walk model is the better representation of the electrokinetic remediation process where the contaminant hydroxide is poorly soluble and the electric potential distribution is not linear.

Comparison between simulations ELK01, ELK02 and ELK03 indicates that as k_e increases electro-osmosis starts to dominate over ion migration as an ionic transport process for the copper sulphate contaminated soil, an effect most clearly seen in ELK03 where there is a significant net movement of both copper and sulphate towards the cathode. A good estimate of k_e is obviously needed where hydroxide formation at the cathode is a significant process, especially for soils whose electro-osmotic permeability is high. A ten-fold increase in k_e gives an approximately seven-fold increase in the width of the copper-free zone at the anode for the predictor-corrector model, an effect which can be ascribed to the observation that the electro-osmotic velocity stays roughly constant in that simulation while ion migration depends on the local electric potential gradient and becomes subdued as copper hydroxide is formed near to the cathode. In contrast, the electro-osmotic discharge reduces sharply in the random walk model for ELK02, so there is little difference between the results for ELK01 and ELK02 using that model, but stays roughly constant in ELK03. It appears that for $k_e = 1 \times 10^{-8}\ m^2 s^{-1} V^{-1}$ the fluid is moving sufficiently rapidly to sweep both copper and sulphate ions into the cathode region quickly enough to prevent the formation of a very narrow zone of low electrical conductivity which would cause the fluid velocity to decrease. The degree of copper accumulation at the cathode given by the random walk model increases as k_e increases, but otherwise the distribution of total copper and sulphate in ELK02 are qualitatively similar to those in ELK01 for both numerical models.

In simulations ELK04 and ELK05 the behaviour predicted by the two numerical models is similar to that for ELKOl. As the initial copper sulphate concentration decreases the electric current also decreases, of course, but the rate of remediation and the final distributions of the two contaminant ions hardly changes. The only noticeable changes as the concentration decreases are that the two numerical models predict increasingly similar Variations in electric current, the width of high copper concentration zone increases slightly in the predictor-correct model, and both models predict slightly greater copper movement away from the anode end. It

appears that the increased mobility of the ions due to the lower ionic strengths of the pore water has little effect on the degree of movement, so dominant is the effect of copper hydroxide formation at the cathode on the transport processes.

The dominance of this effect is also apparent when comparing simulations ELK06, ELK01 , ELK07 and ELK08, since increasing temperature has no effect on the rate of removal of copper in the random walk model and leads to a slight increase in the rate at which extra mass is "created" in the predictor-corrector model, even though the ion mobilities and diffusion coefficients more than double across this range. This behaviour is consistent with the suggestion that the transport will be primarily by electro-osmosis where the formation of relatively insoluble hydroxide and the consequent development of a zone of low electrical conductivity is permitted. This zone develops more rapidly as the temperature increases: in the random walk models the time at which the electric current starts to fall decreases from approximately 18 minutes to approximately 8 minutes and the time for the electric current to stabilise at a low value decreases from approximately 74 minutes to approximately 27 minutes when the temperature increases from 5°C to 45°C. This is consistent with the assumed near doubling of the ion transport properties across this temperature range, which appears to cause the zone of low electrical conductivity at the cathode to develop proportionally earlier. For comparison, in the first author's laboratory tests on Kaolin impregnated with copper sulphate the time for the electric current to stabilise at a low value decreases from approximately 60 minutes to approximately 25 minutes when the temperature increases from 15°C to 45°C, suggesting that, while the rate of increase of ionic conductivity with temperature may in reality be closer to 3%/°C than the 2%/°C assumed in the models, the model predictions are essentially correct. A comparison in figure 89 between the predicted times as a function of temperature for for the random walk models and the measured time in the first author's laboratory experiments shows good agreement between the predicted and the measured results, with the temperature dependence apparently lying in the expetced range. Note that the electro-osmotic permeability was assumed to be independent of temperature. The results also indicate that the mass balance error associated with the predictor-corrector method increases as the migration velocities increase.

Examination of simulations ELK01 , ELK09, ELK10 and ELK1 1 shows that the presence of a background electrolyte does have a significant effect for copper sulphate contamination, even when the background electrolyte concentration is much lower than that of the contaminant. This accords with the assertion in Acar and Gale [1992] that control of the chemistry at the electrodes and proper appreciation of the general electrolyte system within the soil are important for efficient use of electrokinetic remediation. As the background electrolyte concentration increases there is a general increase in the electric current, of course, but there is also less reduction over time. This is noticeable in the predictor-corrector model, although the variation in ELK09 is practically identical to that in ELK01. There is a stronger effect on the current

variation from the random walk model: as the background electrolyte increases, the initial increase in current becomes larger such that in ELK1 1 the current is rising continuously, and the current in the random walk model starts to exceed that in the predictor-corrector model. Raising the electrical conductivity of the pore water generally appears to reduce the deleterious effects of hydroxide formation at the cathode on electrokinetic remediation, and the difference between the two numerical models reflects the observation in simulation ELK01 that while a broad zone of low electrical conductivity develops at the cathode in the predictor-corrector model, in the random walk model this zone is very narrow and has a much lower electrical conductivity. That is, in the random walk model the deleterious effect is more marked, probably because the predictor-corrector model creates mass in this zone so raising the general concentrations, so the beneficial effect of the background electrolyte is also more marked. As indicated by figure 41 for simulation ELK1 1, as the background electrolyte concentration increases the electric potential distribution becomes more linear, reflecting the more uniform electrical conductivity, and the distributions given by the predictor-corrector and by the random walk models become similar.

The predicted contaminant movements are also affected by the background electrolyte concentration: as it increases the degree of remediation of both the copper and the sulphate increase. Both numerical models predict increased accumulation of copper near to the cathode, while the random walk model in particular gives a zone of enhanced removal of copper close to the anode. For the predictor-corrector model the width of the zone with almost complete anion removal increases from about 0·05m to about 0·07m as the background electrolyte concentration rises to 0· lmol L^{-1}, while for the random walk model it increases from about 0·005m to about 0·05m. The presence of other non-reacting ions in solution clearly has a marked beneficial effect on the transport, an effect which will be much more significant at the low contaminant concentrations found in the field than at the much higher contaminant concentrations sometimes used in laboratory work.

The previous discussion concerns simulations of short duration tests. In ELK12 the duration was increased from that in ELK01 by a factor of ten to 80 hours while in ELK13 it was increased by a further factor of ten. The trends identified in simulation ELK01 continue, although the fluctuations caused by the stochastic nature of the random walk model become stronger, especially in the variation of electric current for ELK13. This may result from the temporary formation of narrow adjacent zones of low and high pH, due to the fluctuations in the concentration distributions and the enforcement of electroneutrality, as such zones would both have high electrical conductivity. The predictor-corrector model gives a generally declining electric current throughout.

After 80 hours the random walk model gives an approximately 5% reduction in copper and almost no reduction in sulphate, while the predictor-corrector model gives approximately 30% and 90% respectively; the mass balance error associated with the predictor-corrector model still

dominants the variation for copper, but the simulated period is now long enough for the amount of copper to start falling. The predictor-corrector model predicts that approximately half of the soil is free of copper but the random walk model predicts only slight movement away from the anode, again indicating the relative importance of electro-osmosis as a transport process in these two simulations. However, the random walk model gives high copper concentrations close to the cathode only, while the predictor-corrector model gives a broad band of copper accumulation. The random walk model gives acid conditions everywhere except in the cathode well, while the predictor-corrector model gives a slightly more alkaline cathode zone occupying over half the soil, behaviour consistent with the erroneous creation of copper in the predictor-corrector model, as discussed above.

The predictor-corrector model gives a small amount of sulphate still present near to the anode, consistent with the high degree of removal, but in the random walk model there is almost no sulphate movement. For both models the distribution of electric potential after 80 hours is similar to that after 8 hours. Similar behaviour was observed for a lead contaminated kaolin by Acar and Gale [1992]: in their laboratory Test 1 electrokinetic remediation has been applied long enough to clean up about half of the sample which also shows a central region of lower electrical conductivity, not present in their longer Test 5.

After 800 hours both numerical models predict complete removal of the copper sulphate contaminant: in the random walk model copper remediation is complete after about 300 hours and sulphate remediation after about 470 hours, while the predictor-corrector model gives approximately 140 hours and 110 hours respectively. The distribution of final pH is similar for both models.

The behaviour in the simulations for a sodium chloride contaminant is qualitatively very different from that for a copper sulphate contaminant. The difference arises because sodium hydroxide is highly soluble while copper hydroxide is poorly soluble. A principal feature is that the results from the two numerical models are much more similar than for the copper sulphate, and there is now no evidence of mass balance errors in the predictor-corrector model. In ELK14 the electric current rises from 0·22A to about 0·38A over the first five hours and then falls to about 0·05A by eight hours; however, the predictor-corrector model gives a smooth variation during these two periods while the random walk model indicates a rapid change from one level to another. The specific discharge through the soil stays constant, reflecting the fact that no zone of low electrical conductivity is formed in the filters for the sodium chloride contaminant. The final distributions of dissolved and total sodium are almost identical for each numerical model, except that a small amount of hydroxide is indicated at the cathode where the pH rises to about 13. The pH of the alkali zone is higher than in the simulations for copper sulphate, reflecting the fact that there is little removal of hydroxy ions by complexation with the sodium. Both models predict substantially the same variation over time in the percentage of dissolved sodium with 40–50% being removed in the eight hours,

except that the random walk method gives a slightly higher rate of removal initially and a dropping off in the rate at about five hours, coinciding with a sudden drop in the electric current. The random walk model does predict almost no removal of the chloride, however, compared with about 70% removal in the predictor-corrector model.

The final distributions of the concentration of sodium and of chloride are roughly the same in both numerical models, although the random walk model shows large fluctuations, less chloride movement, and an accumulation of sodium at the cathode and of chloride at the anode. As with the copper sulphate simulations, it is not clear whether the random walk model is giving erroneously large accumulations at the electrodes or whether numerical dispersion in the predictor-corrector model is suppressing the accumulation. The numerical models give substantially the same final pH distribution: an alkali half of about pH 13 and an acidic half of about pH 2. This indicates that the acid front originating at the anode and following the cations has met the alkali front originating at the cathode and following the anions, leaving a central zone of neutral pH in which the ionic strength and the electrical conductivity are low. In the random walk model this zone is much narrower than in the predictor-corrector model, as can be seen in the final distribution of electric potential: the former model gives a step-like distribution, so that ionic migration has practically ceased, while the latter has a similar but much smoother distribution.

Doubling the simulated test duration to 16 hours results in little additional movement of the sodium chloride in the random walk model but noticeably more movement in the predictor-corrector model, as shown by comparing the results of ELK14 and ELK15. In the random walk model the behaviour has become dominated by a clean, low electrical conductivity zone near the middle of the sample causing the electric potential gradient to be very small where the contaminant concentrations are still significant. Since transport due to ionic migration is neglible in this case remediation is dependent on the slower processes of electro-osmosis and dispersion. The final distribution of sodium and of chloride are smoother than in ELK14, as a result of dispersion over the additional 8 hours.

In the simulation series ELK12, ELK16 and ELK17 for a copper sulphate contaminant the applied voltage was halved for each subsequent simulation while the test duration was doubled. Apart from the scale change of the time axis there is very little difference in the results: the mass balance error increases slightly in the predictor-corrector model as does the amount of remediation in the random walk model. If, as therefore seems likely, the electrical conductivity is the same at homologous times in the three simulations, and noting that the percentage reduction was found to be approximately linear with the increase in time for constant voltage, this implies that the degree of remediation is approximately proportional to the total amount Of energy expended. This accords with the results of published experimental work [Lageman *et al.*, 1989; Hamed *et al.*, 1991; Acar et *al.*, 1992; Acar et al., 19941. For the random walk model the final copper distributions did become slightly smoother along the series. with the

the sulphate, which indicates that it is the difference in the calculated voltage distribution between the random walk model and the predictor-corrector model which caused the random walk to give little anion removal, and not some inherent direction sensitive effect in the numerical algorithms. The width of the remediated zone is similar in both models, as is the final distribution of pH except that the stochastic nature of the random walk model is evident across the central part of the sample where the pH still has its initial value. Enforcing a linear electric potential distribution is equivalent to assuming that the electrical conductivity is constant, so the electric current is constant. This is reflected in the much higher degree of remediation in simulation ELK20 than in ELK01 : after eight hours approximately twice as much copper has been removed in ELK20 than in ELK01 for both numerical models, and there is now significant remediation of the sulphate in the random walk model. It must be remembered that in ELK20 the conductivity of the pore water is not correctly modelled. However, the conductivity change due to copper hydroxide formation would be small where copper is not the principal cation in solution and this explains why the results from ELK20 resemble those from ELK1 1, a simulation with a background electrolyte concentration equal to that of the copper sulphate contaminant.

There is no evidence of mass balance errors accumulating in the predictor-corrector models for ELK1 1 and ELK20, nor for a sodium chloride chloride contaminant, so it appears that this unphysical behaviour arises because of that model's inability to cope with large changes in the electric potential gradient and hence in the transport velocity within the sample, and not from the discontinuity in the contaminant cation concentration distribution caused by the creation of high pH zones where the cation is present principally as the hydroxide. That is, the predictor-corrector model performs badly where there are large spatial variations of velocity, and where the grid Peclet number becomes very large.

Increasing the temperature for a sodium chloride contaminant by 40°C between simulation ELK14 and simulation ELK21 results in only a slight increase in the amount of remediation after 8 hours. The electric current variation with time is similar to that in ELK14, with an initial rise and a sudden decrease to a low value, except that in ELK21 the levels are nearly twice those in ELK14 and the decrease occurs at just longer than half the time taken in ELK14. Both numerical models give final amounts of dissolved sodium and chloride only slightly lower than the corresponding final amounts for ELK14 but significantly higher initial rates of remediation. As before, the slow down in the rate of remediation coincides with the decrease in the electric current. The final voltage distribution given by the random walk method is identical to that in ELK14 and the distribution given by the predictor-corrector method is very similar to that in ELK14 except that the low conductivity zone is broader. The relative increase in electrical current and the initial rate of remediation is consistent with the assumed near doubling of the ion transport properties due to the higher temperature and causes the central zone of substantially clean soil to develop proportionally earlier than in ELK14. Thereafter, the electric

field strength is low in the zones where ions are still present and the electrokinetic remediation process is dominated by this central clean zone, as in ELK12 and ELK14. The higher temperature increases the diffusion coefficients and results in some additional clean up, but the concentration distributions at the time when this central zone of low ionic strength forms are probably largely independent of temperature and the final states are about the same at 25°C and 65°C. Similar conclusions were drawn above for the effects of temperature in simulations of copper sulphate contaminated soil, although there it was the development of a high pH, low ionic strength zone at the cathode which dominated the process.

Comparing the results of simulations ELK14 and ELK22 shows that adding a background electrolyte does result in enhanced remediation for a sodium chloride contaminated soil, just as it did for a copper sulphate contaminated soil. In ELK22 both numerical models predict that the electric current will initially rise and subsequently fall. However, the fall is not as dramatic as it was in ELK14 and just as in ELK1 1 for a copper sulphate contaminated soil the presence of the background electrolyte prevents the development of a zone of very low electrical conductivity and therefore increases the total amount of remediation. This effect is more marked for the random walk method predictions, which in ELK14 gave nearly zero electric potential gradients over most of the sample. Consequently the variation in percentage dissolved sodium given by the predictor-corrector method is almost the same in ELK22 as in ELK14, but that given by the random walk model no longer shows the sudden decrease in the rate of removal, and the two models give almost the same final amounts. The final distribution of dissolved sodium given by the predictor-corrector method is almost the same as in ELK14, while that given by the random walk method is similar to that in ELK14 except that the distribution is smoother and the contaminated zone is smaller, reflecting the higher degree of remediation. As before, the random walk method predicts an accumulation of sodium around the cathode while the predictor-corrector method does not.

CONCLUSIONS

Complex transport, electrochemical and physico-chemical processes govern the migration of water, ions and other chemical species in contaminated soils during electrokinetic remediation, in which DC electric fields are applied across the soil. Both physical and numerical modelling of electrokinetic remediation present a significant challenge to the researcher in environmental geotechnics, who must draw on work from ground improvement, geochemistry, soil contaminant transport, hydrogeology, electrochemistry and aqueous solution chemistry to develop a proper understanding of these processes, for the parameters in the transport equations change as transport takes place. In this paper a simplified, physically based numerical model is developed for the electrokinetic remediation of laboratory samples, using both a finite difference method and a stochastic method for solving the transport equations. The basic behaviour in the models can be understood by consideration of the effects of the

replacement with hydronium ions of cations moving away from the anode towards the cathode, the replacement with hydroxy ions of anions moving away from the cathode towards the anode, the reversible equilibration reactions for the association of the contaminant cation into its uncharged aqueous and solid hydroxide forms, and the autoprotolysis of water molecules.

Two contaminants were selected for the numerical study: copper sulphate, as an example of a contaminant whose cation hydroxide is relatively insoluble; and sodium chloride, as an example of one in which the cation hydroxide is relatively soluble. Simulations were performed to study the effects of the magnitude of electro-osmotic flow, temperature, contaminant concentration, duration of voltage application and the presence of a background electrolyte in the pore water. Electra-osmotic permeabilities in the range 0 – 1 x $10^{-8} m^2 s^{-1} V^{-1}$, temperatures in the range 5–65°C, durations at 40V in the range 8-800 hours for copper sulphate and 8–16 hours for sodium chloride, and background electrolyte concentrations up to those of the contaminant electrolyte were considered.

Neither numerical model was entirely satisfactory. The predictor-corrector model is not inherently mass-conservative and was found to create mass erroneously in the simulations for copper sulphate, apparently because of an inability to handle large spatial changes in the advective component of the transport equations. If the electric potential variation across the sample remained nearly linear then the predictor-corrector model seemed to perform satisfactorily, and generally gave much smoother concentration distributions than did the random walk model. The stochastic nature of the random walk model was apparent in all the simulations, but the consequences seemed more acute in the sodium chloride ones. Given the sensitivity of the transport to local values of the electric field strength and the concentration gradient, and the way in which the transport parameters depend on the concentration distributions, there is a clear need for a mass conservative, high accuracy numerical algorithm for solving the advection-dispersion equation with temporally and spatially varying transport parameters which can cope satisfactorily with large grid Peclet numbers and ideally also with large grid Courant numbers. In the absence of a satisfactory general method, the results suggest that the random walk model should be used where the hydroxides of the contaminant cation are relatively insoluble and the dissolved contaminant is the dominant electrolyte in the pore water, in which case the grid Peclet number may become very large, while the predictor-corrector model should be used otherwise.

For both contaminants the remediation behaviour comes to be dominated by a narrow zone of low ionic strength, low electrical conductivity pore water unless precautions are taken to prevent this zone forming. The low electrical conductivity zone causes the overall electrical resistance of the sample to rise significantly, so that the electric current falls, and also significantly reduces the electric potential gradient in zones where contaminant ions are still present. As a result, there is very little migration of the ions due to the electric field and continued clean up is largely due to electro-osmosis and diffusion. In such a situation, a good

estimate Of the electro-osmotic permeability of all the materials present is essential, and the results show that if k_e is at the upper end of the range encountered in practice then the direction of ion movement may change.

For a copper sulphate contaminated soil the low electrical conductivity zone results from the formation of relatively insoluble uncharged aqueous copper hydroxide in the alkaline cathode end of the sample, so that almost all of the applied electric potential difference is dropped over a very narrow region close to the cathode. If this zone was sufficiently narrow it may lie entirely within the filters used to restrain the soil, in which case the potential difference across the soil and therefore the rate of water movement due to electro-osmosis becomes very small. The electric current falls by about a factor of four over the first one to four hours as this zone develops. The rate of clean up is a lot less than would be expected from tests on contaminants where the metal hydroxide is relatively soluble, or from calculations done assuming a linear variation in electric potential, and increasing the mobility of the ions by either lowering the concentration or by increasing the temperature does not produce enhanced remediation when there was no background electrolyte. The primary effect of temperature was to decrease the time taken for the low electrical conductivity zone to develop, with the factor reduction in time being approximately linear with temperature and about the same as the factor increase in the ion mobility with temperature assumed in the model. The deleterious effect of copper hydroxide formation on electrokinetic remediation could be suppressed by adding a background electrolyte, since this prevented the ionic strength and therefore the electrical conductivity close to the cathode from falling to a very low value. Background electrolyte concentrations of the same order as the contaminant concentration are sufficient to produce throughout the test an approximately linear variation in electrical potential across the sample and a rate of contaminant migration similar to the initial rate. On the absence of a background electrolyte the remediation time was about ten days for a sample of length $L = 0 \cdot 2\text{m}$ subjected to an electric potential difference of 40V, and using half the electric potential produced approximately the same pattern of migration after twice the time.

For a sodium chloride contaminated soil the low electrical conductivity zone appears when the acid front from the anode meets the alkali front from the cathode, hydronium and hydroxy ions recombine to give water, and a central zone of substantially clean pore water develops. Sodium hydroxide is relatively soluble so only small quantities form at the cathode. It is when the contaminant cation distribution and the contaminant anion distribution no longer overlap that electrokinetic remedation becomes suppressed, because almost all of the applied electric potential difference is dropped over a very narrow region in the centre of the sample. As with copper sulphate, increasing the temperature does not enhance the remediation but rather reduces the time taken for this low electrical conductivity zone to develop. Again, the deleterious effect of this zone on electrokinetic remediation is suppressed when a background electrolyte is

added, since this prevented the ionic strength and therefore the electrical conductivity from falling to a very low value.

The limited comparison with experimental data that was possible indicates that the numerical models successfully represent the physical behaviour. The random walk model's predictions for a copper sulphate contaminated sample of the variation in electric current with time, the final electric potential distribution, the overall pattern of copper movement, and the effect of temperature on the time taken for the low conductivity cathode zone to develop gives good agreement with the first anthor's short duration laboratory tests. The behaviour is also similar to that reported by others working on electrokinetic remediation of heavy metal contaminated soils. The predictor-corrector model's predictions for a sodium chloride contaminated sample of the final distributions of sodium, chloride and electric potential agree with those measured experimentally by Hellawell [1994]. In general the numerical results also accord with the frequently made assertions that the degree of remediation is proportional on the total amount of energy expended and that appreciation of the overall electrolyte conditions in the pore water is important for efficient use of electrokinetic remediation.

It therefore appears that the numerical solutions developed here successfully model the essential features of the various transport, electrochemical and physico-chemical processes occuring during electrokinetic remediation of heavy metal contaminated soils. Further laboratory testing is needed to assess the accuracy of the predicted effects due to a background electrolyte, since the modelling of background electrolytes is not very realistic. However, the results are encouraging and indicate that the numerical models should be a useful tool in specifying and assessing further experimental work, both in the laboratory and in the field.

ACKOWLEDGEMENTS

This research was completed at the University of Cambridge Department of Engineering, and was funded by the U.K. Science and Engineering Research Council under the grant title "Study of pollutant spillage and electro-kinetic soil remediation (GR/JO5644)". The authors wish to thank Ms. Maddy Penn Dr. Rod Lynch for their advice and comments.

FIGURES

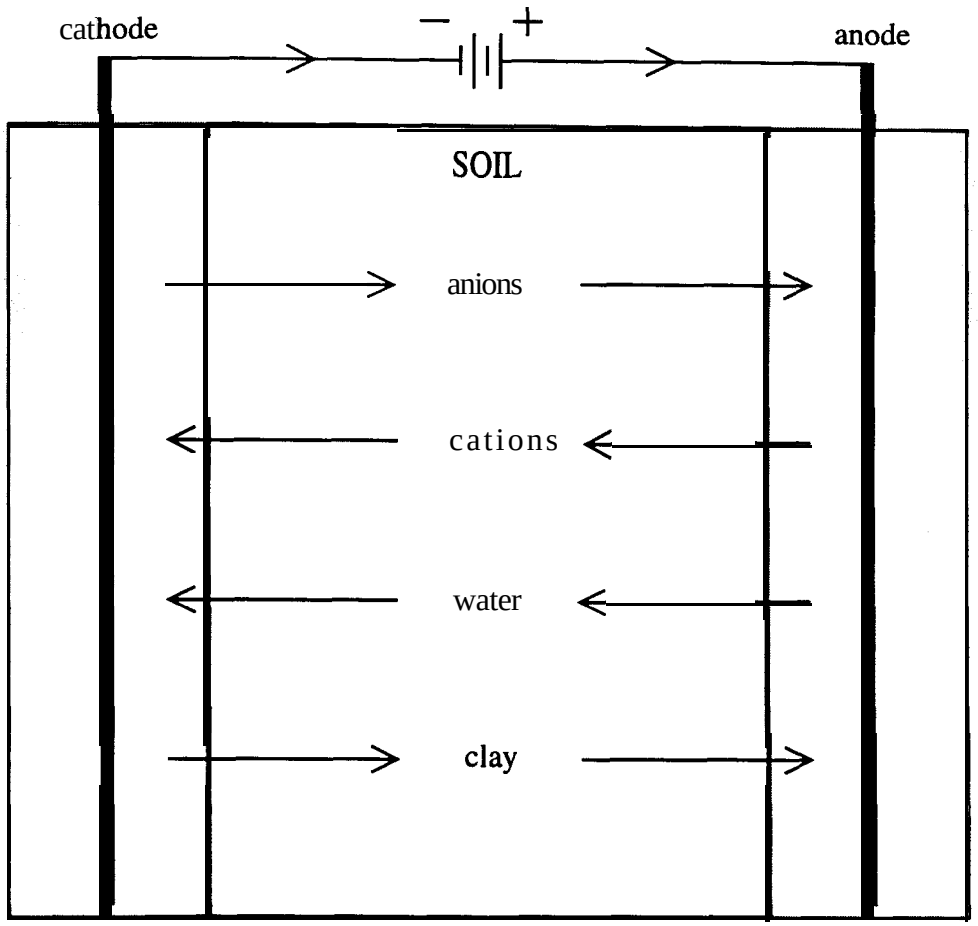

Figure 1 Movements and electric currents in an electrokinesis cell

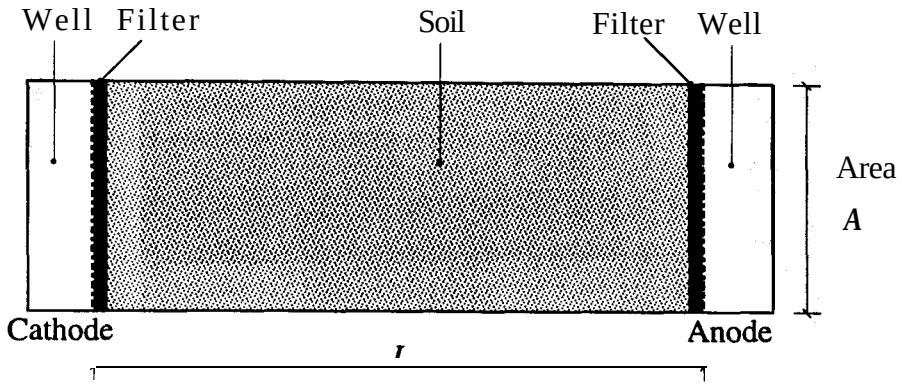

Figure 2 Basic geometry for the ELK program

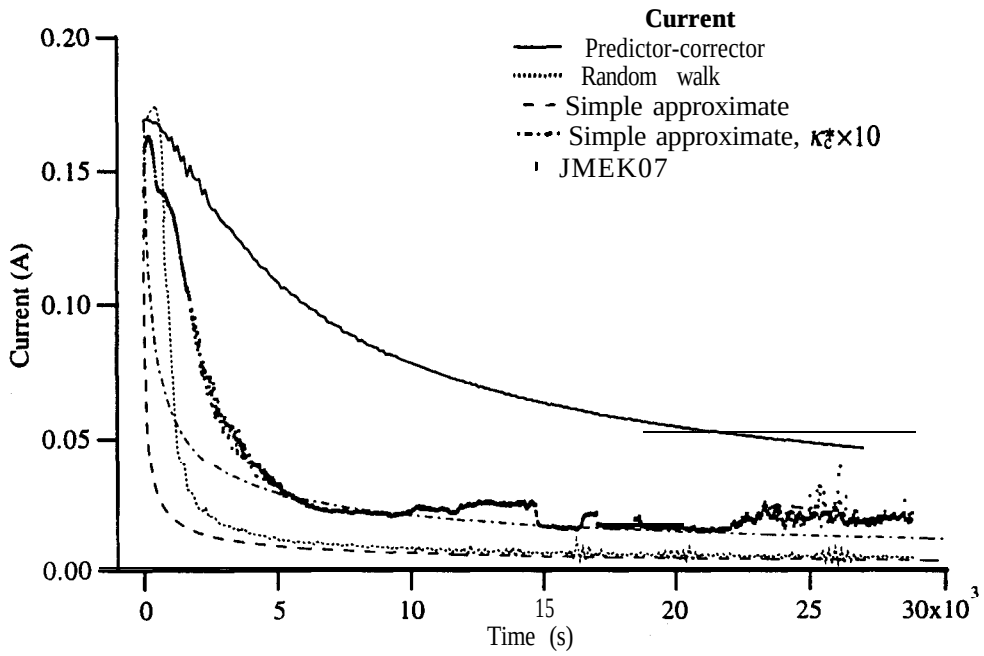

Figure 3 Variation in current with time for ELK01 and JMEK07

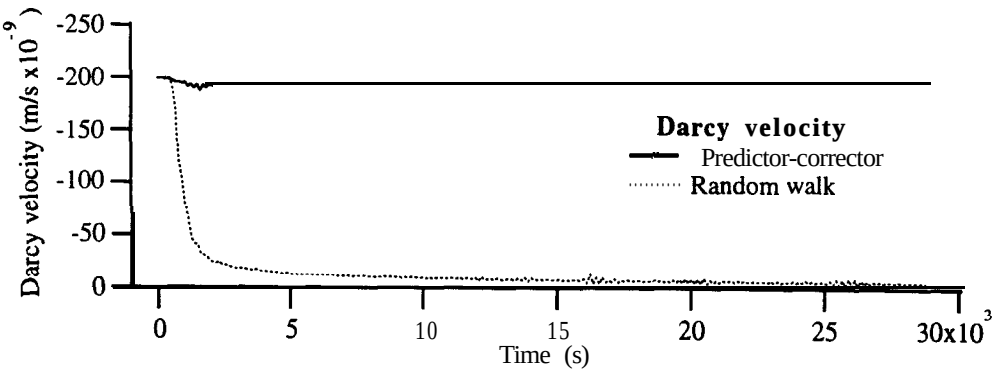

Figure 4 Variation in specific discharge with time for ELK01

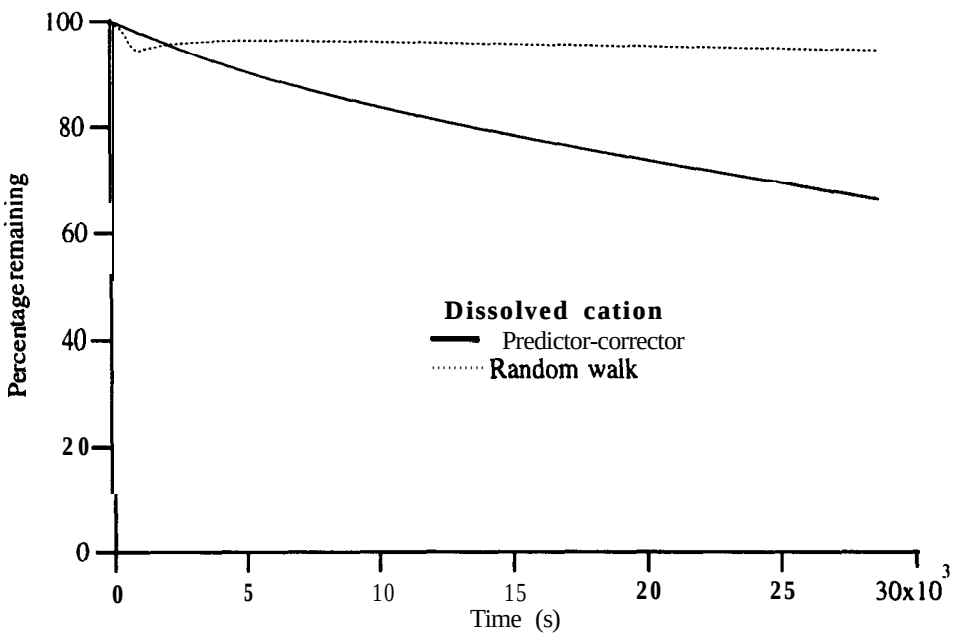

Figure 5 Variation in percentage dissolved copper with time for ELK01

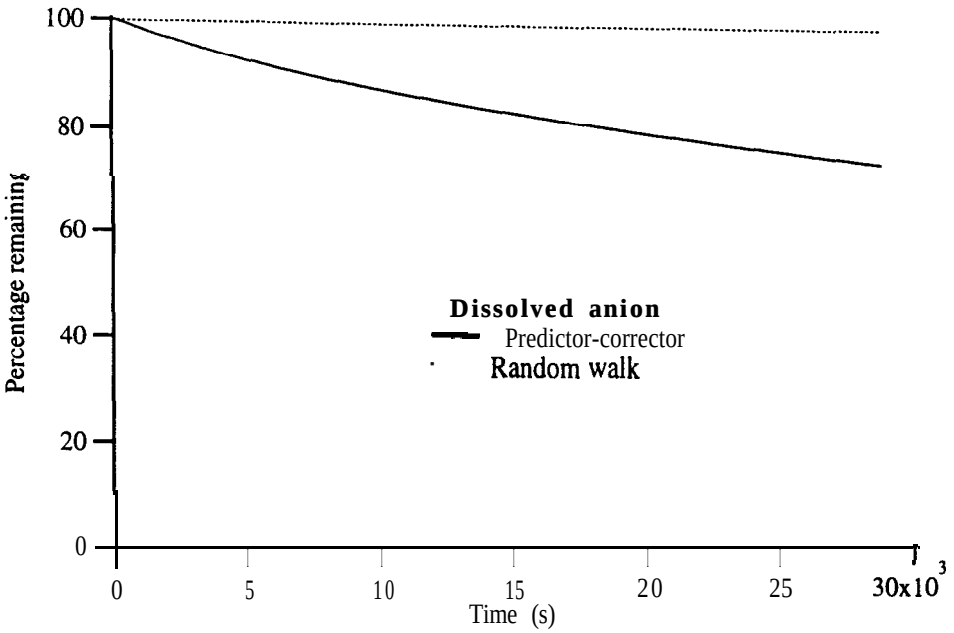

Figure 6 Variation in percentage sulphate with time for ELK01

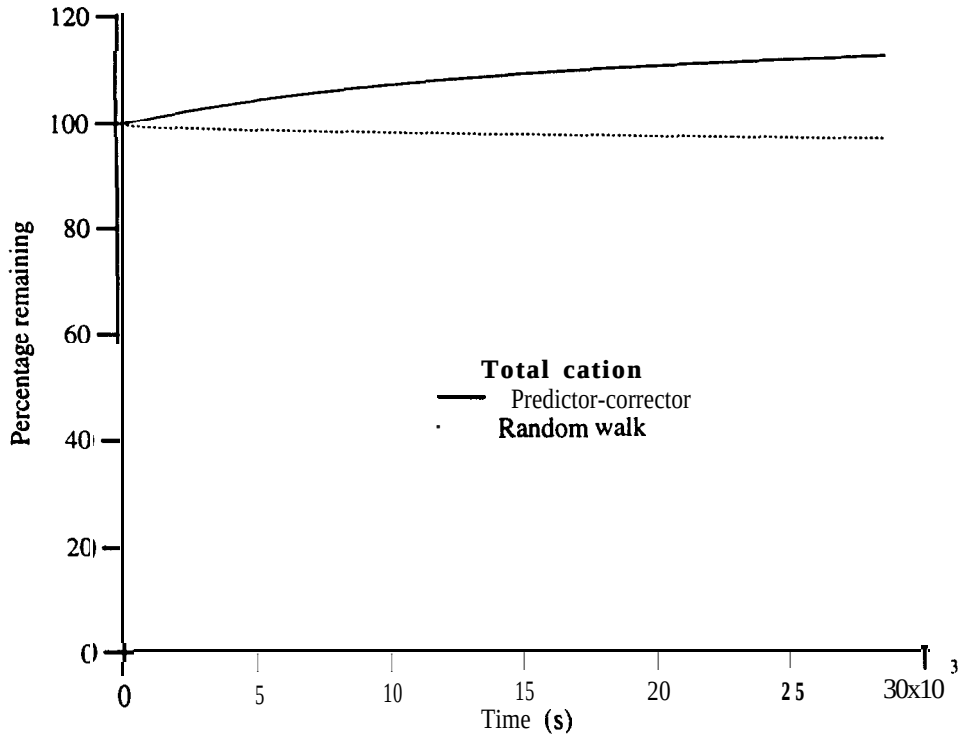

Figure 7 Variation in percentage total copper with time for ELK01

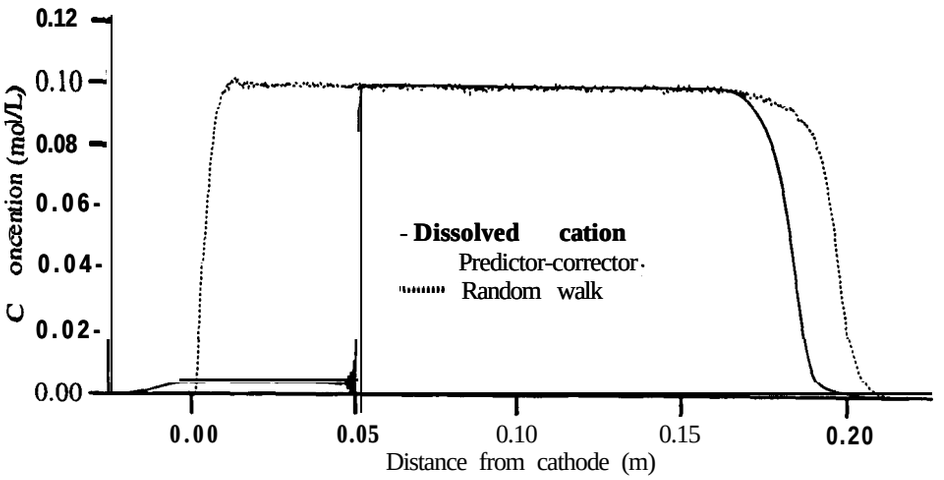

Figure 8 Final distribution of dissolved copper for ELK01

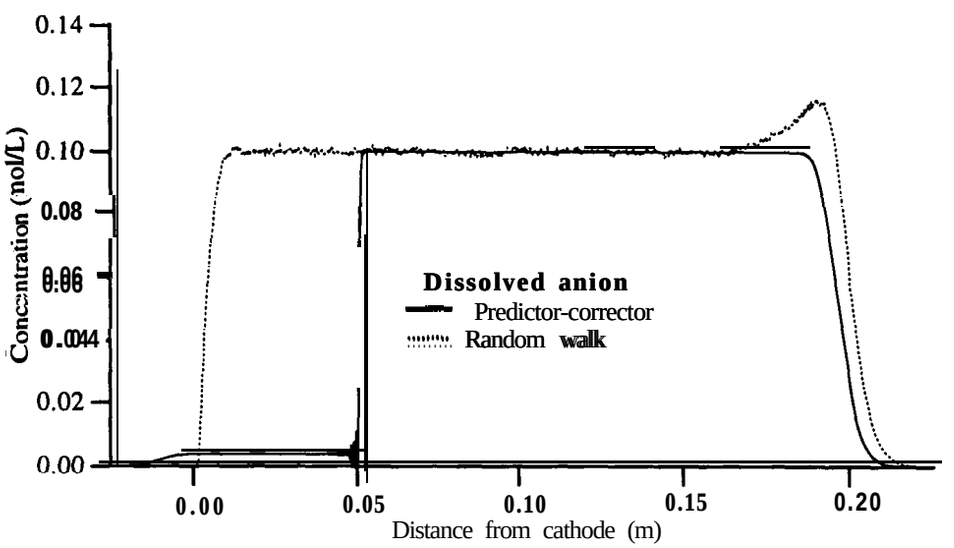

Figure 9 Final distribution of sulphate for ELK01

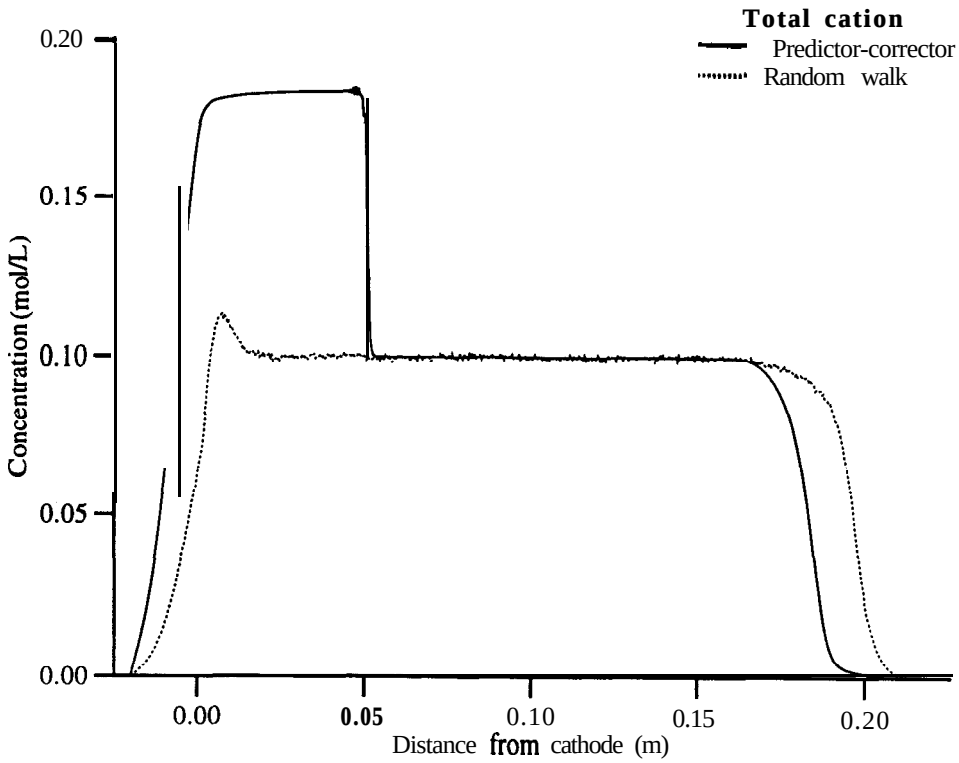

Figure 10 Final distribution of total copper for ELK01

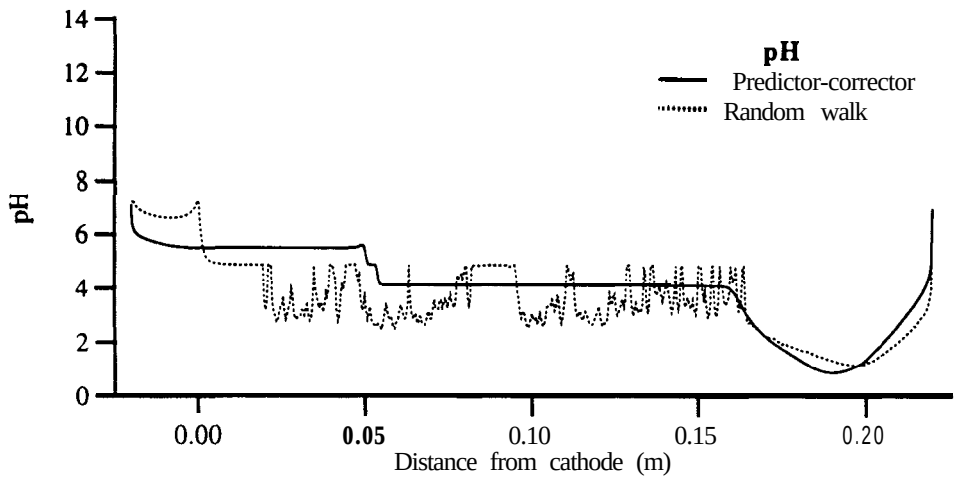

Figure 11 Final distribution of pH for ELK01

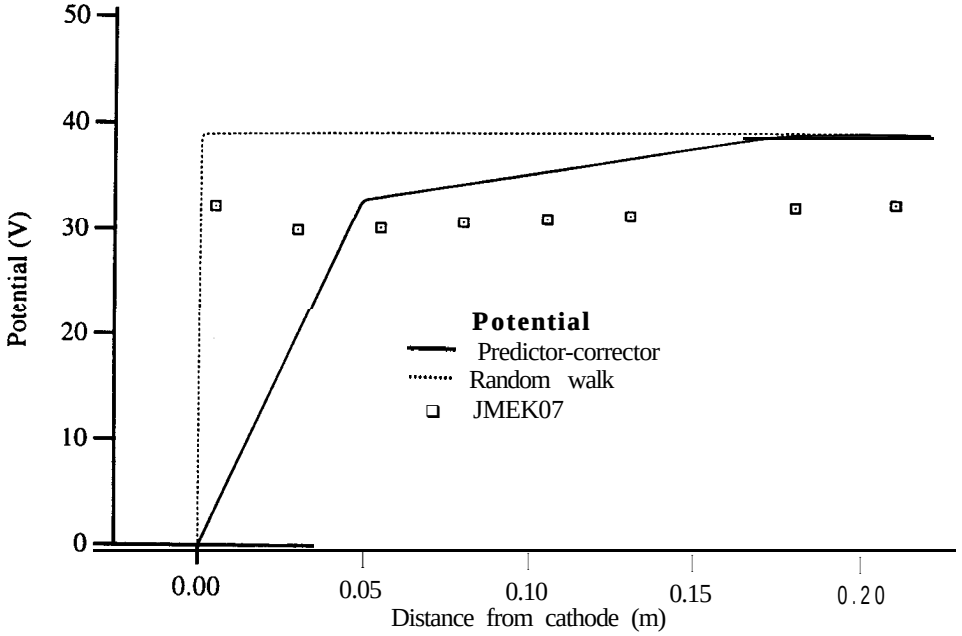

Figure 12 Final distribution of voltage for ELK01 and JMEK07

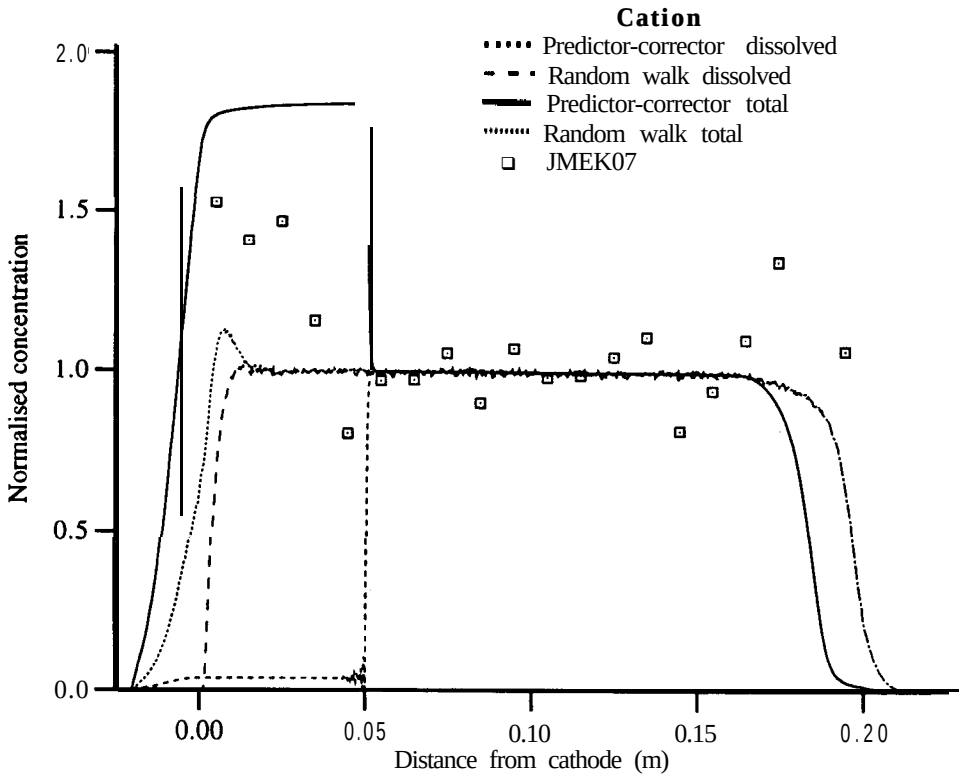

Figure 13 Final distribution of copper for ELK01 and JMEK07

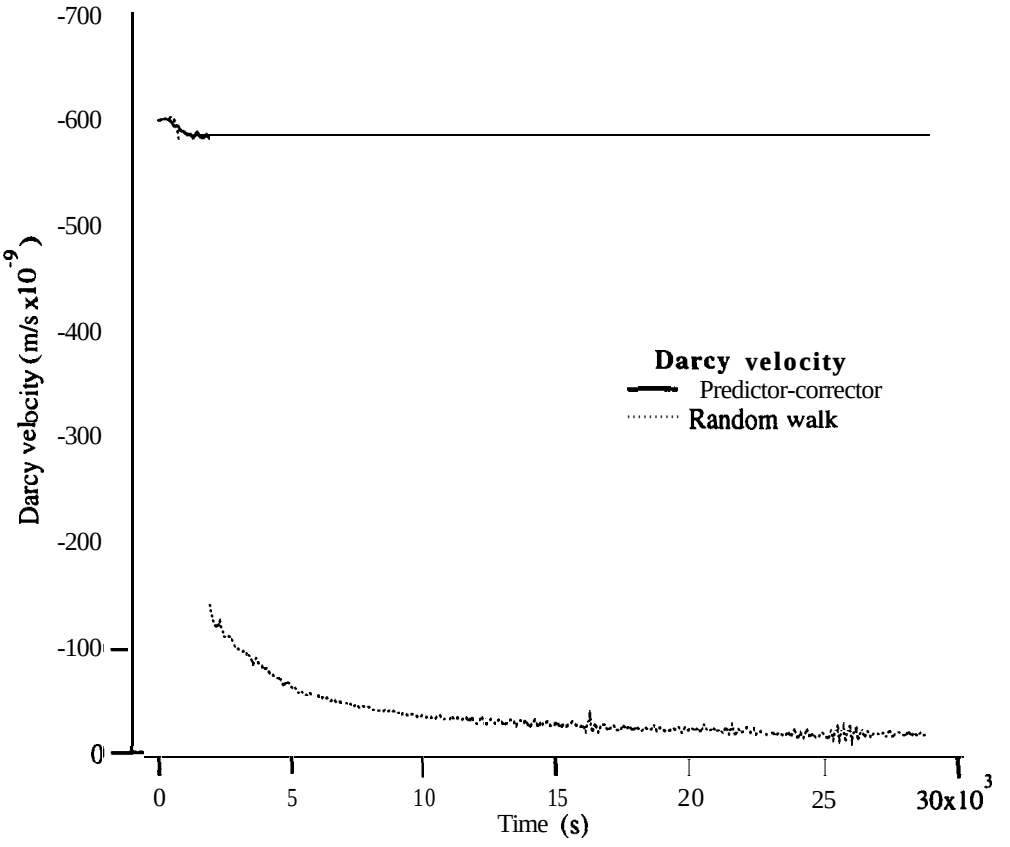

Figure 14 Variation in specific discharge with time for ELK02

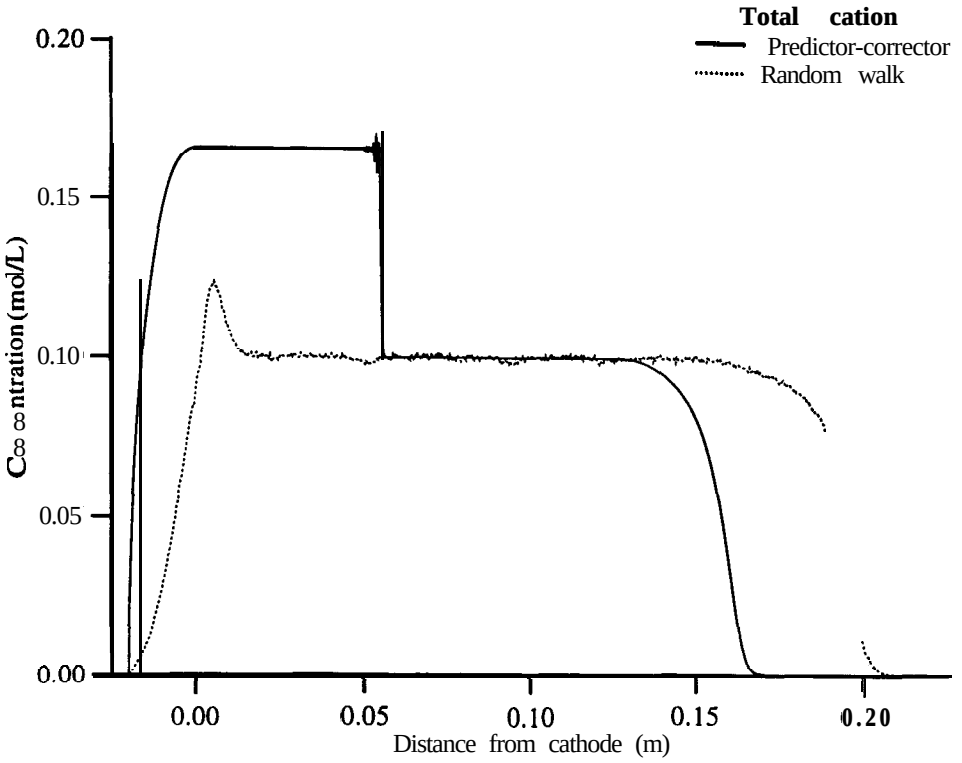

Figure 15 Final distribution of total copper for ELK02

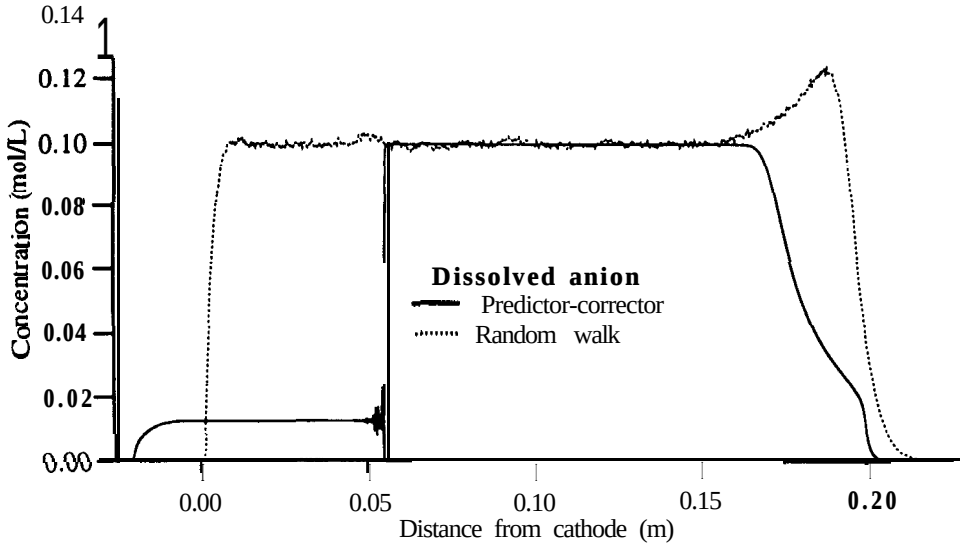

Figure 16 Final distribution of sulphate for ELK02

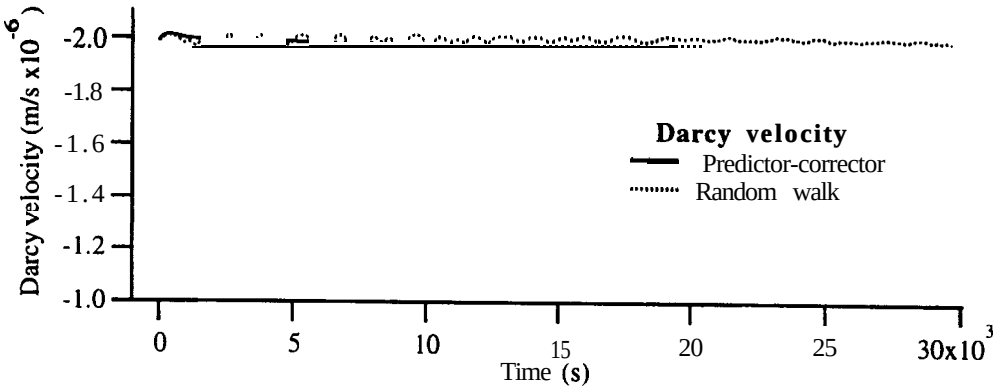

Figure 17 Variation in specific discharge with time for ELK03

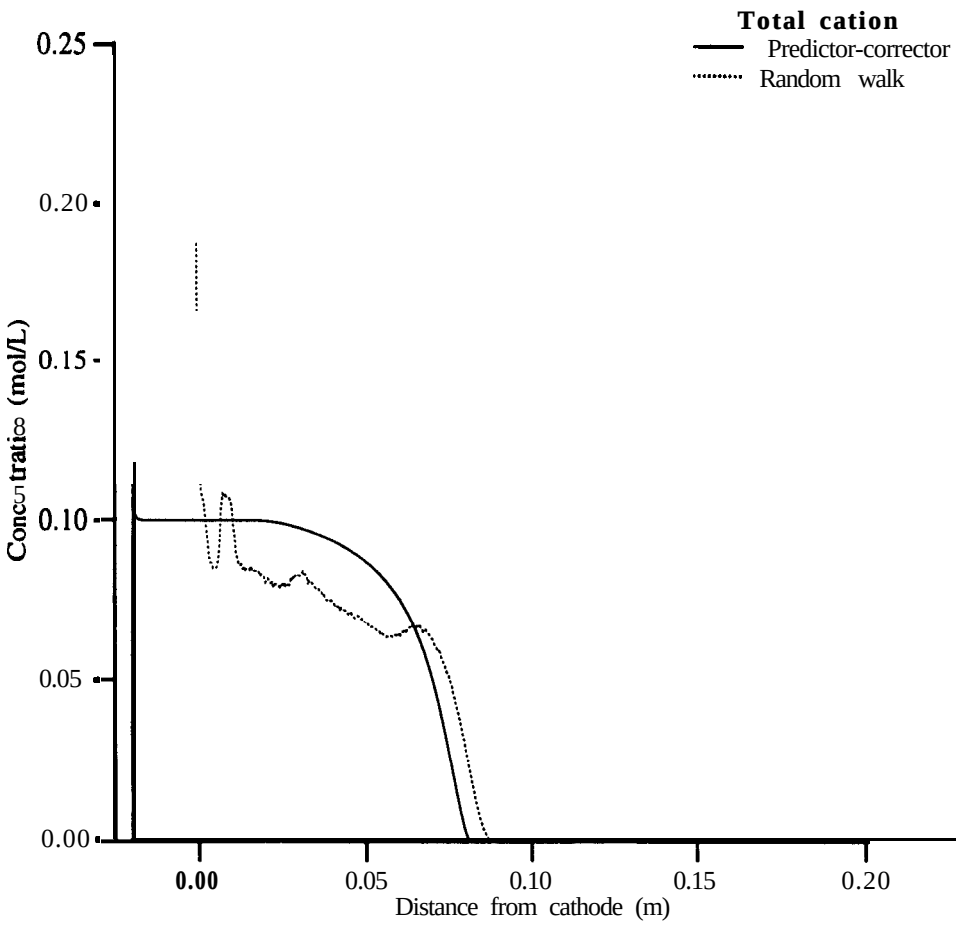

Figure 18 Final distribution of total copper for ELK03

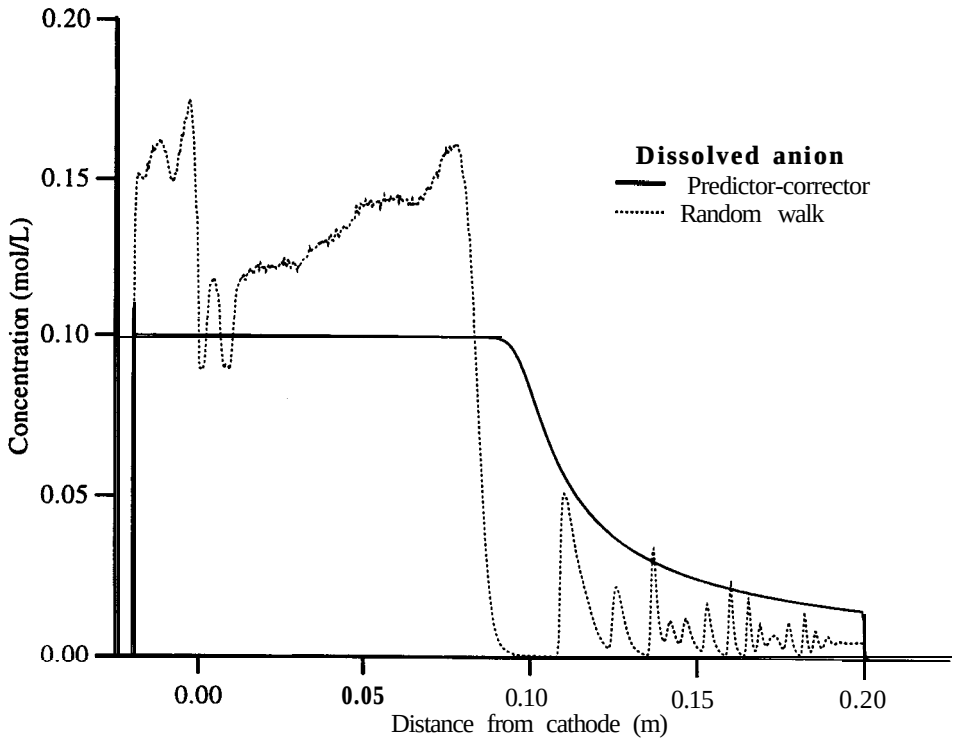

Figure 19 Final distribution of sulphate for ELK03

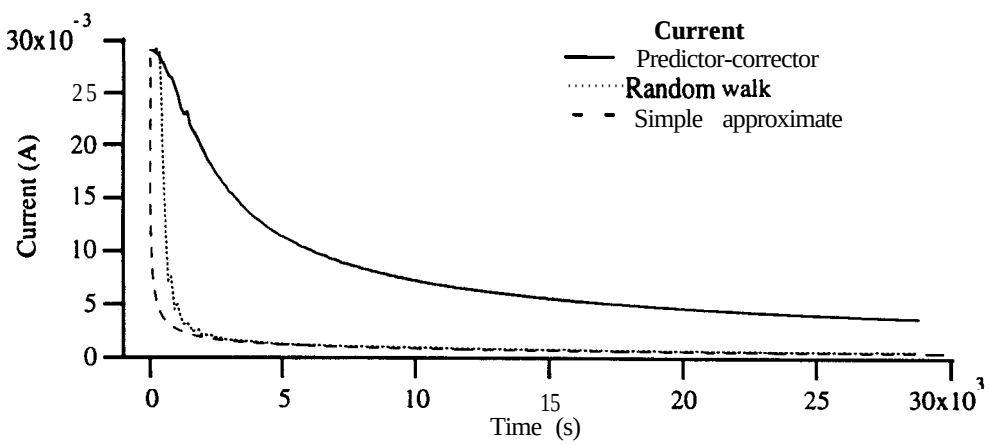

Figure 20 Variation in current with time for ELK04

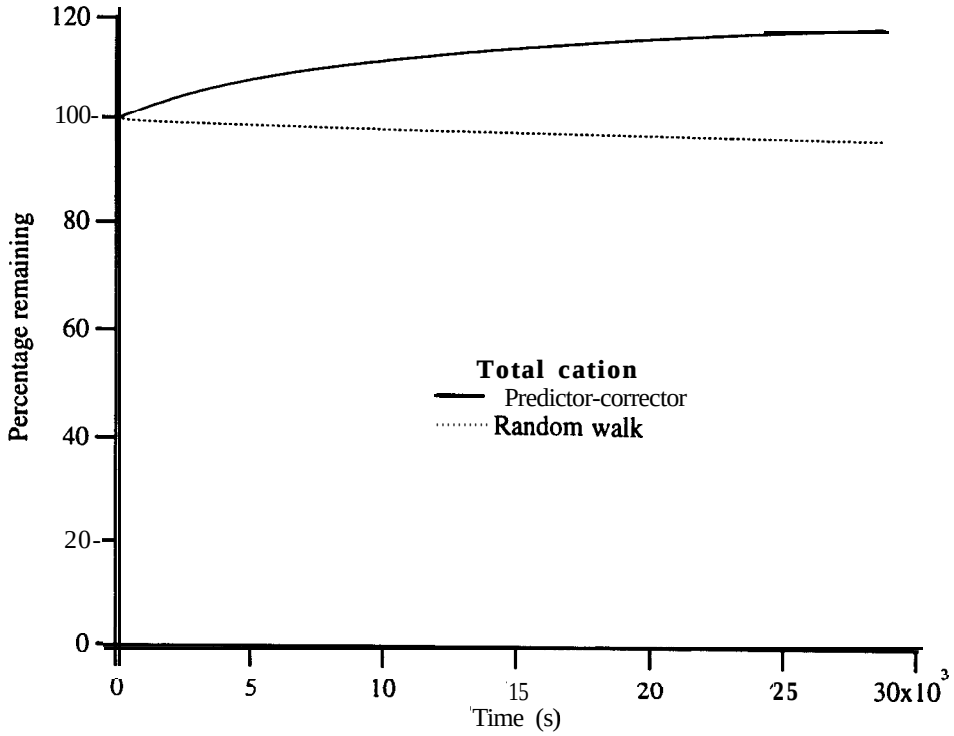

Figure 21 Variation in percentage total copper with time for ELK04

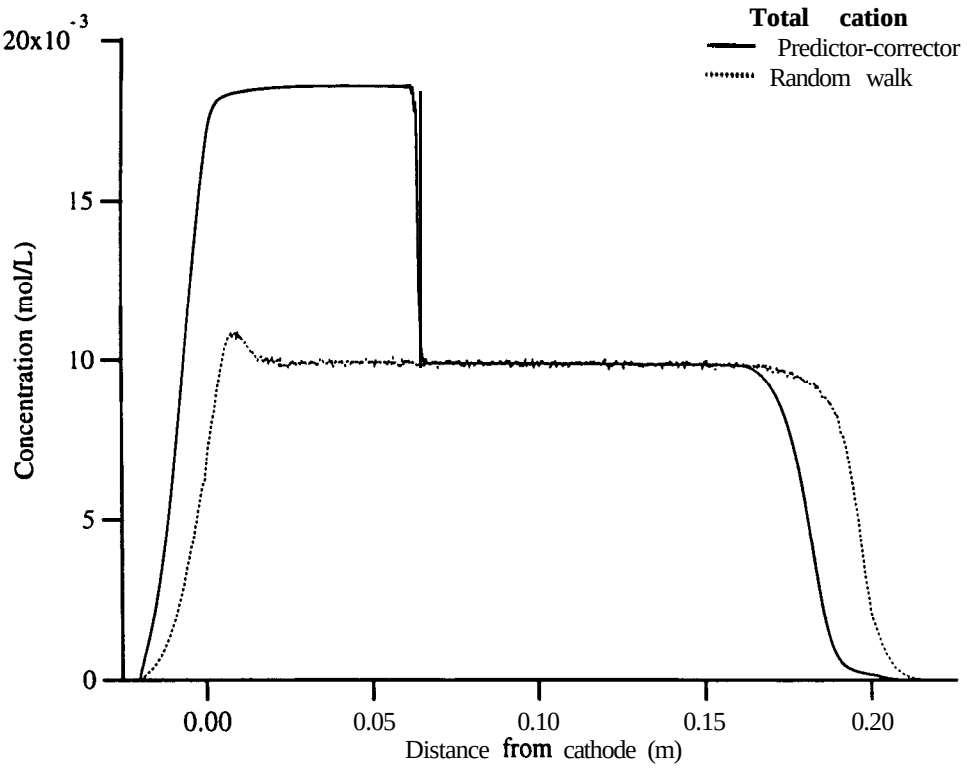

Figure 22 Final distribution of total copper for ELK04

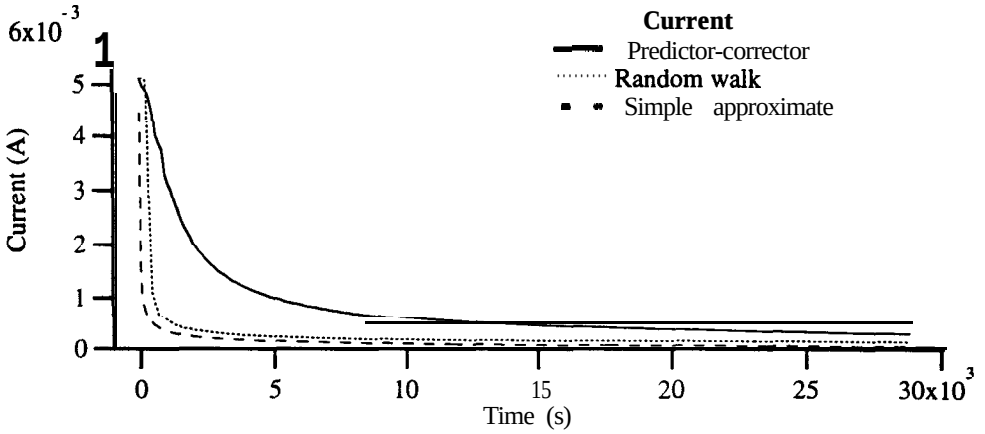

Figure 23 Variation in current with time for ELK05

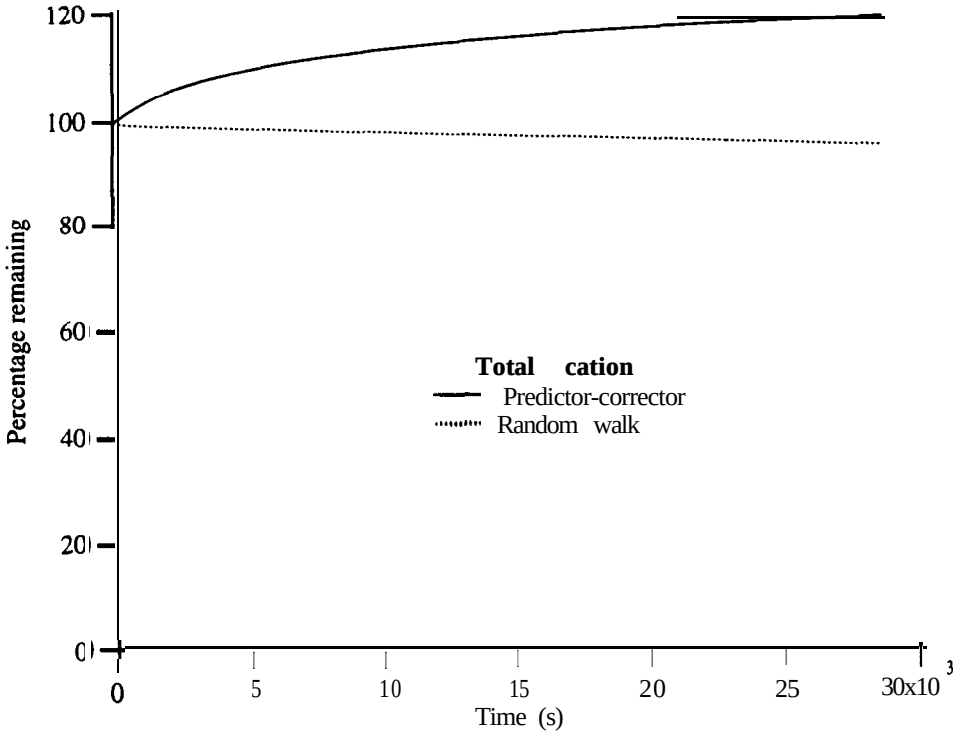

Figure 24 Variation in percentage total copper with time for ELK05

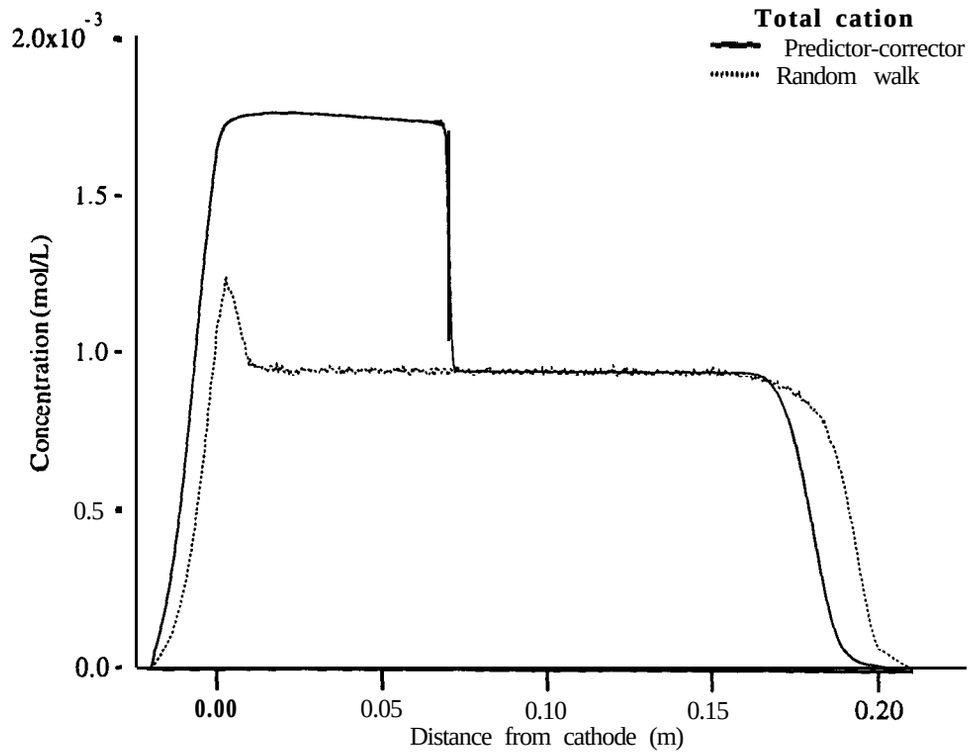

Figure 25 Final distribution of total copper for ELK05

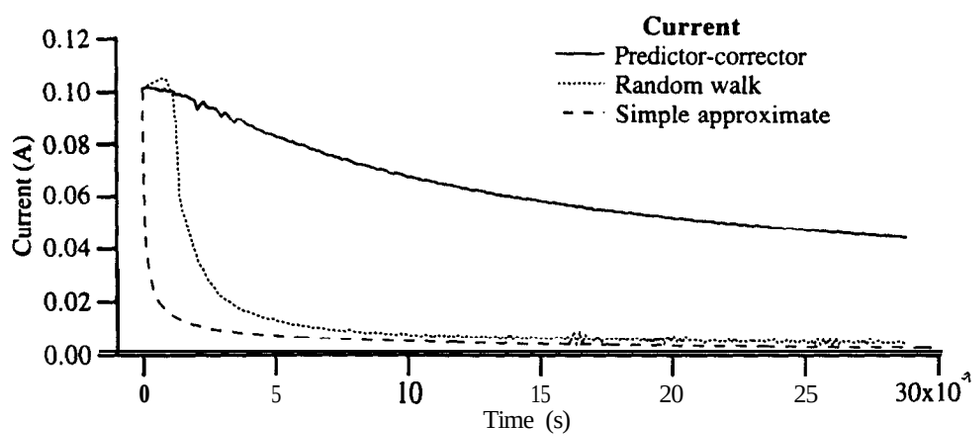

Figure 26 Variation in current with time for ELK06

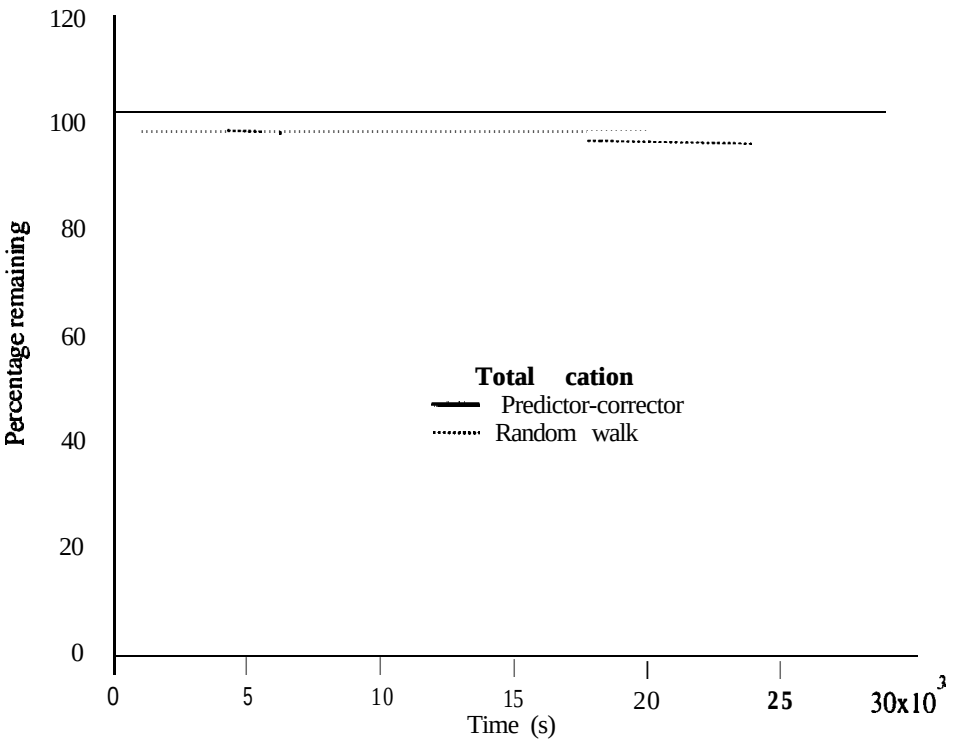

Figure 27 Variation in percentage total copper with time for ELK06

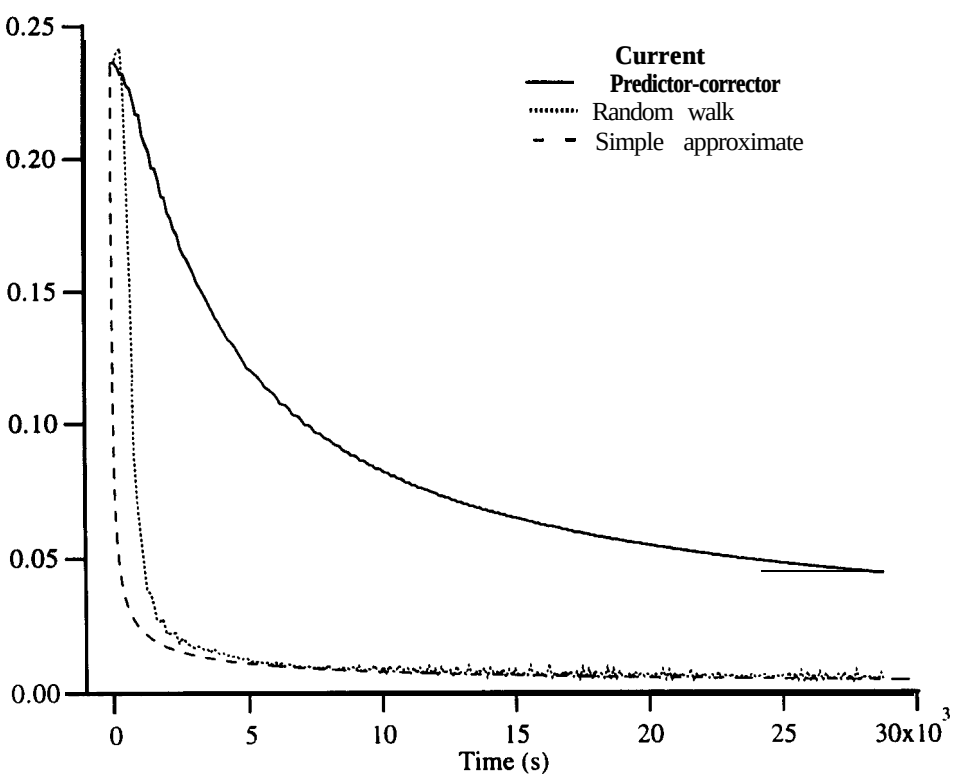

Figure 28 Variation in current with time for ELK07

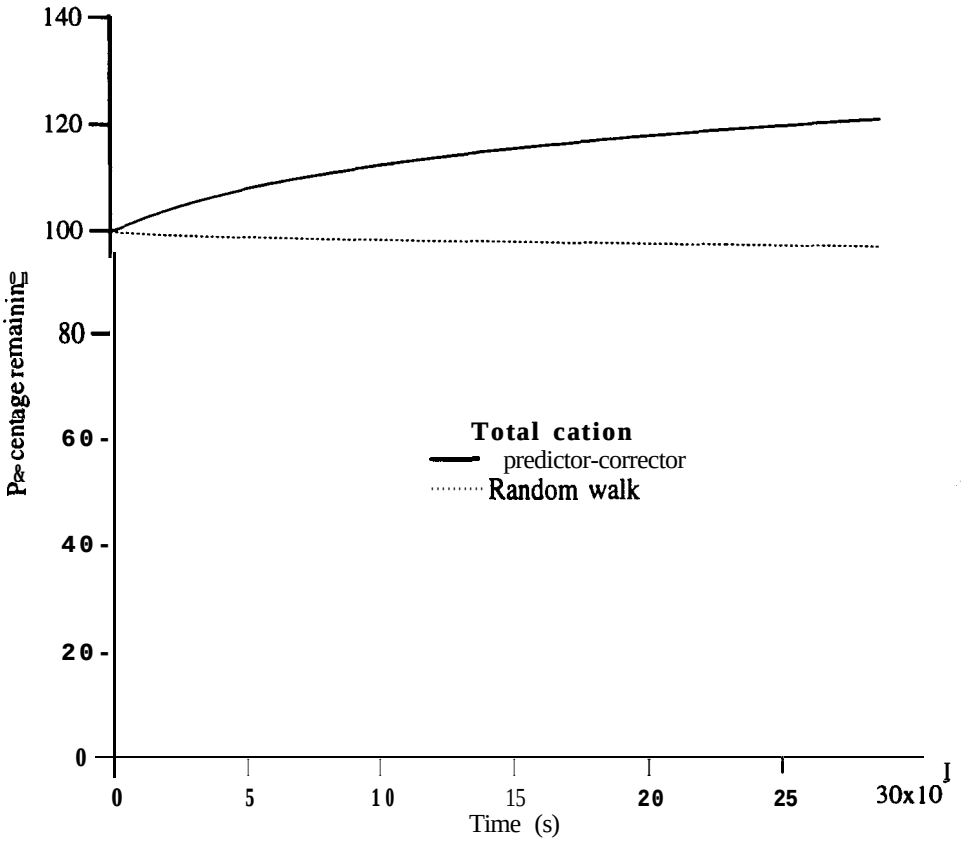

Figure 31 Variation in percentage total copper with time for ELK08

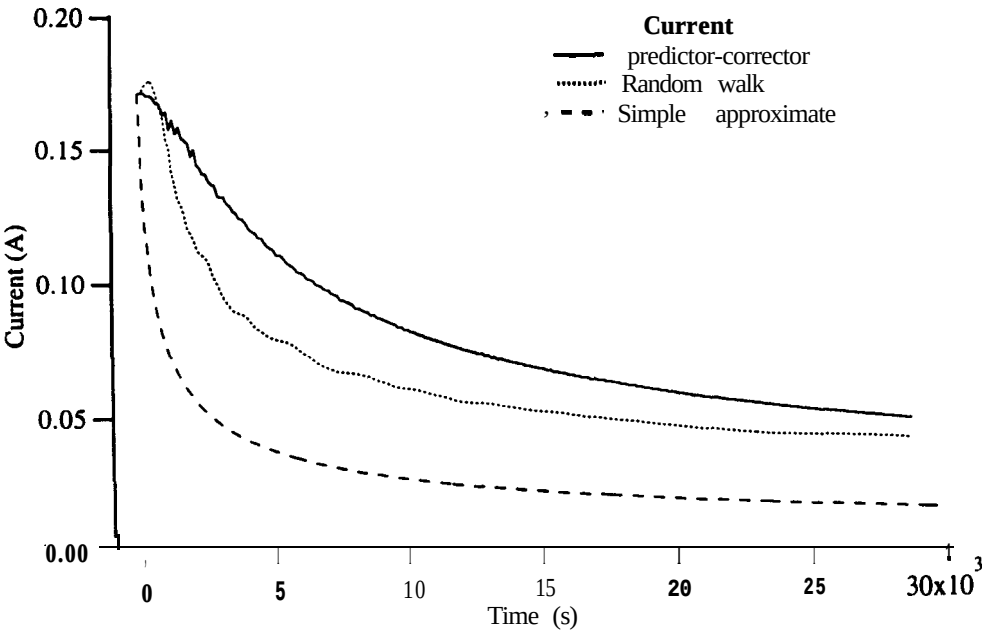

Figure 32 Variation in current with time for ELK09

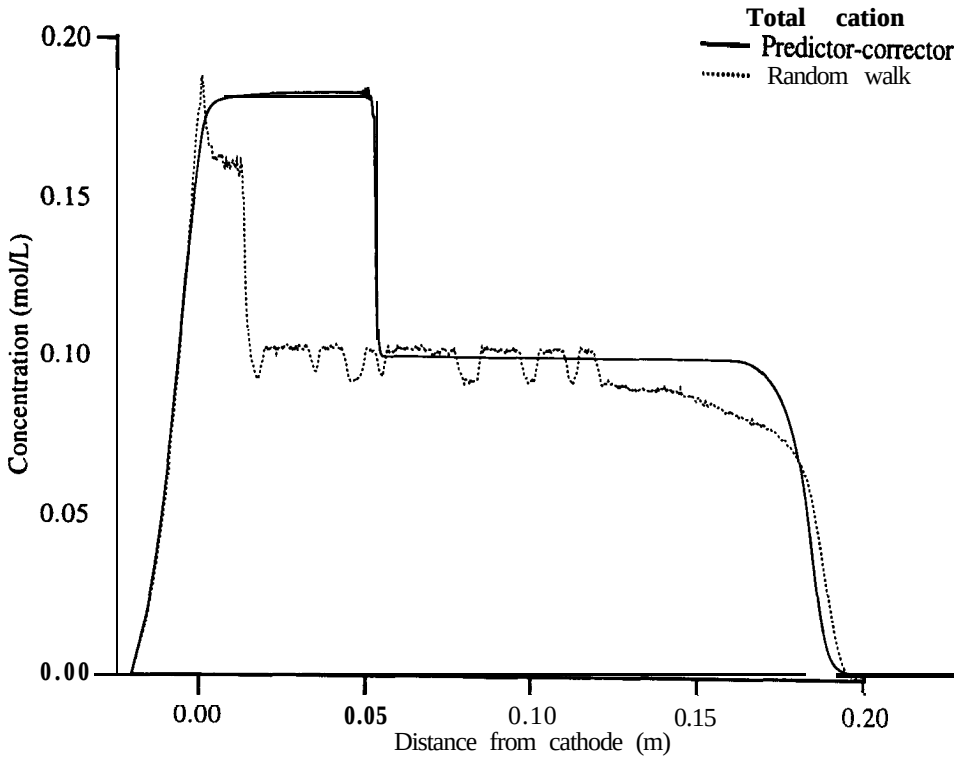

Figure 33 Final distribution of total copper for ELK09

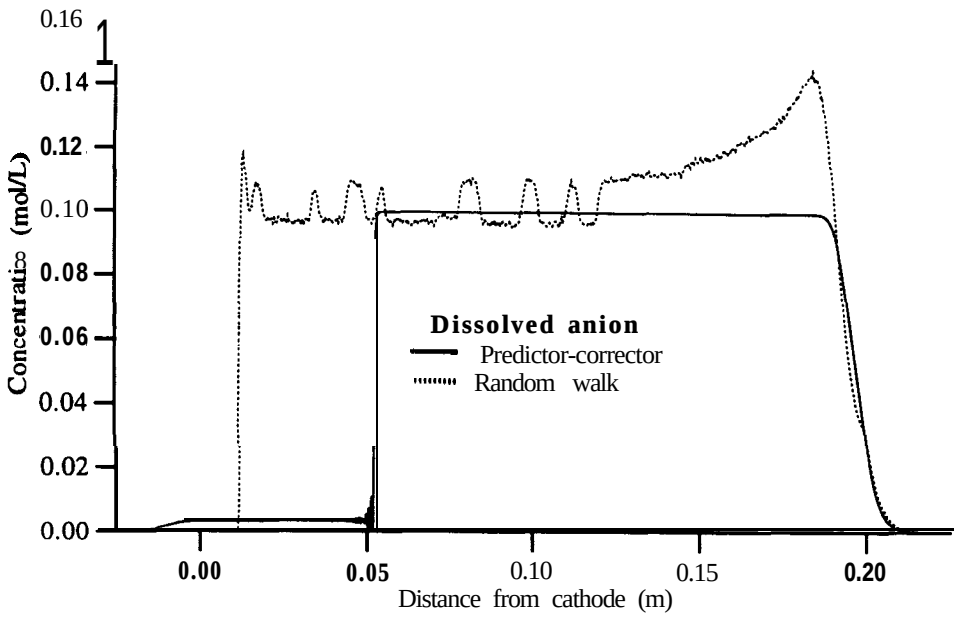

Figure 34 Final distribution of sulphate for ELK09

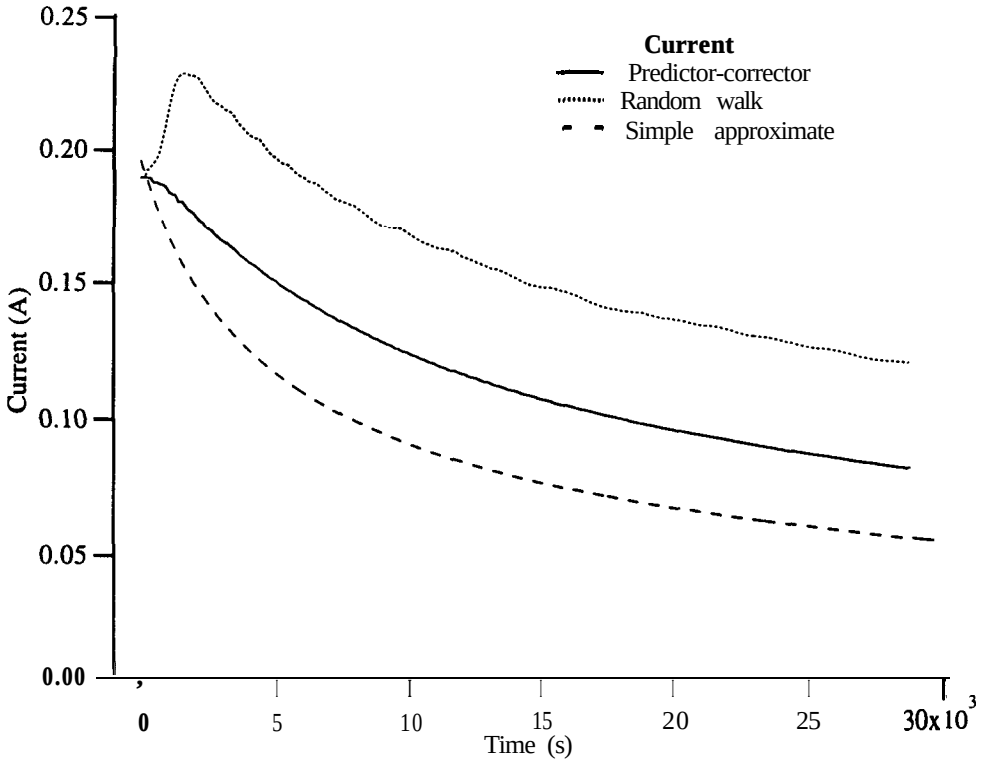

Figure 35 Variation in current with time for ELK10

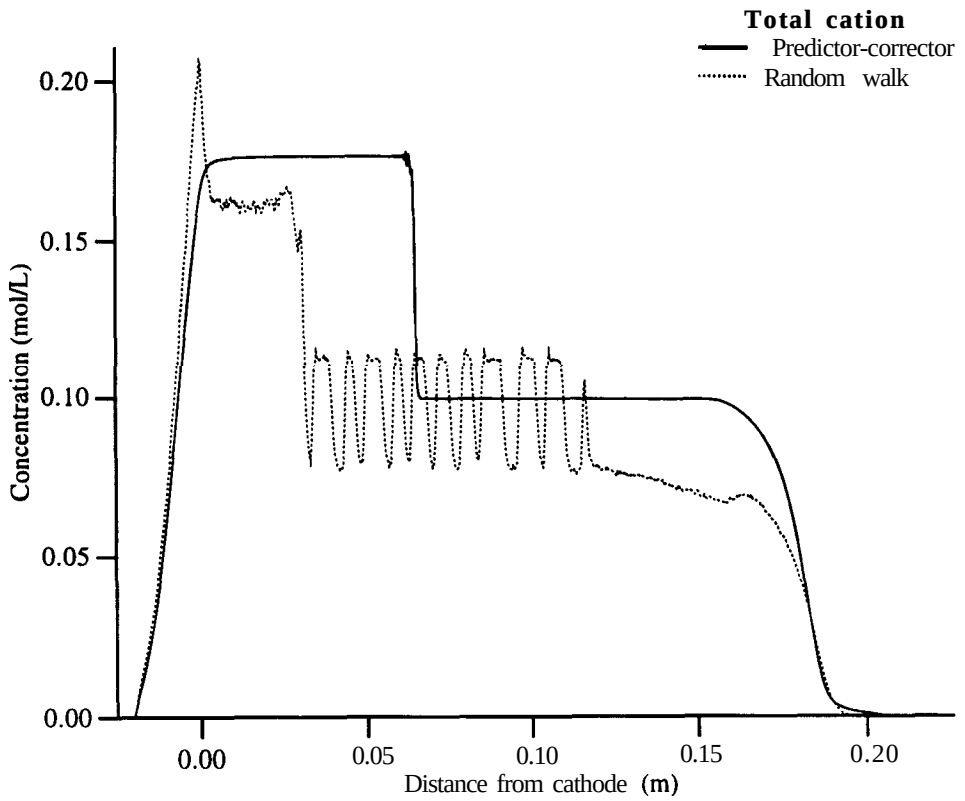

Figure 36 Final distribution of total copper for ELK10

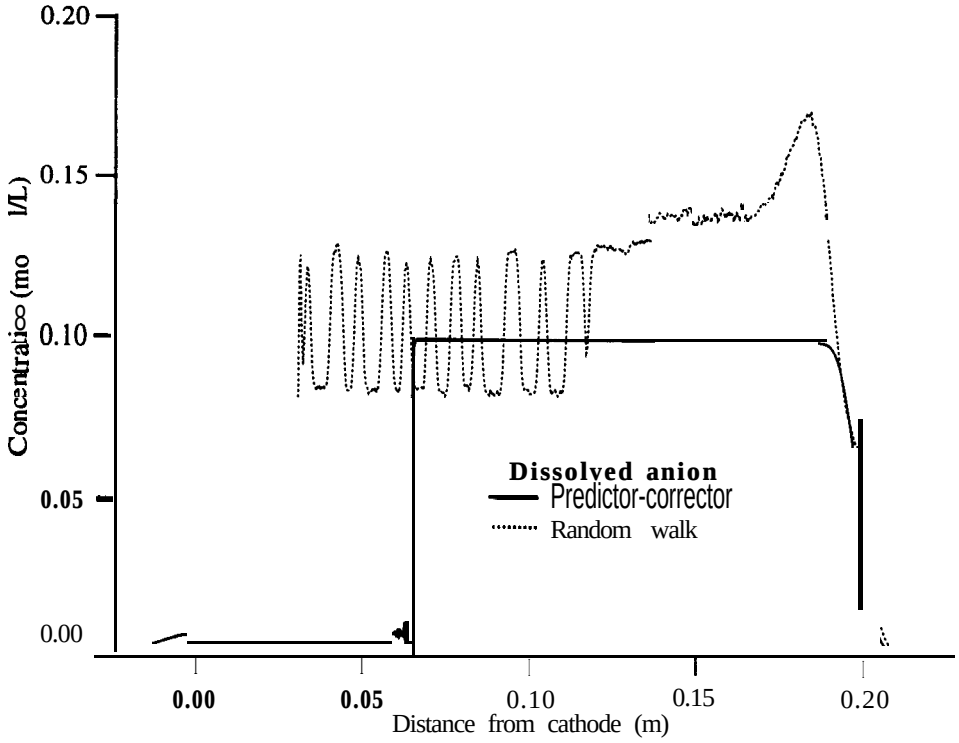

Figure 37 Final distribution of suiphate for ELK10

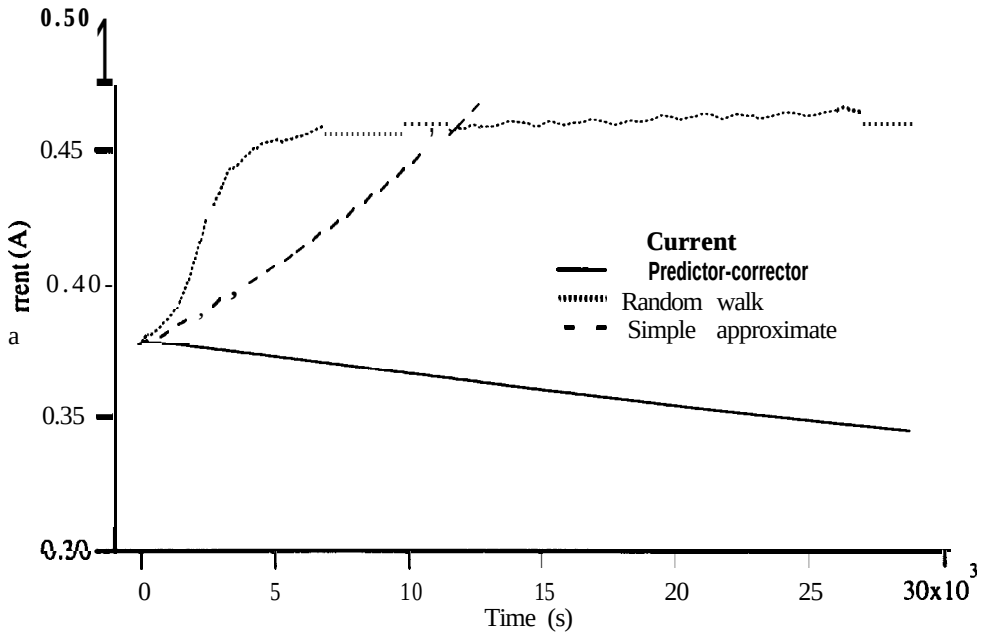

Figure 38 Variation in current with time for ELK11

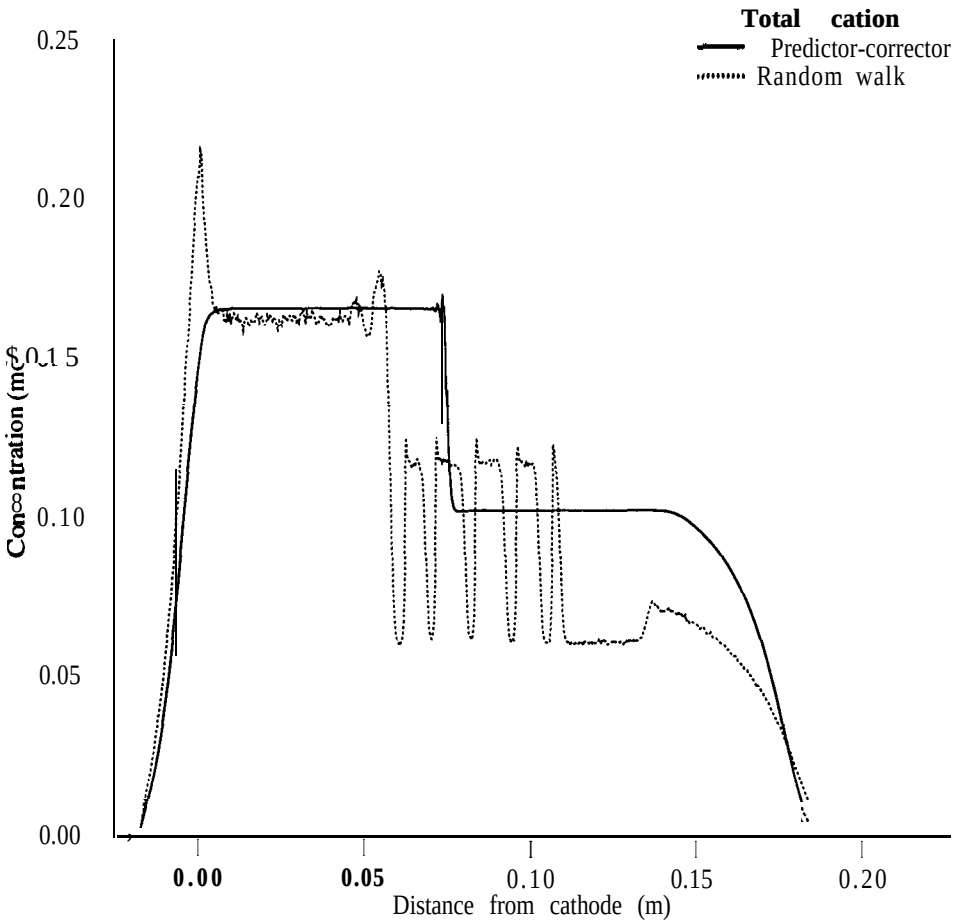

Figure 39 Final distribution of total copper for ELK11

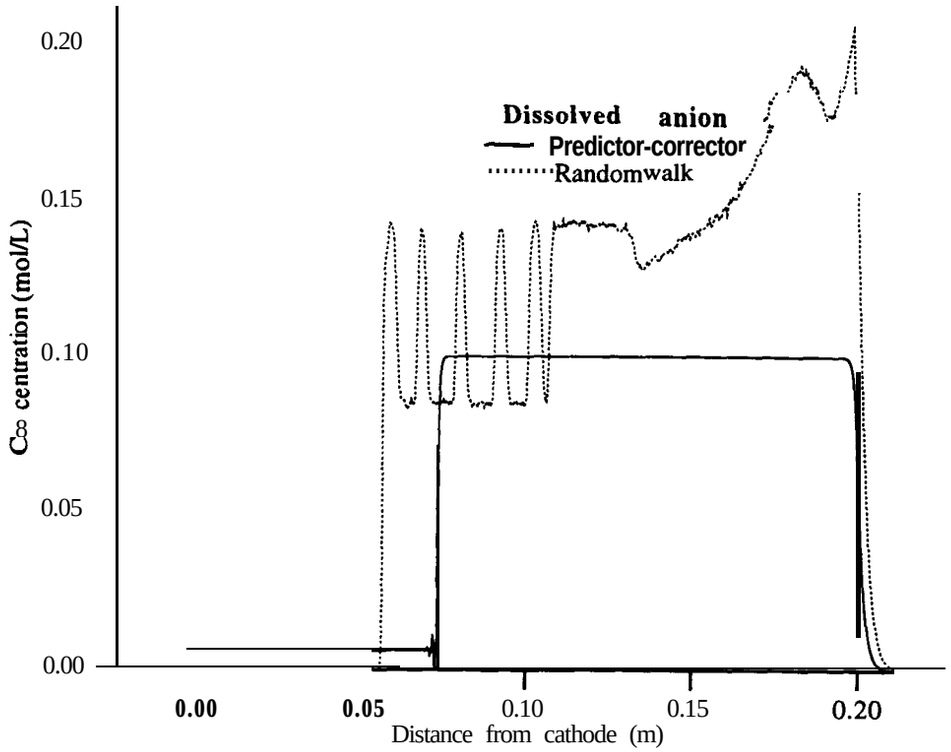

Figure 40 Final distribution of sulphate for ELK11

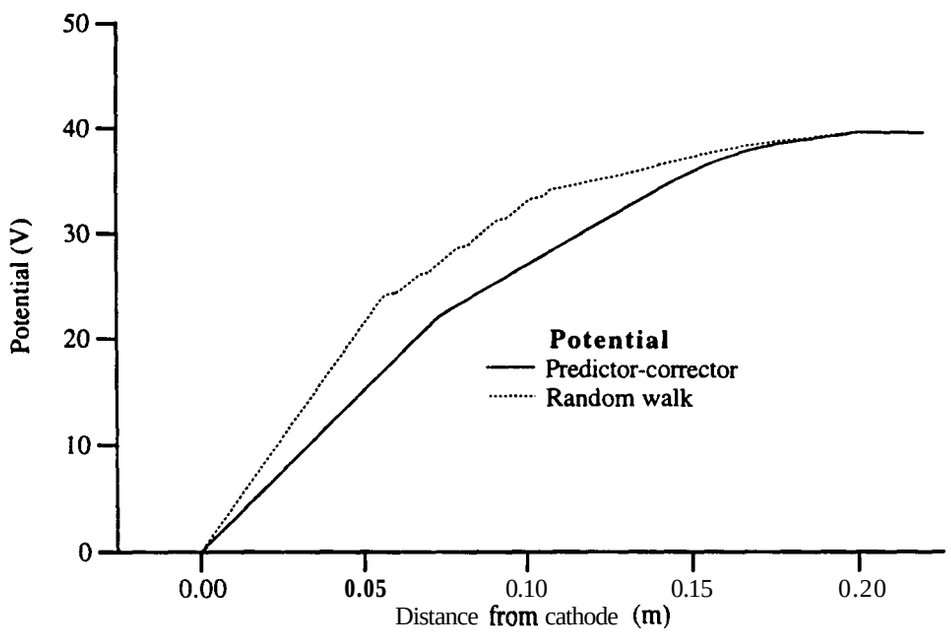

Figure 41 Final distribution of voltage for ELK11

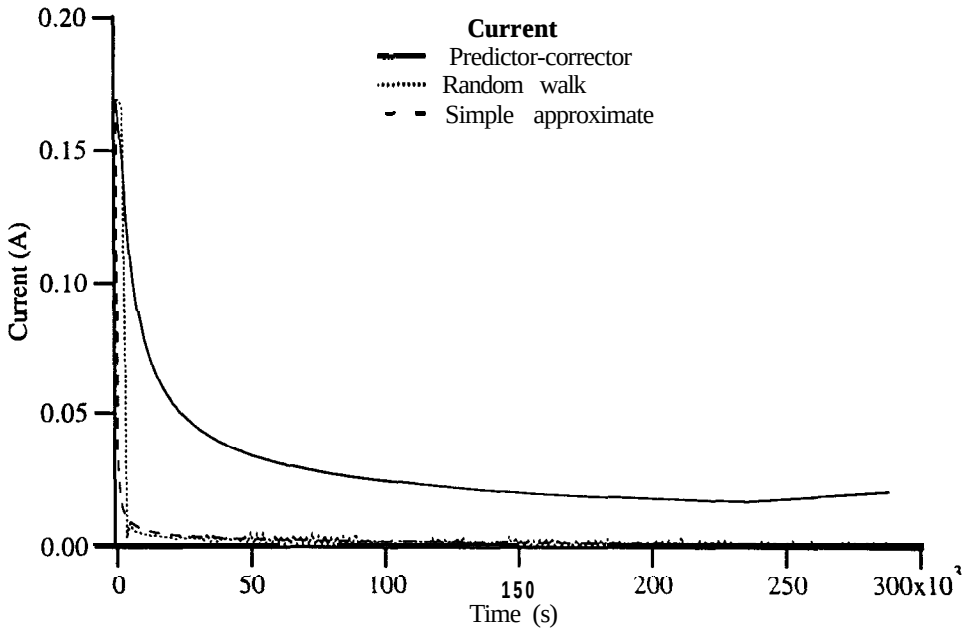

Figure 42 Variation in current with time for ELK12

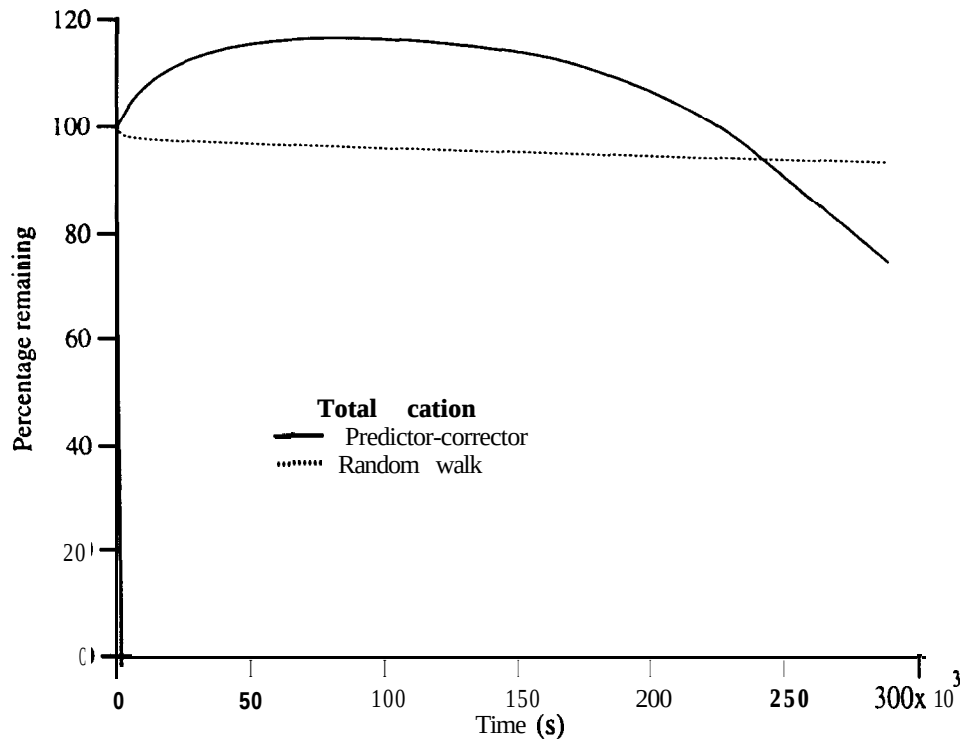

Figure 43 Variation in percentage total copper with time for ELK12

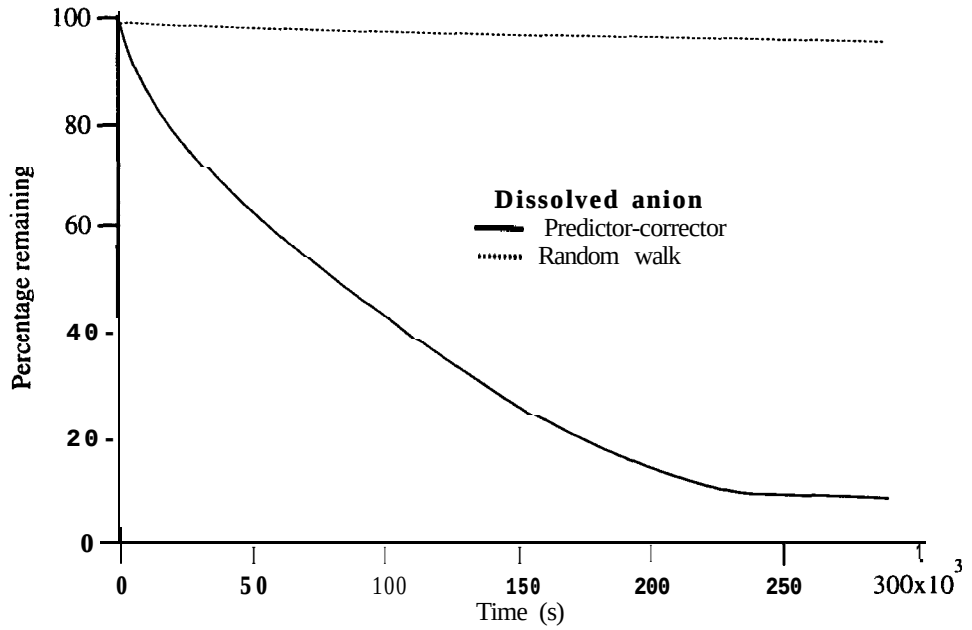

Figure 44 Variation in percentage sulphate with time for ELK12

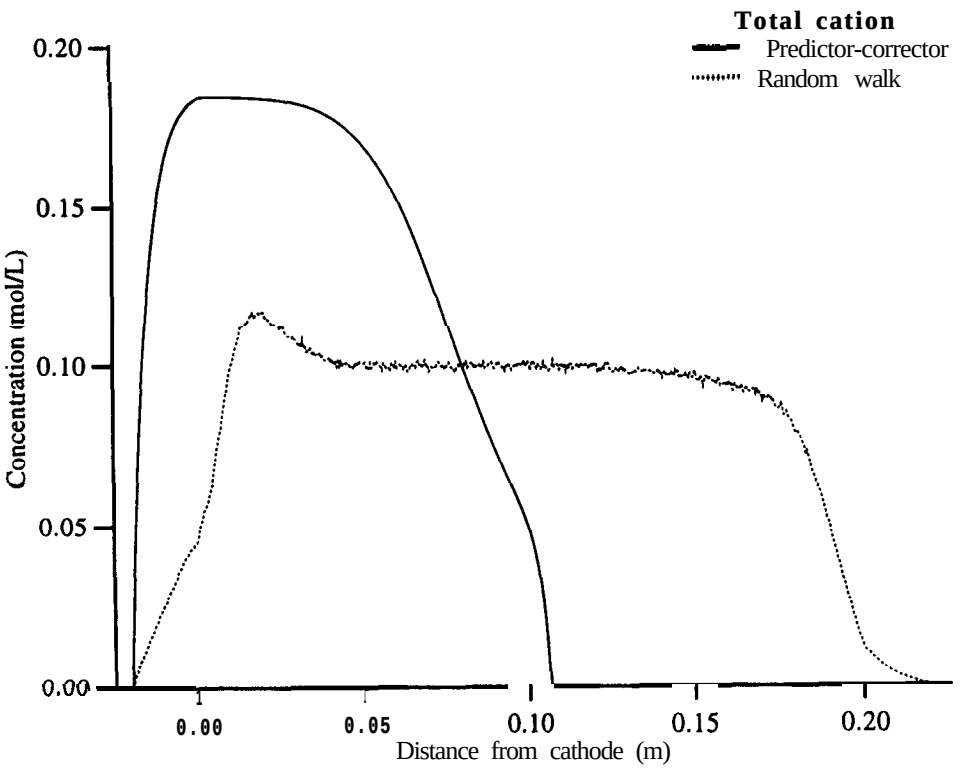

Figure 45 Final distribution of total copper for ELK12

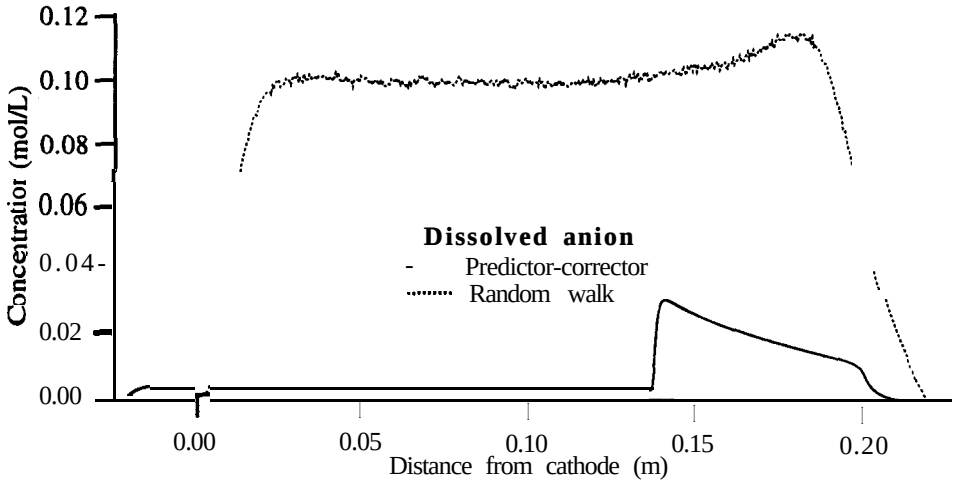

Figure 46 Final distribution of sulphate for ELK12

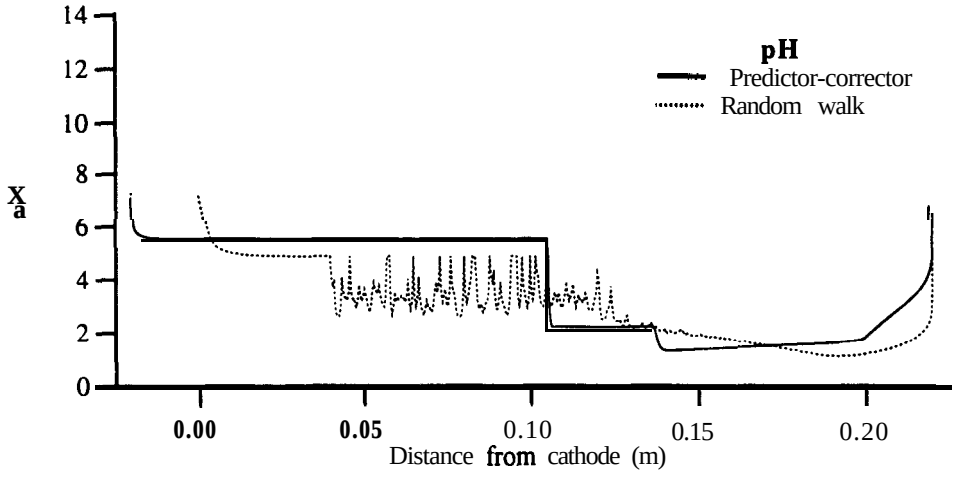

Figure 47 Final distribution of pH for ELK12

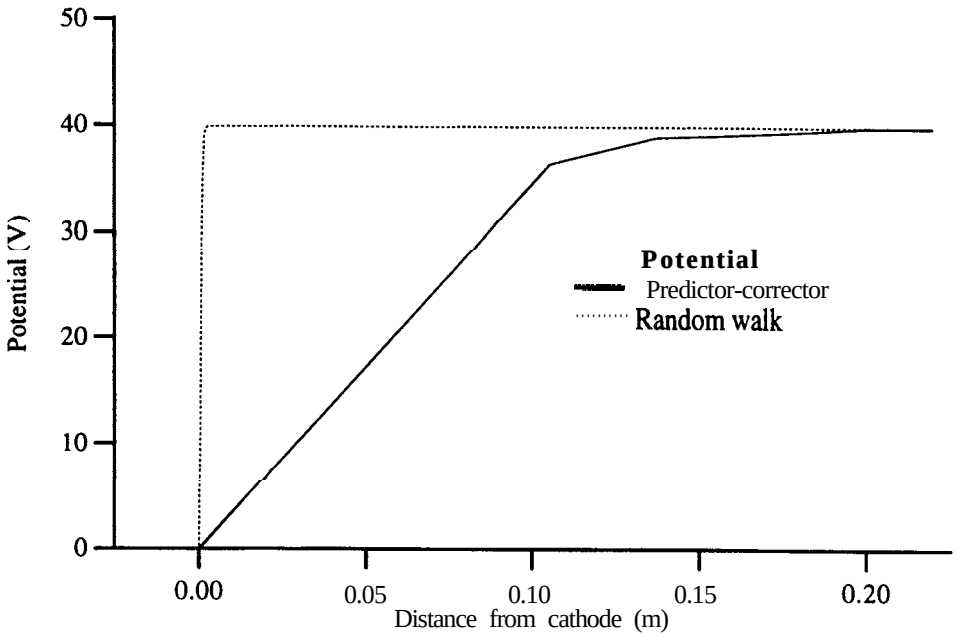

Figure 48 Final distribution of voltage for ELK12

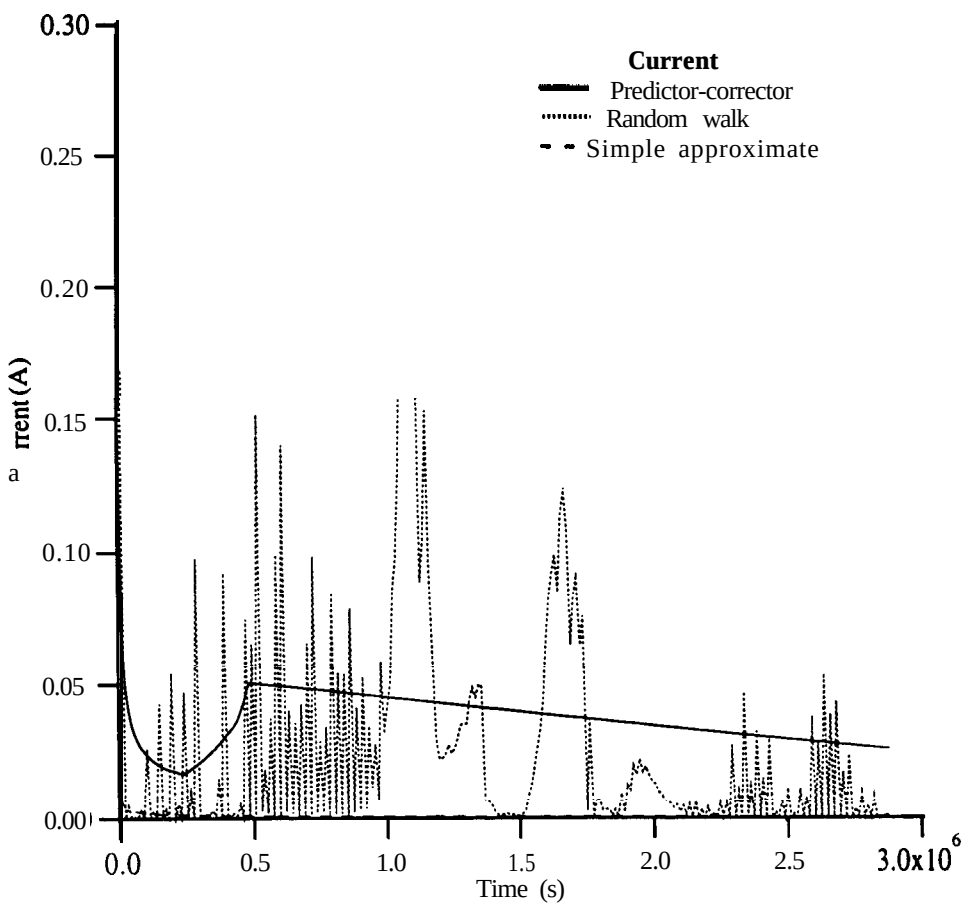

Figure 49 Variation in current with time for ELK13

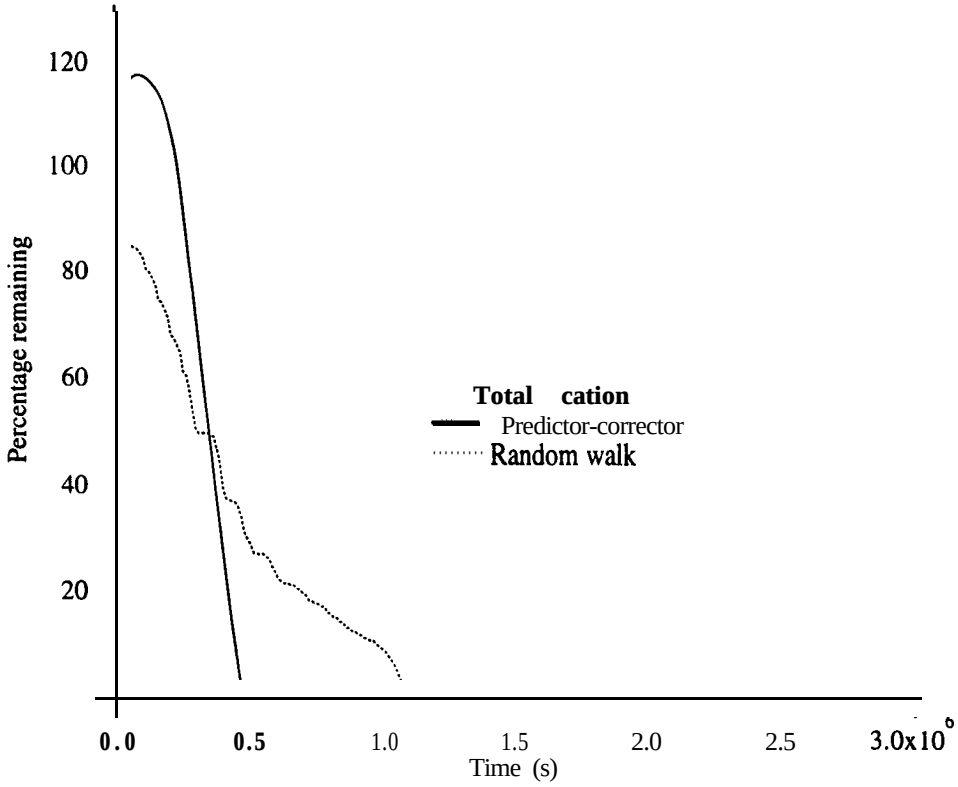

Figure 50 Variation in percentage total copper with time for ELK13

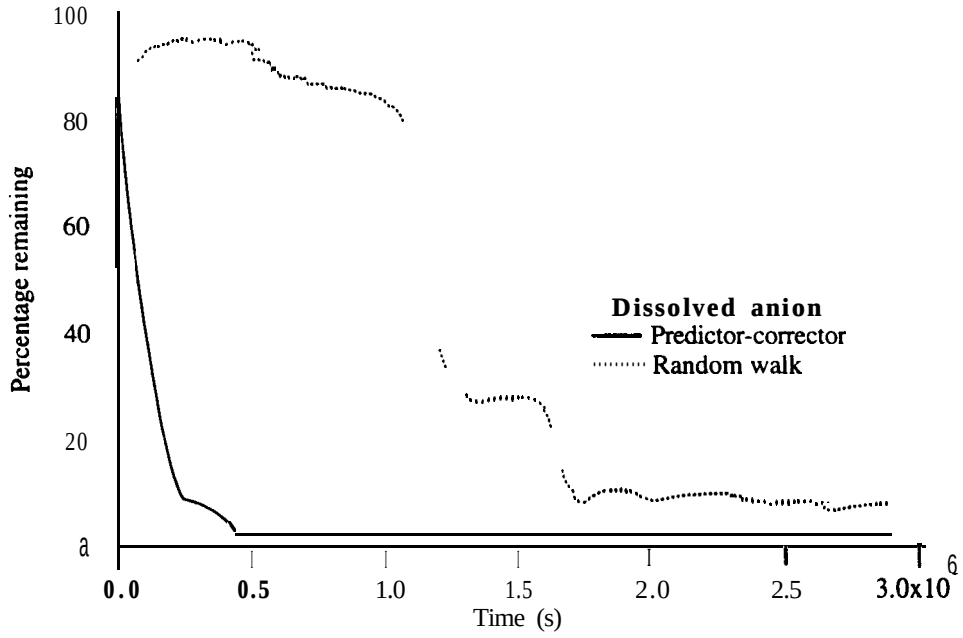

Figure 51 Variation in percentage sulphate with time for ELK13

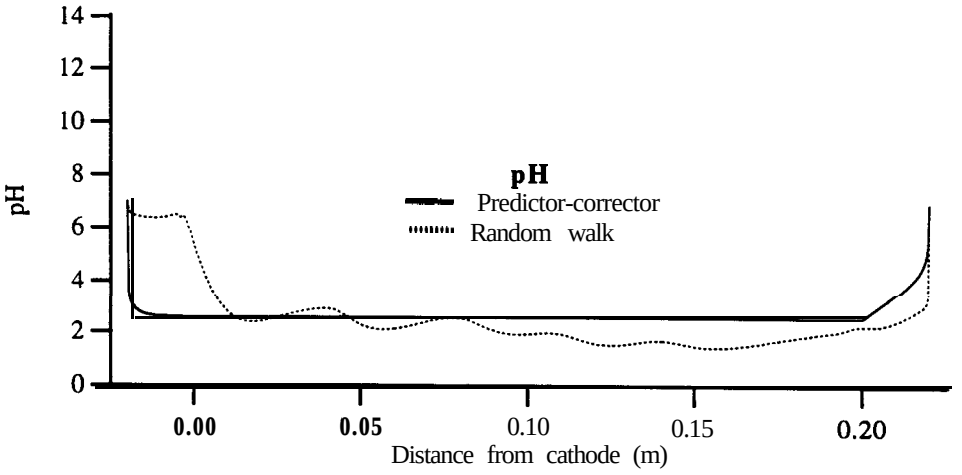

Figure 52 Final distribution of pH for ELK13

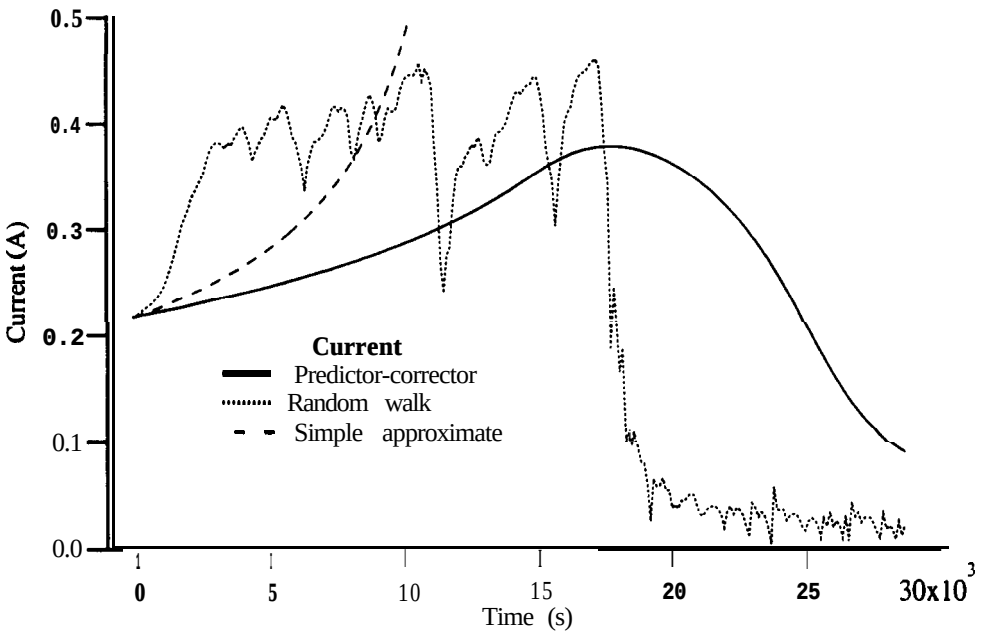

Figure 53 Variation in current with time for ELK14

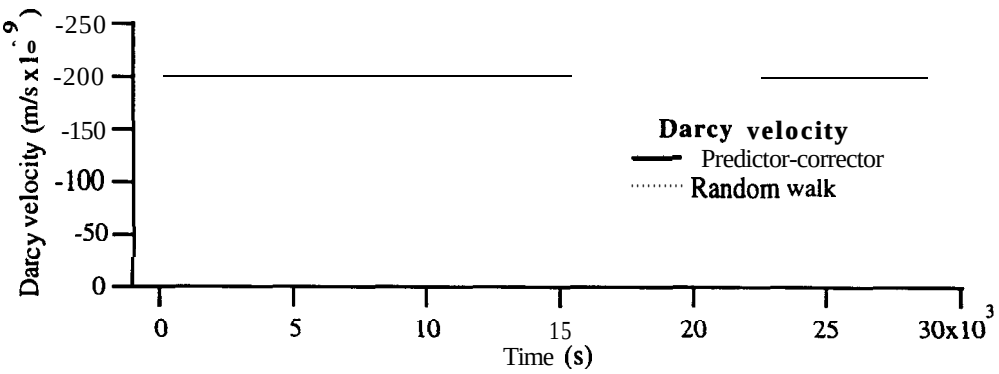

Figure 54 Variation in specific discharge with time for ELK14

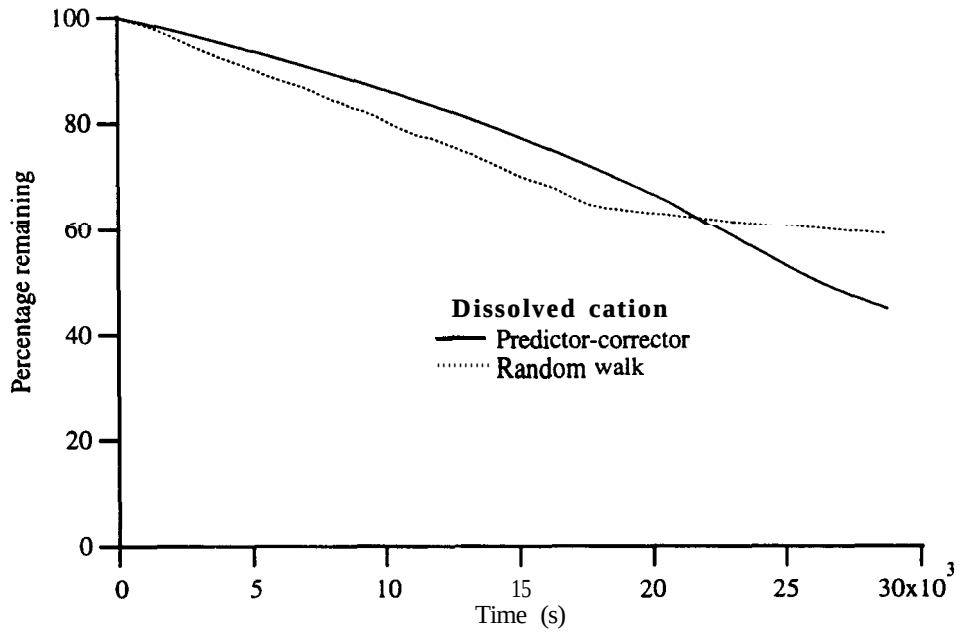

Figure 55 Variation in percentage dissolved sodium with time for ELK14

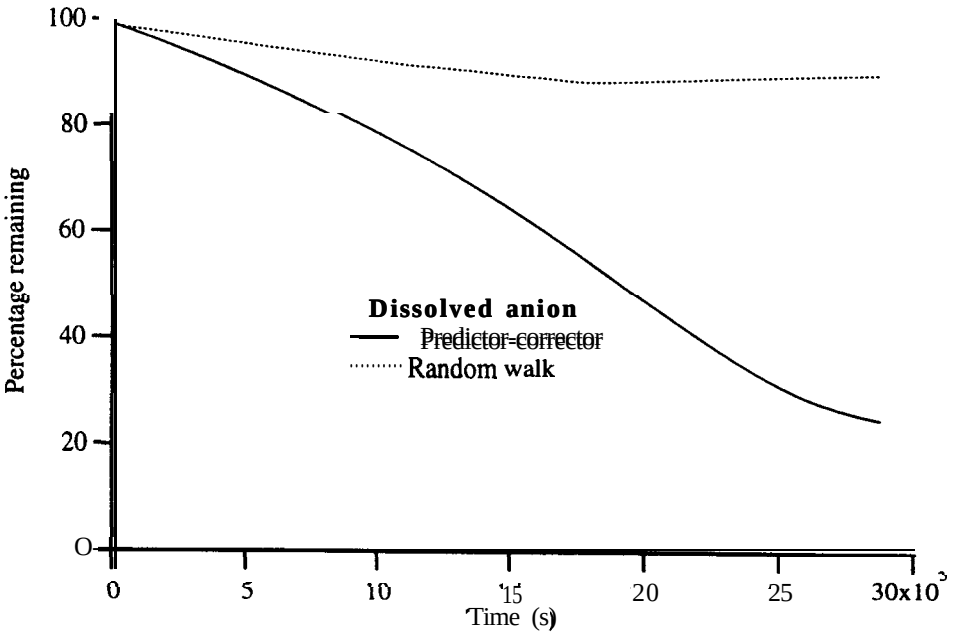

Figure 56 Variation in percentage chloride with time for ELK14

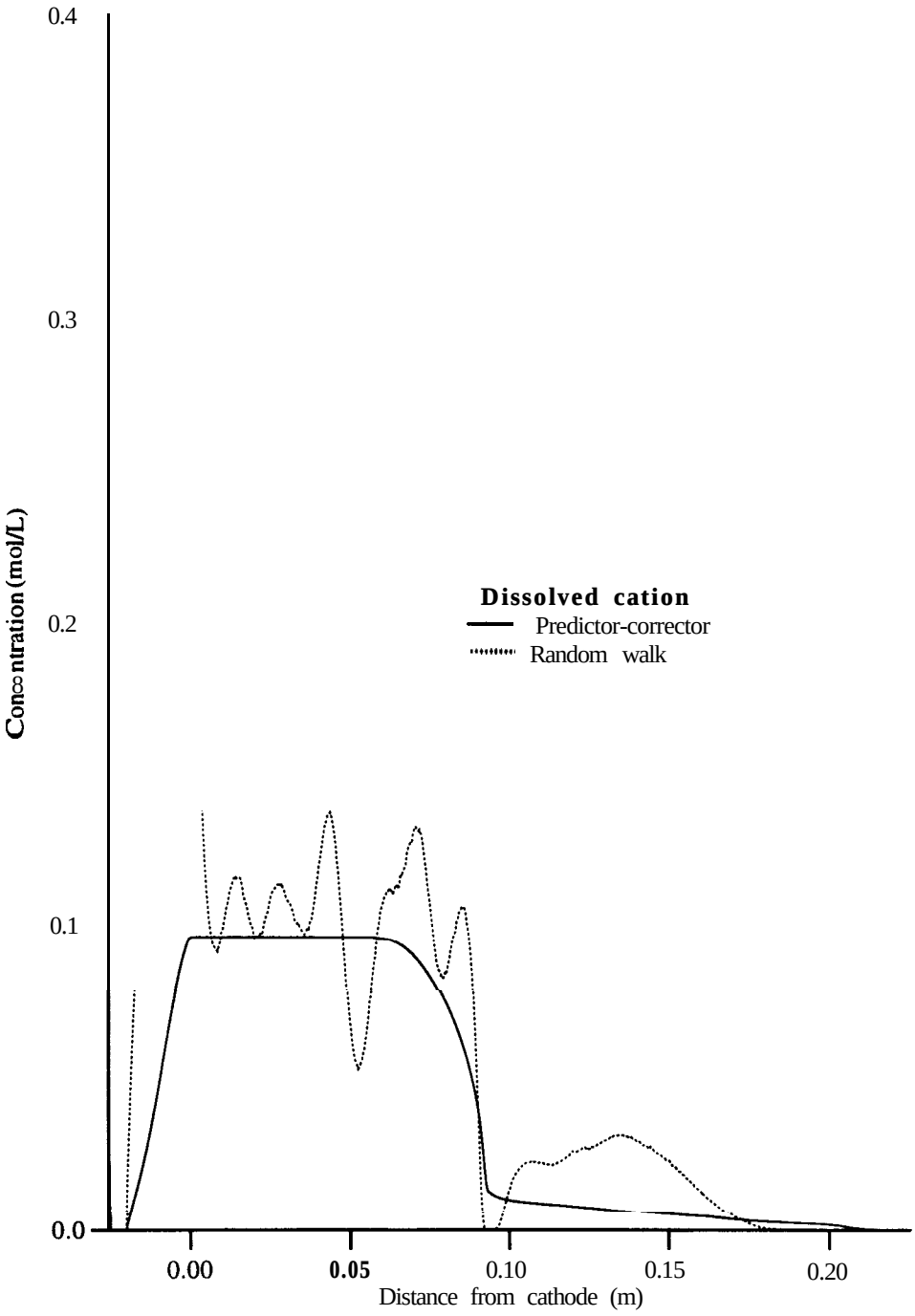

Figure 57 Final distribution of dissolved sodium for ELK14

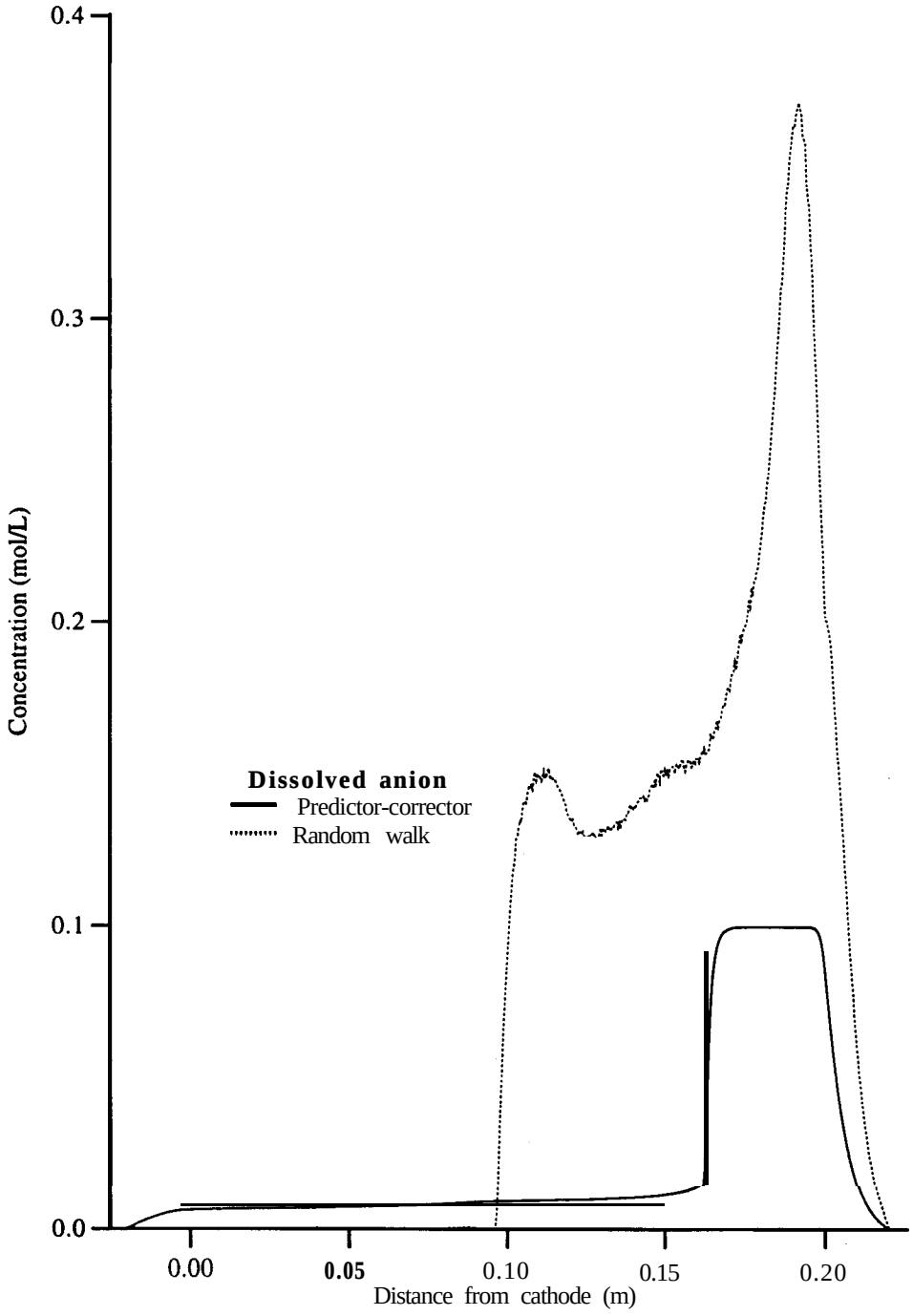

Figure 58 Final distribution of chloride for ELK14

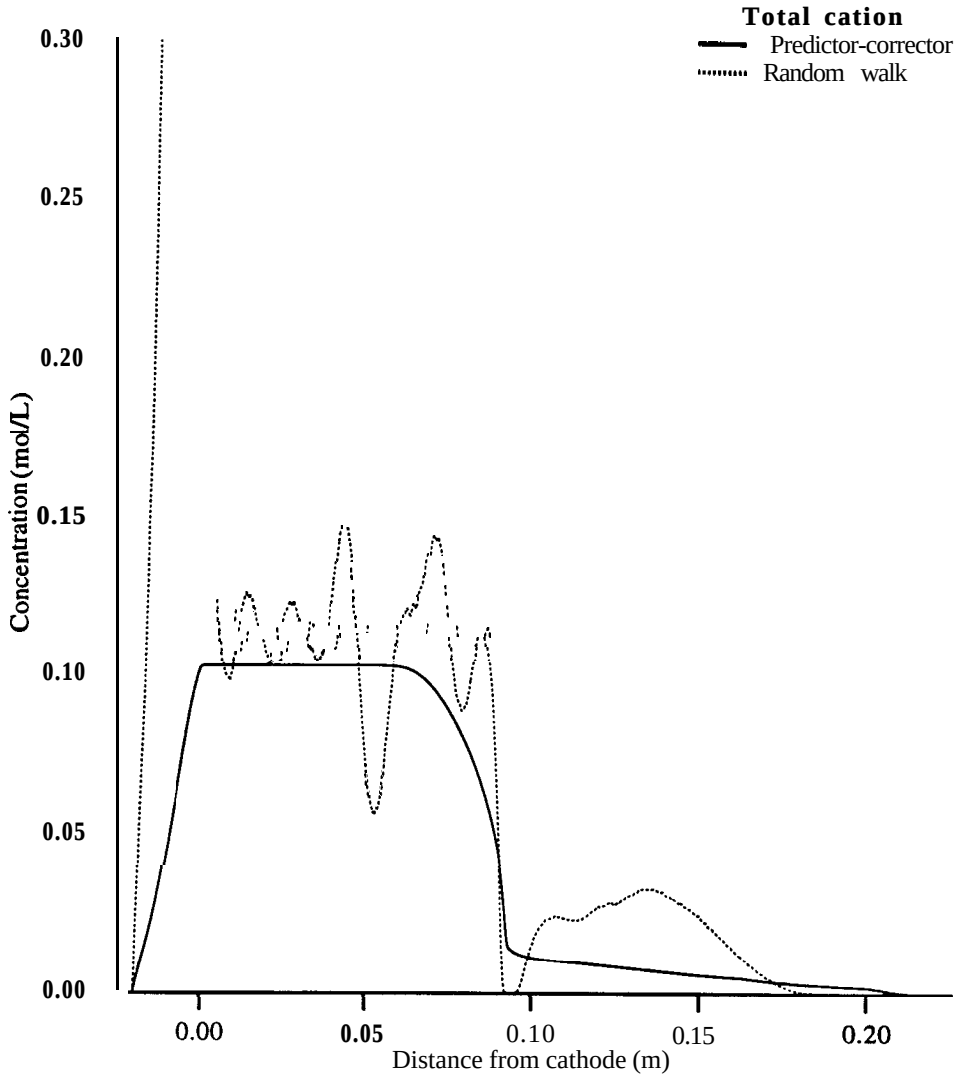

Figure 59 Final distribution of total sodium for ELK14

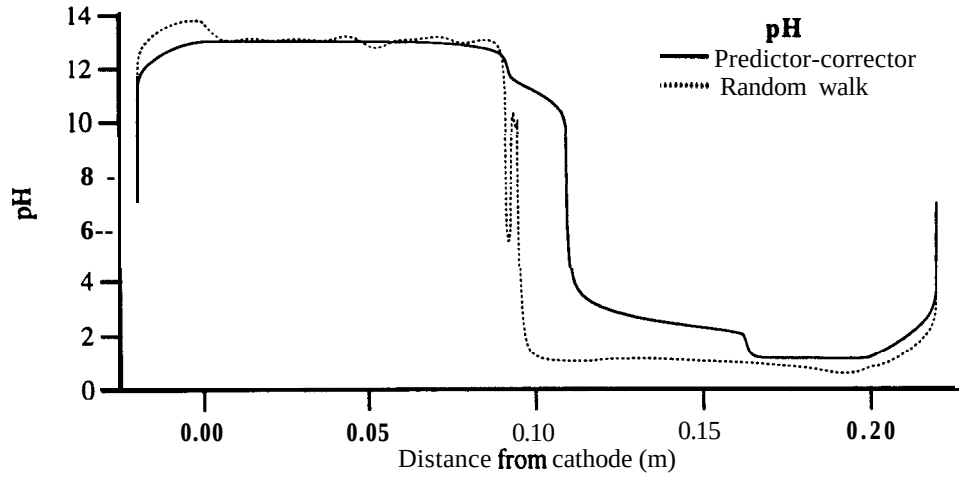

Figure 60 Final distribution of pH for ELK14

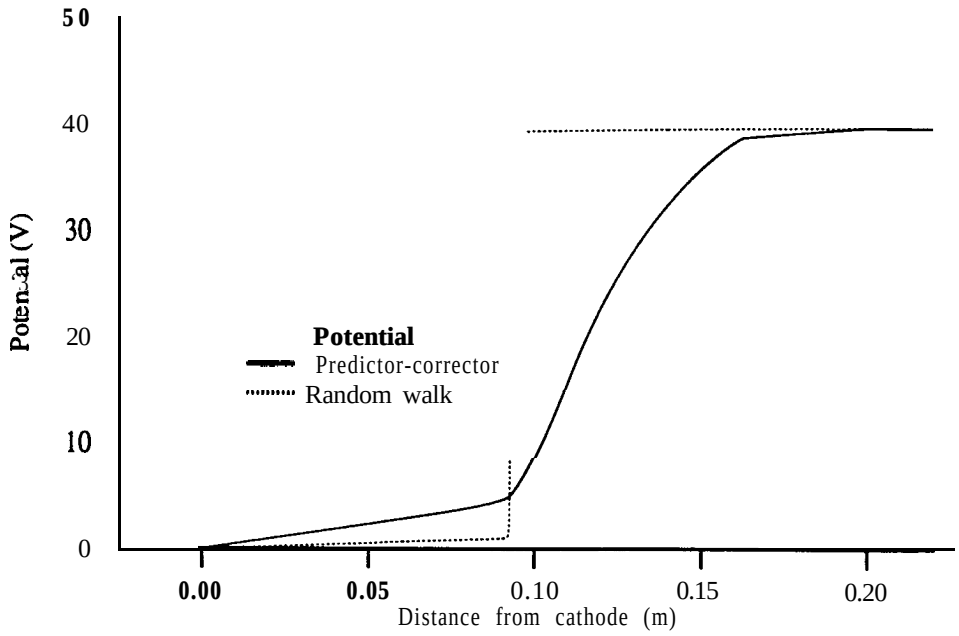

Figure 61 Final distribution of voltage for ELK14

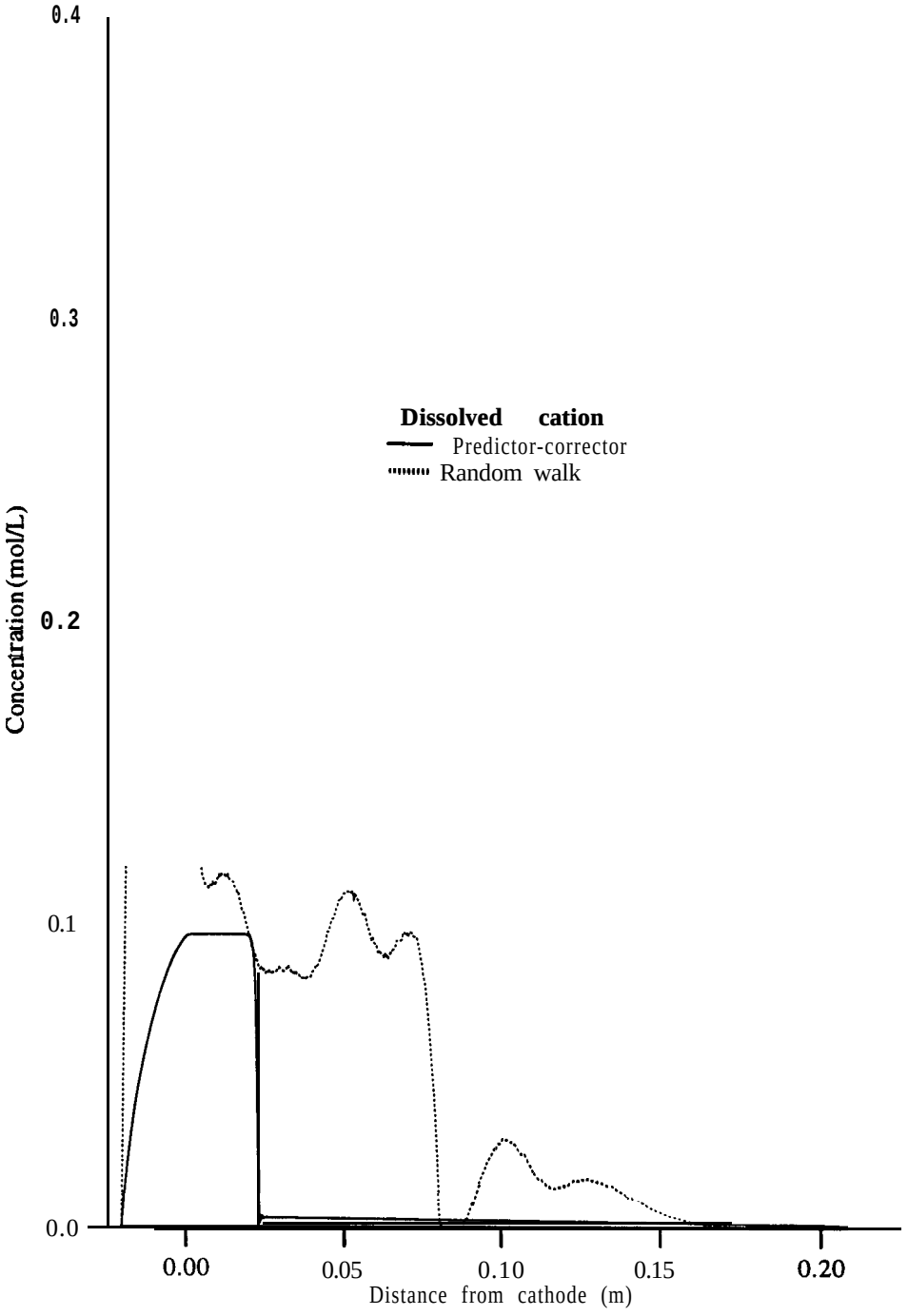

Figure 62 Final distribution of dissolved sodium for ELK15

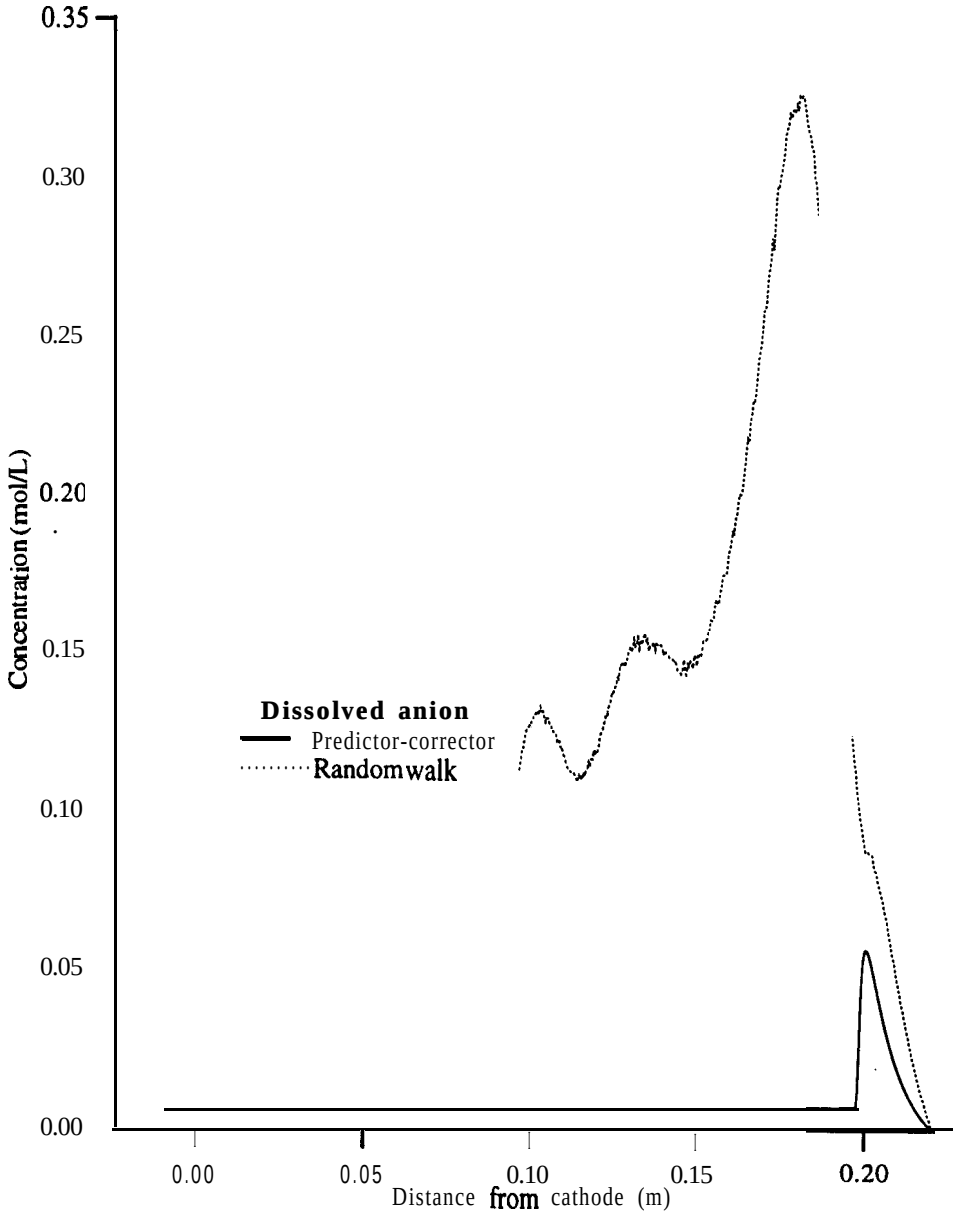

Figure 63 Final distribution of chloride for ELK15

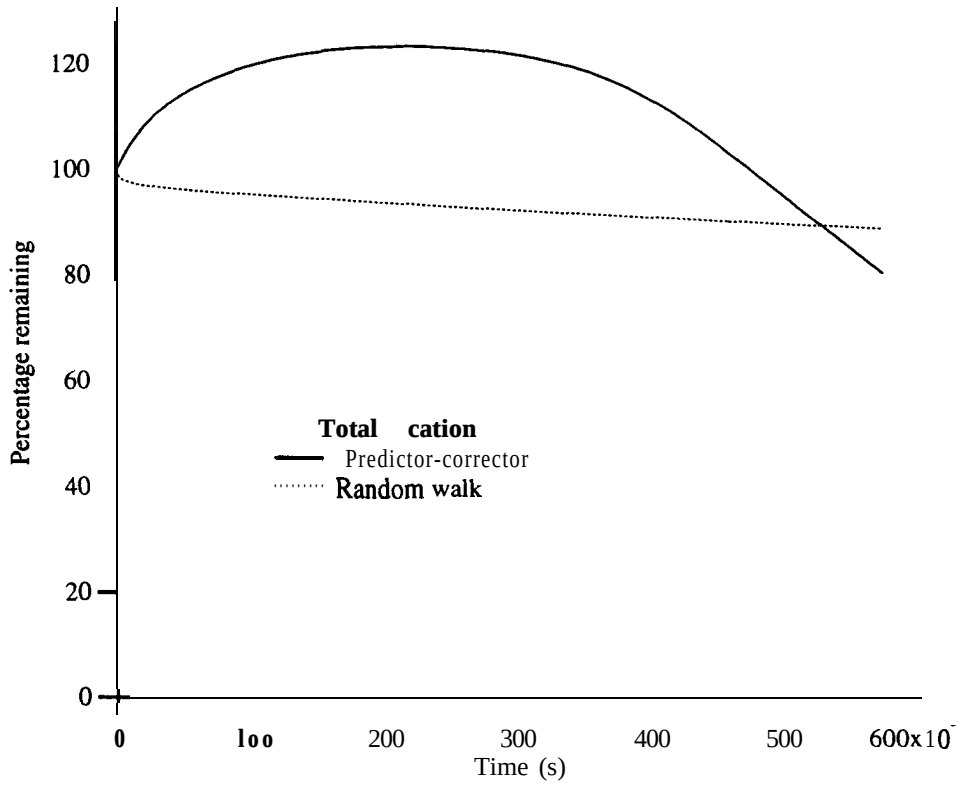

Figure 64 Variation in percentage total copper with time for ELK16

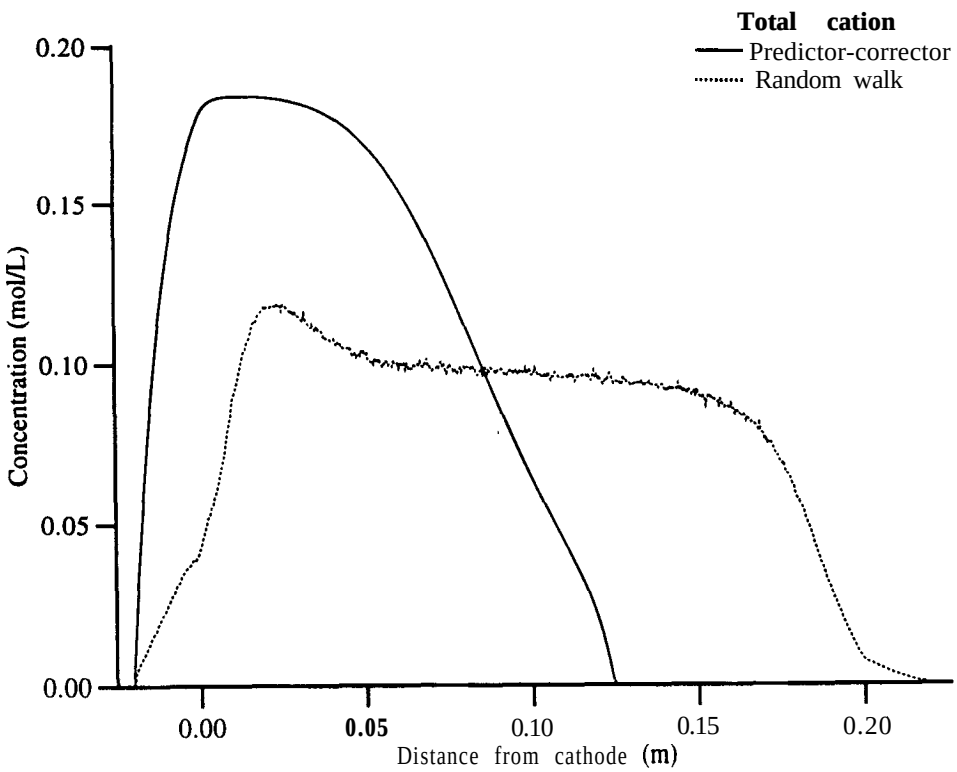

Figure 65 Final distribution of total copper for ELK16

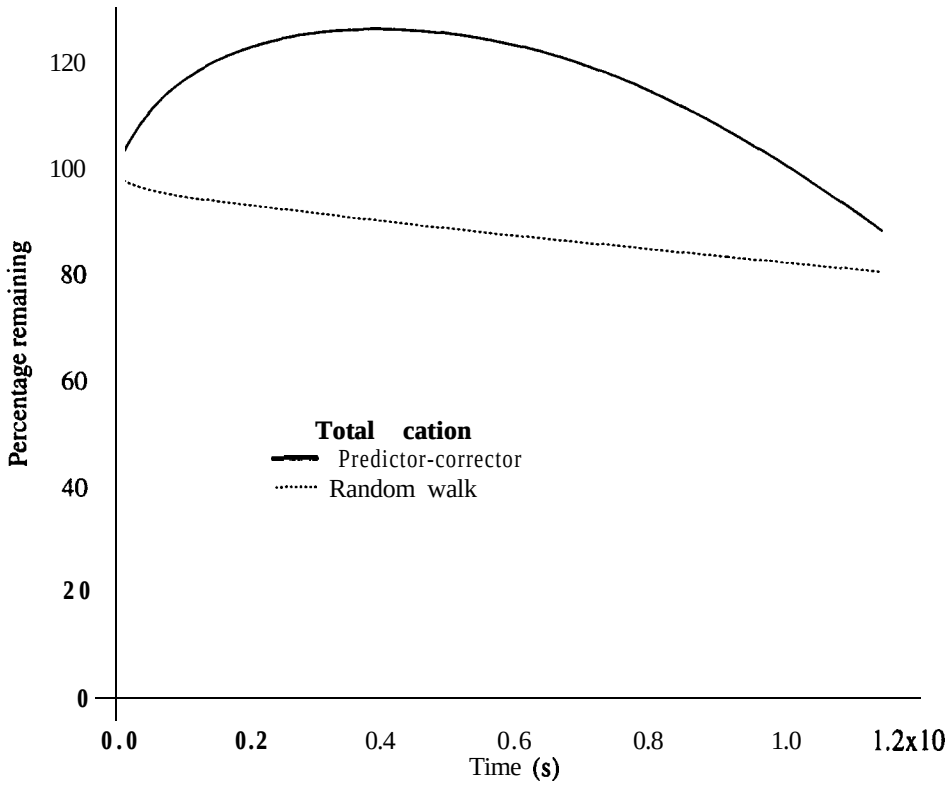

Figure 66 Variation in percentage total copper with time for ELK17

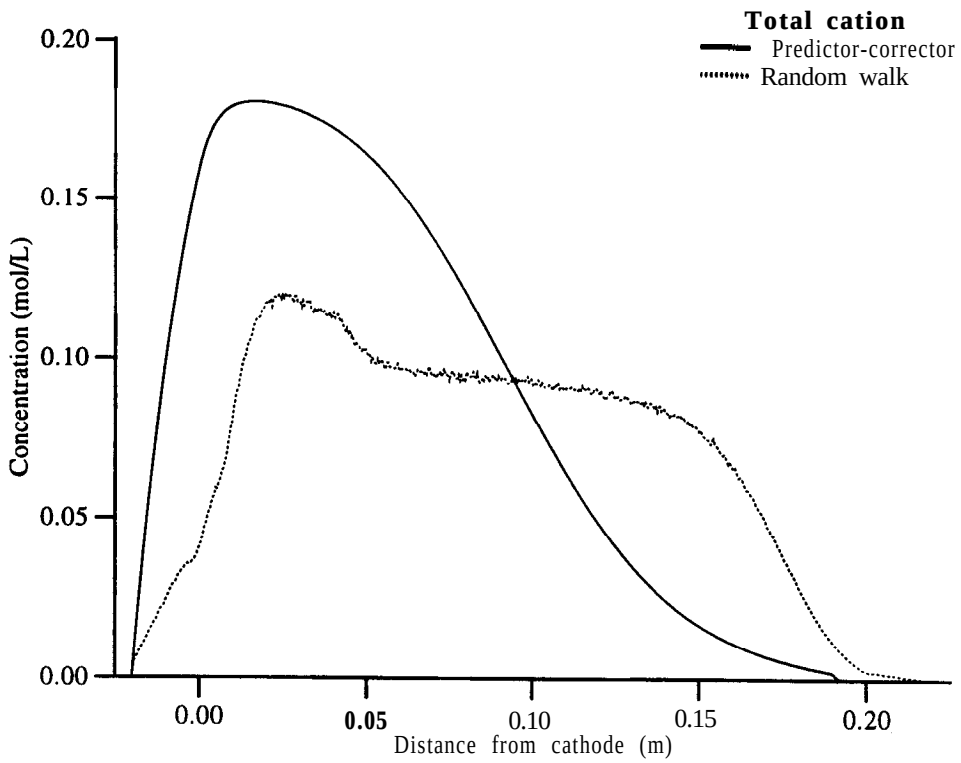

Figure 67 Final distribution of total copper for ELK17

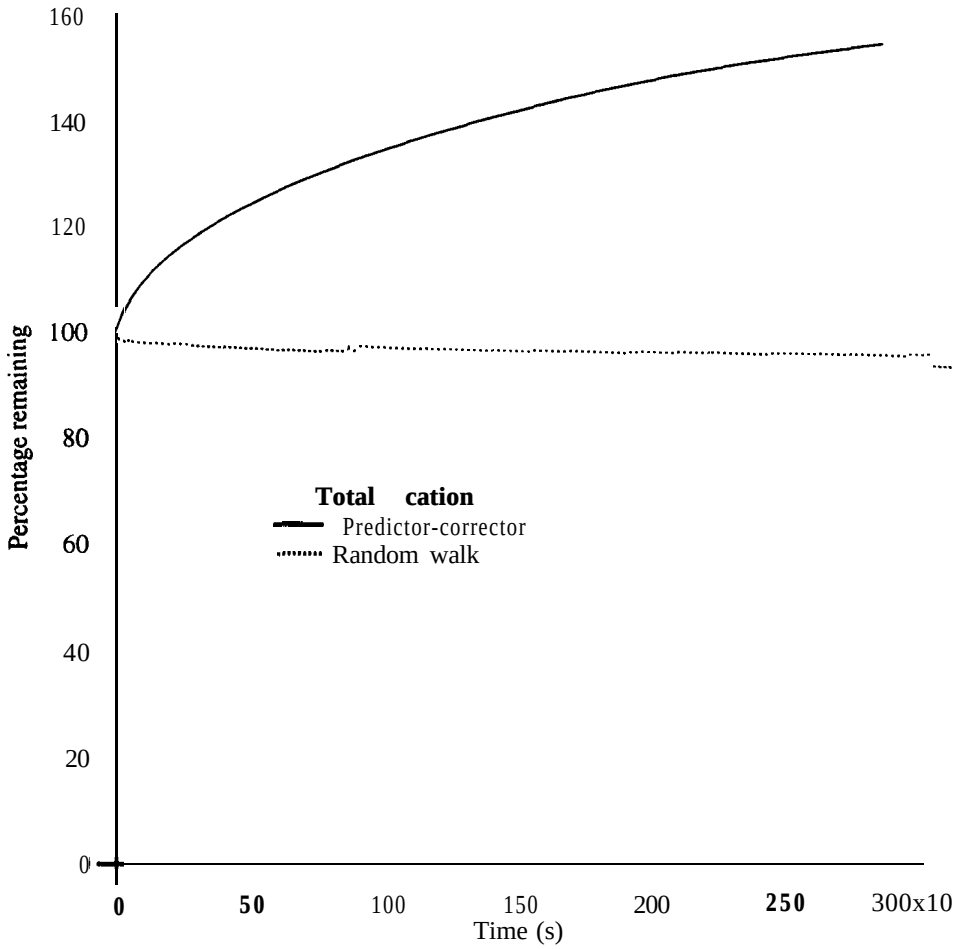

Figure 68 Variation in percentage total copper with time for ELK18

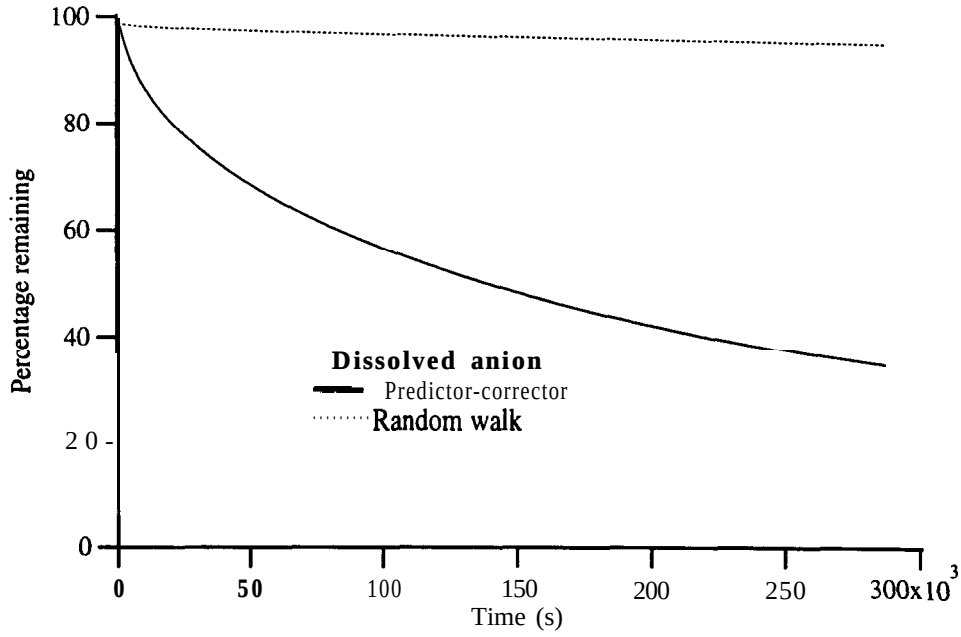

Figure 69 Variation in percentage sulphate with time for ELK18

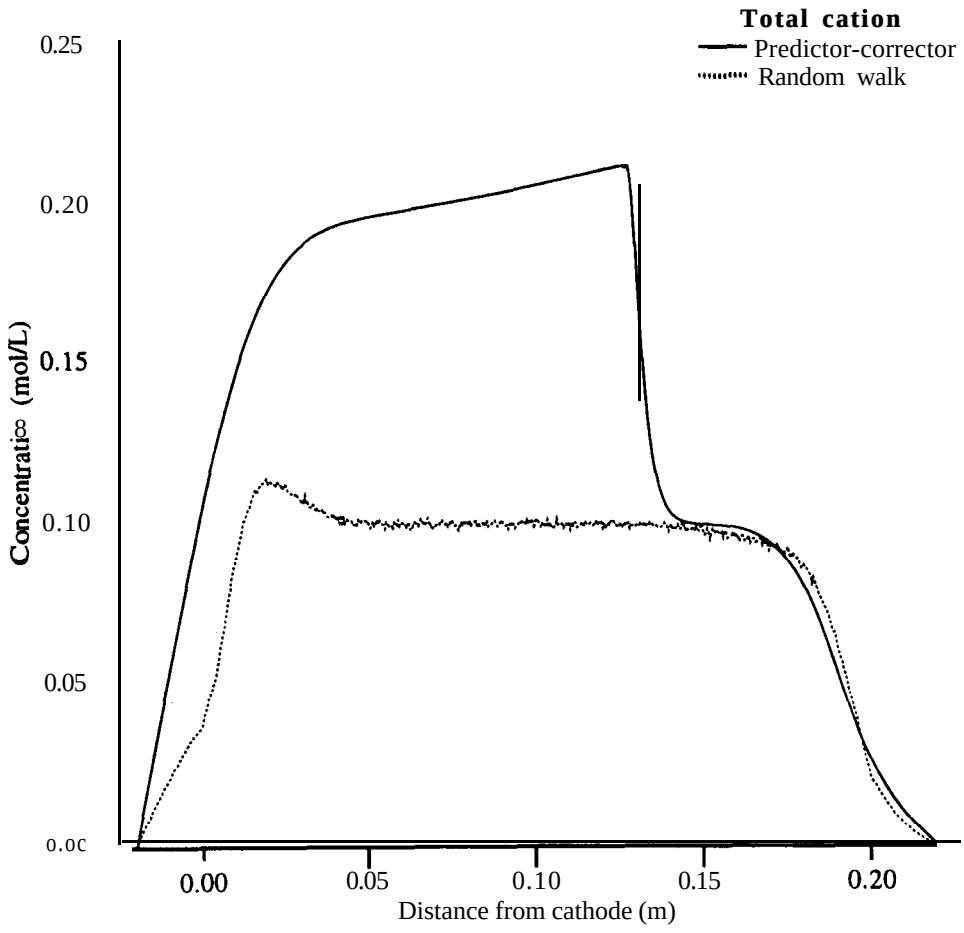

Figure 70 Final distribution of total copper for ELK18

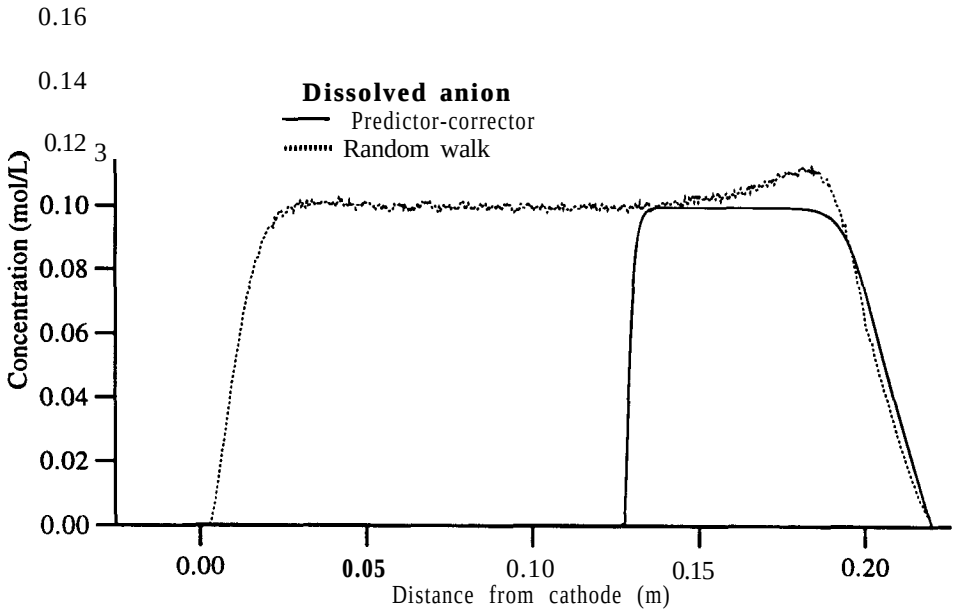

Figure 71 Final distribution of sulphate for ELK18

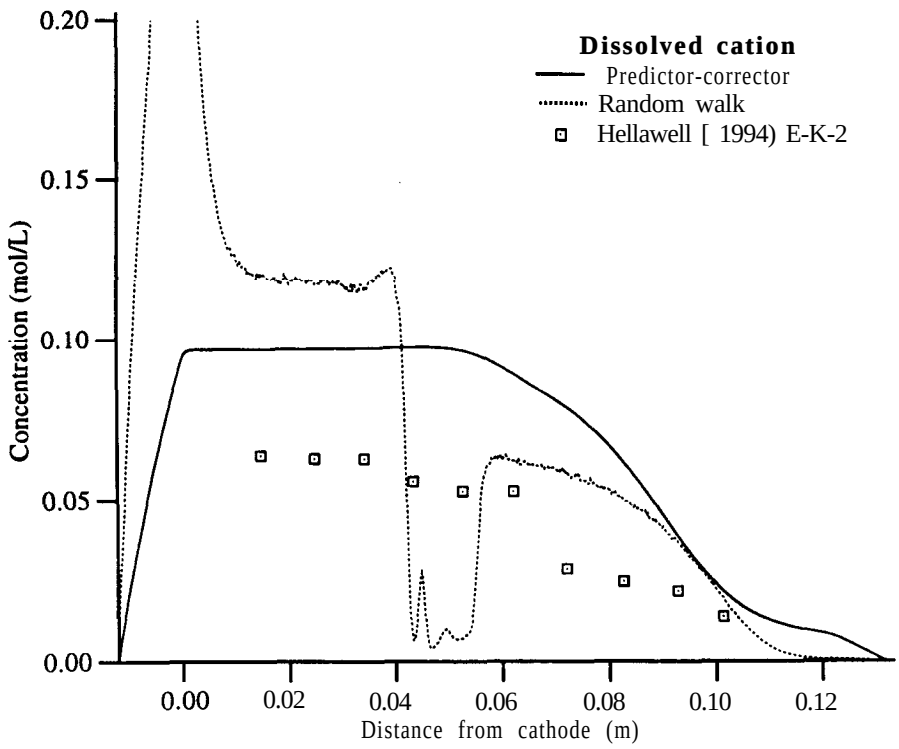

Figure 72 Final distribution of dissolved sodium for ELK19

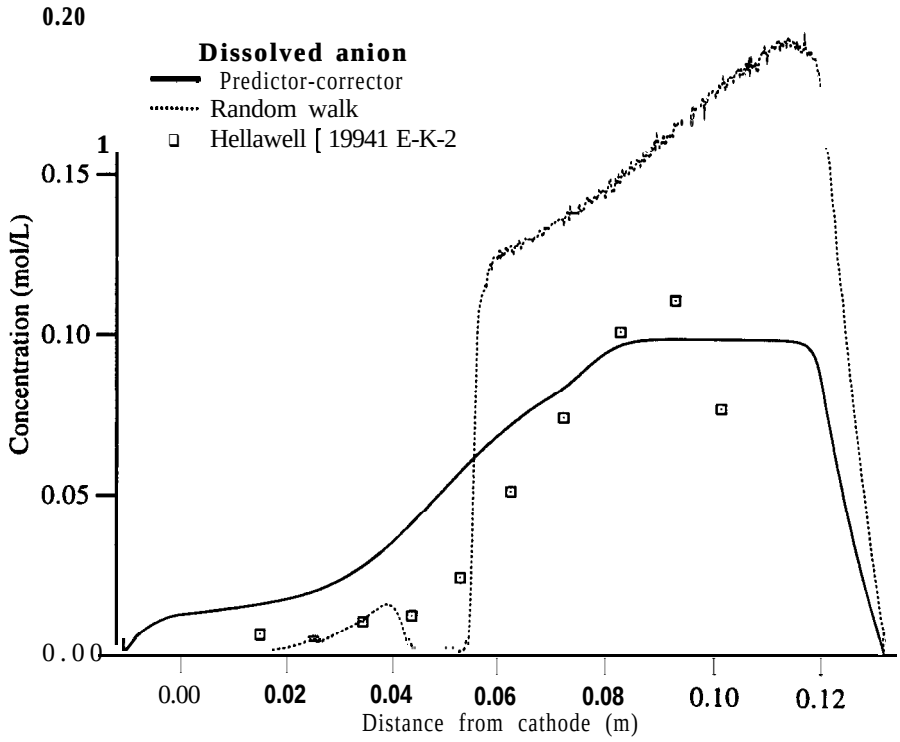

Figure 73 Final distribution of chloride for ELK19

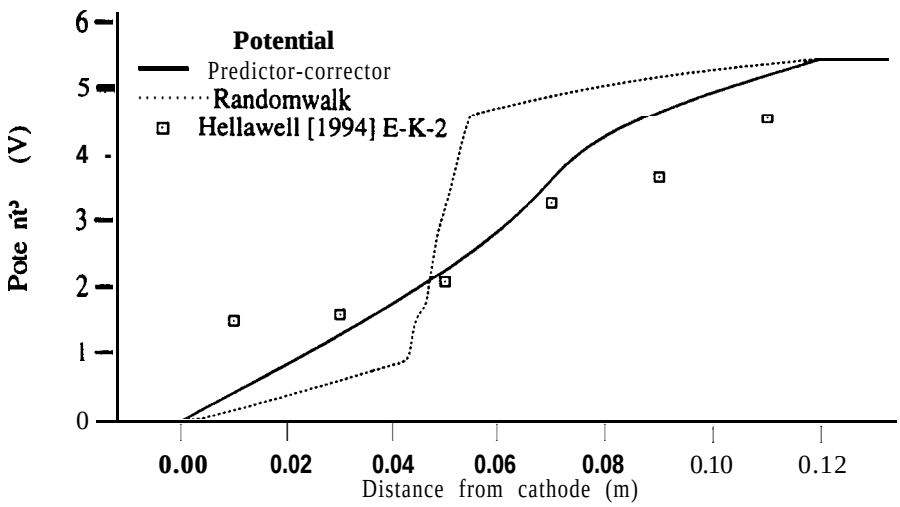

Figure 74 Final distribution of voltage for ELK19

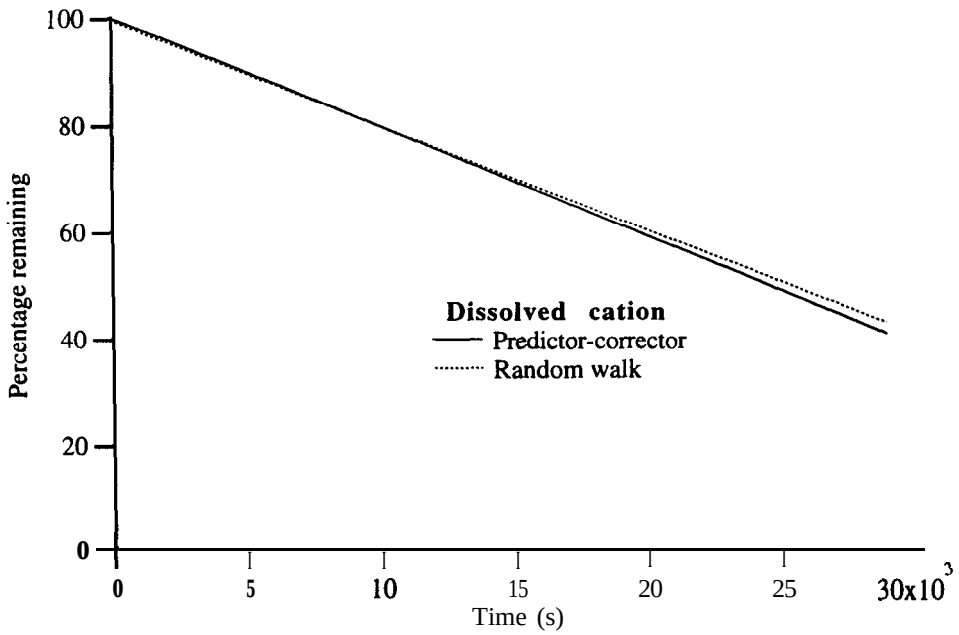

Figure 75 Variation in percentage dissolved copper with time for ELK20

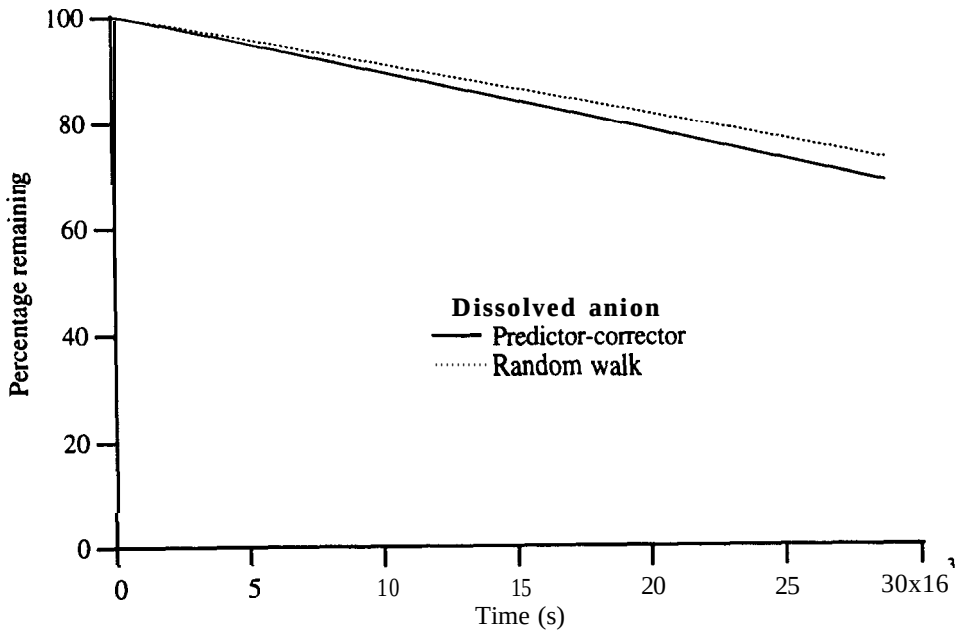

Figure 76 Variation in percentage sulphate with time for ELK20

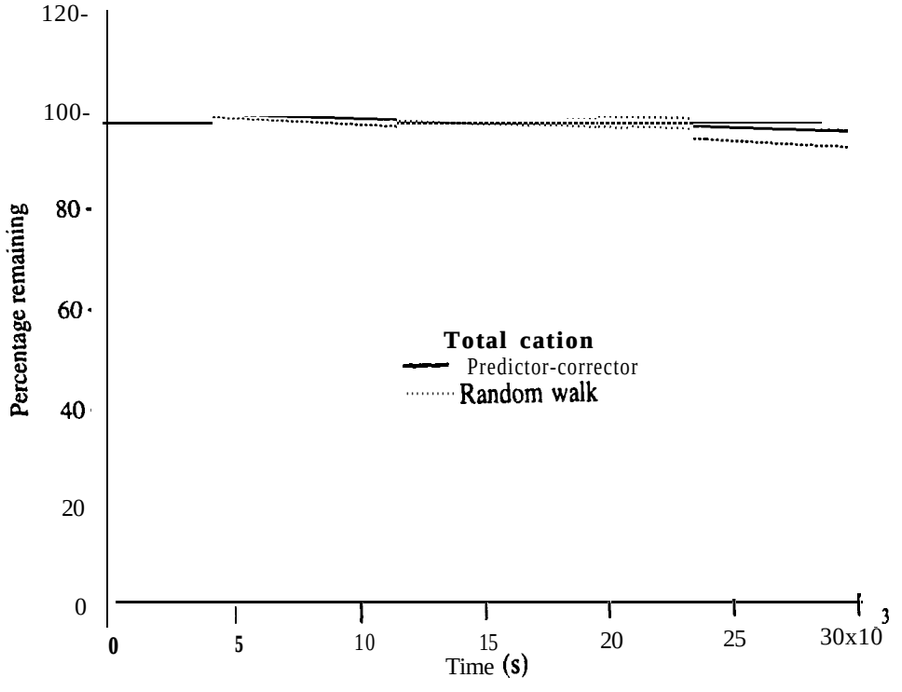

Figure 77 Variation in percentage total copper with time for ELK20

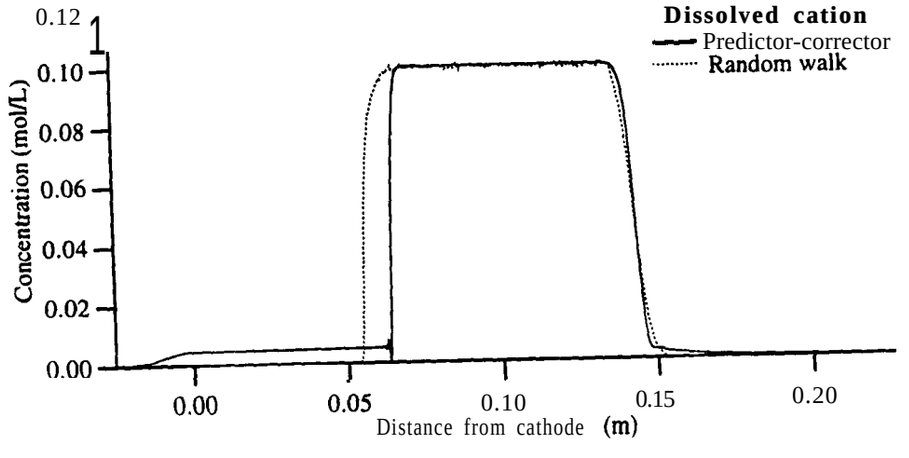

Figure 78 Final distribution of dissolved copper for ELK20

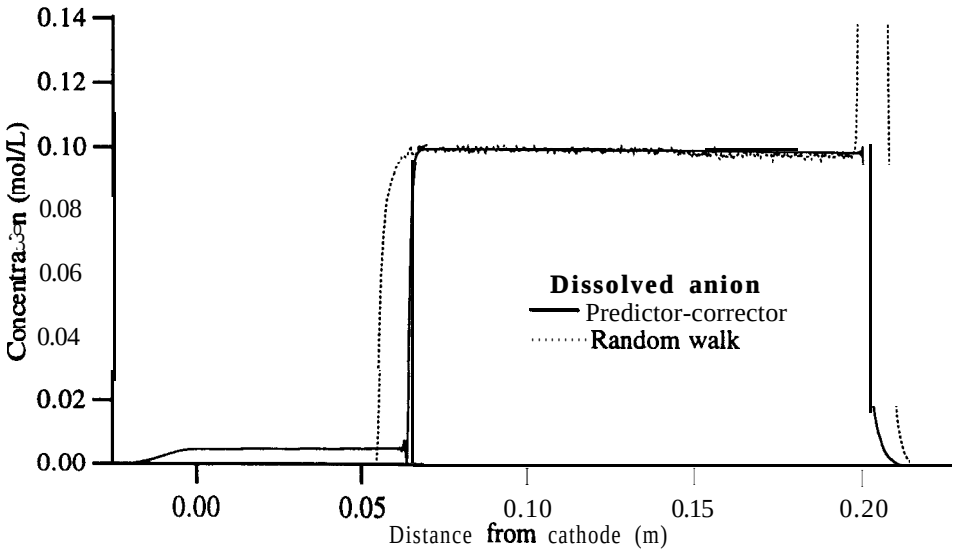

Figure 79 Final distribution of sulphate for ELK20

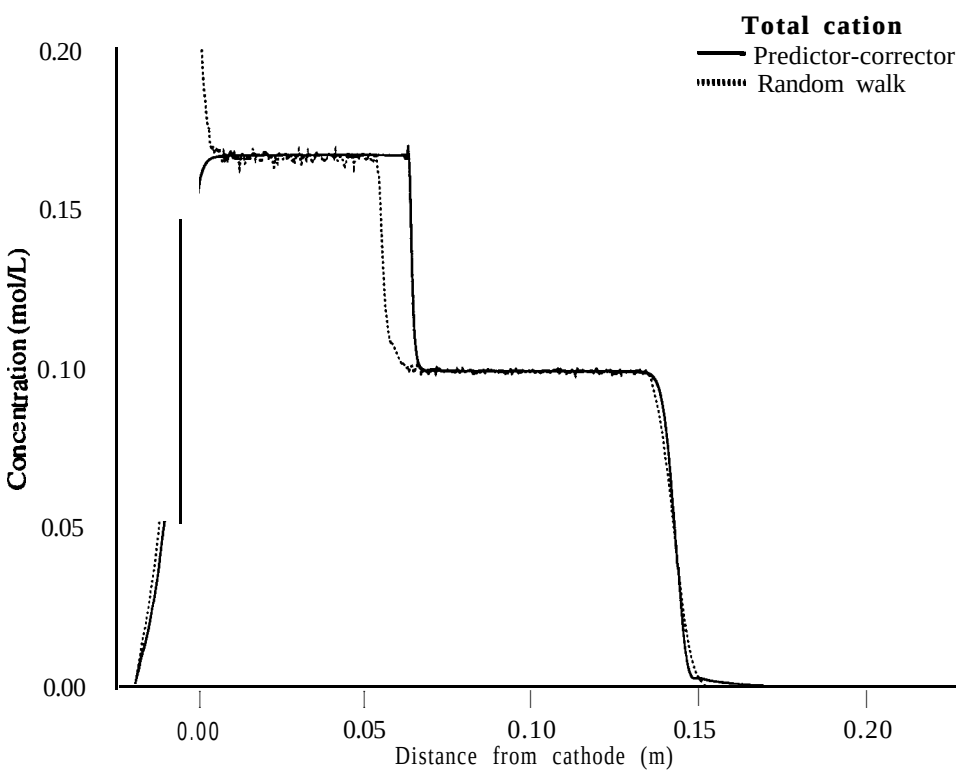

Figure 80 Final distribution of total copper for ELK20

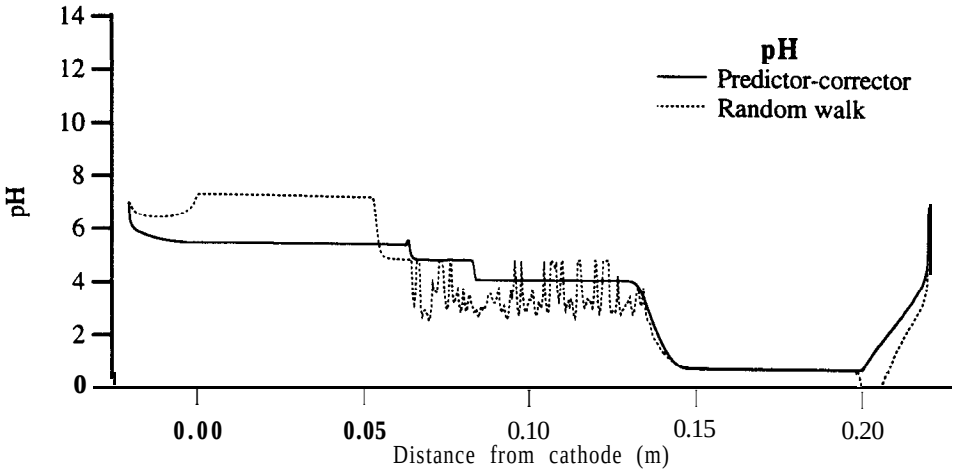

Figure 81 Final distribution of pH for ELK20

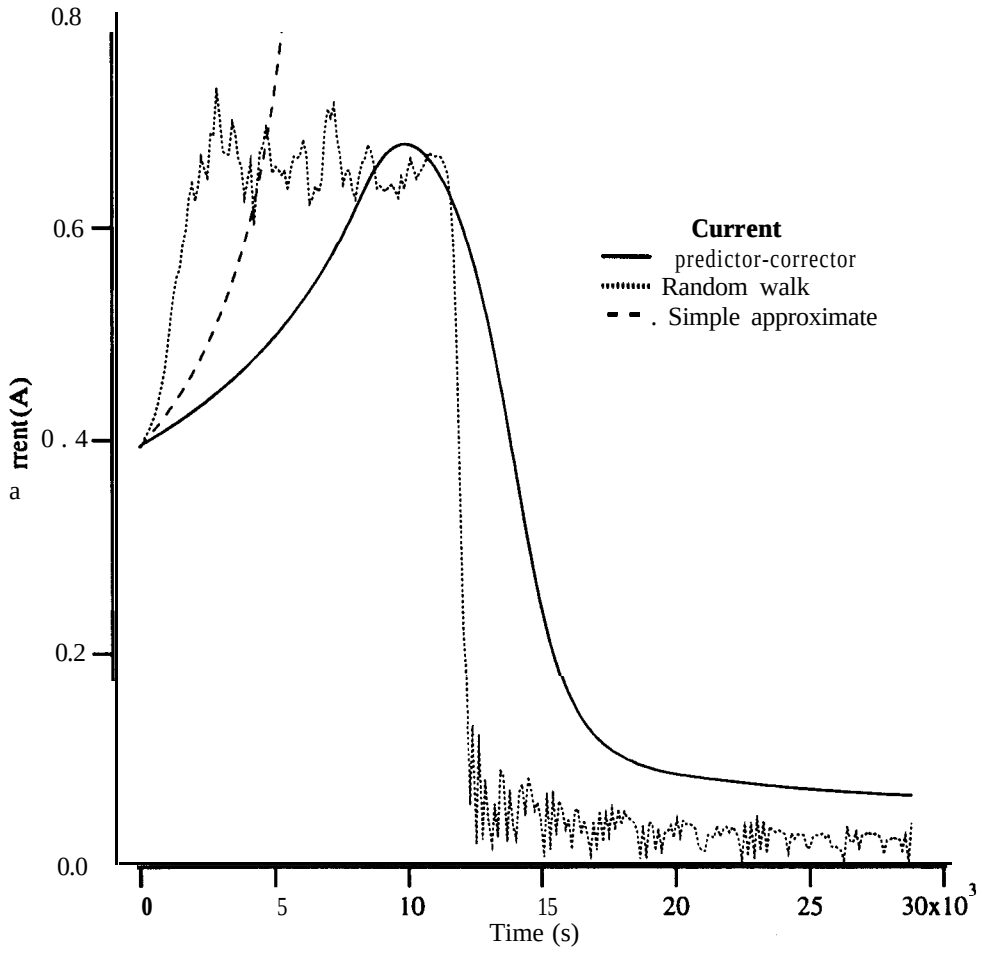

Figure 82 Variation in current with time for ELK21

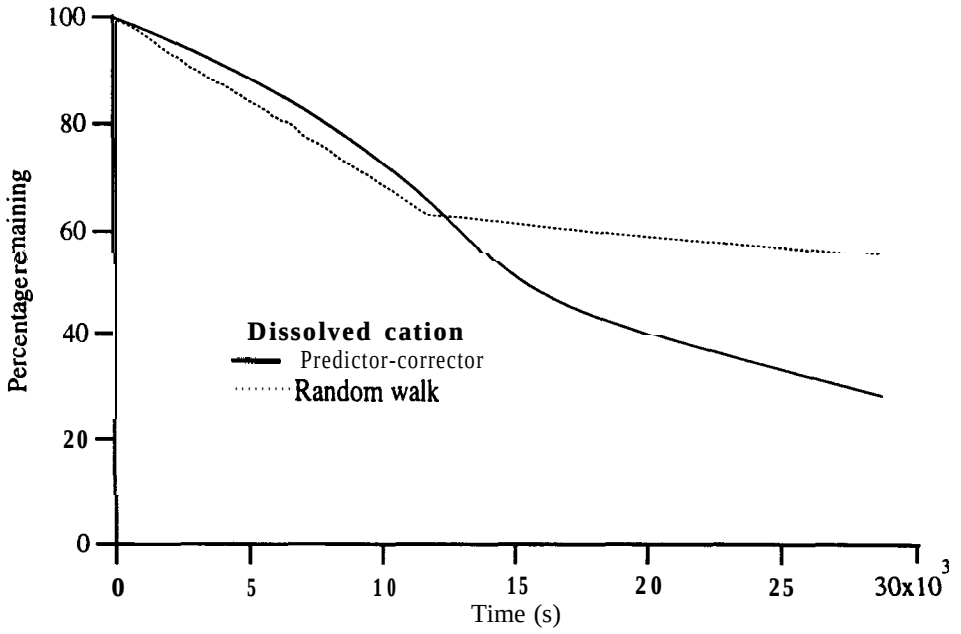

Figure 83 Variation in percentage dissolved sodium with time for ELK21

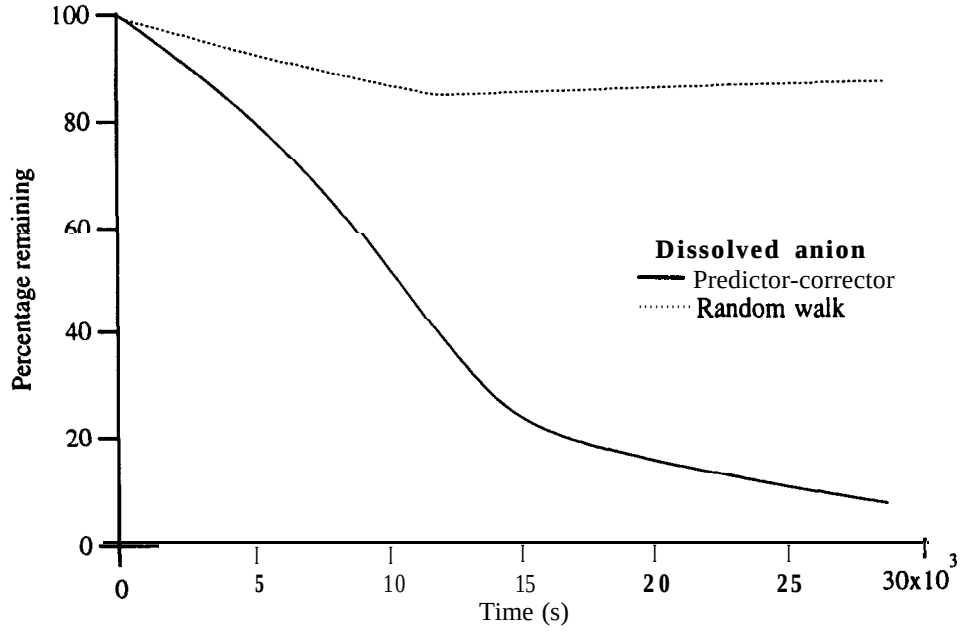

Figure 84 Variation in percentage chloride with time for ELK21

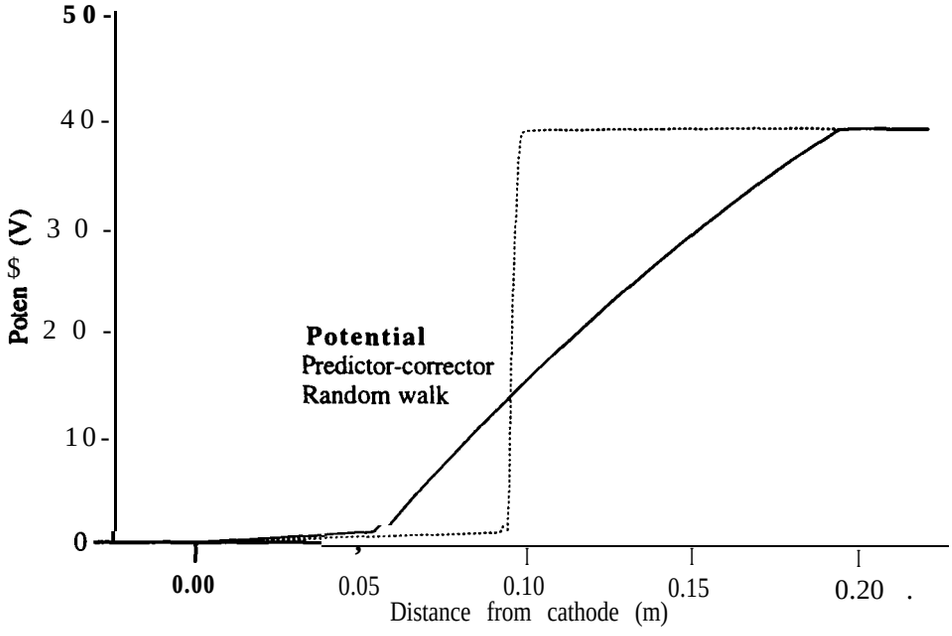

Figure 85 Final distribution of voltage for ELK21

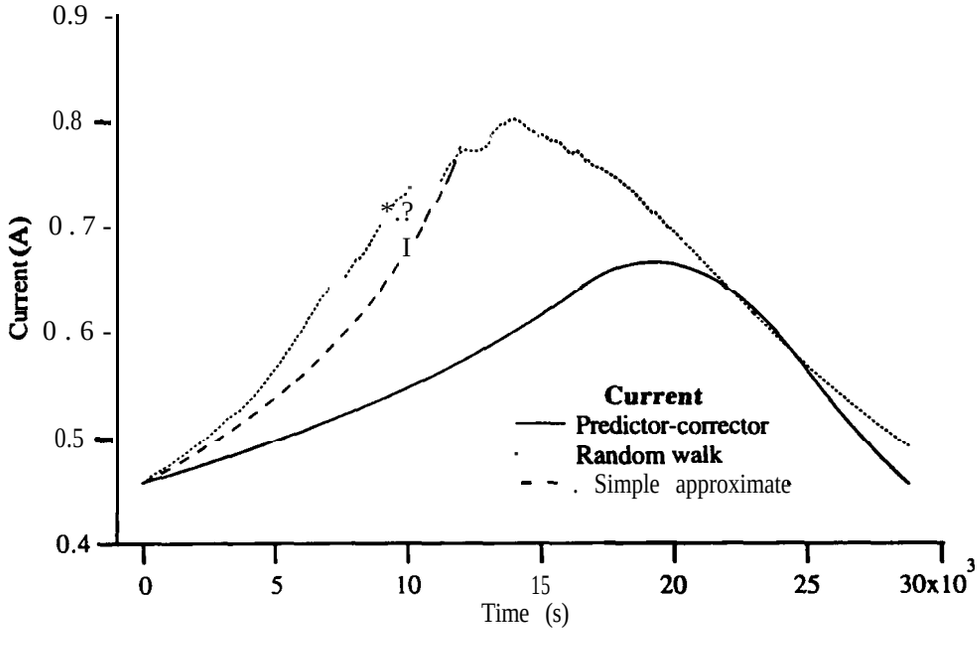

Figure 86 Variation in current with time for ELK22

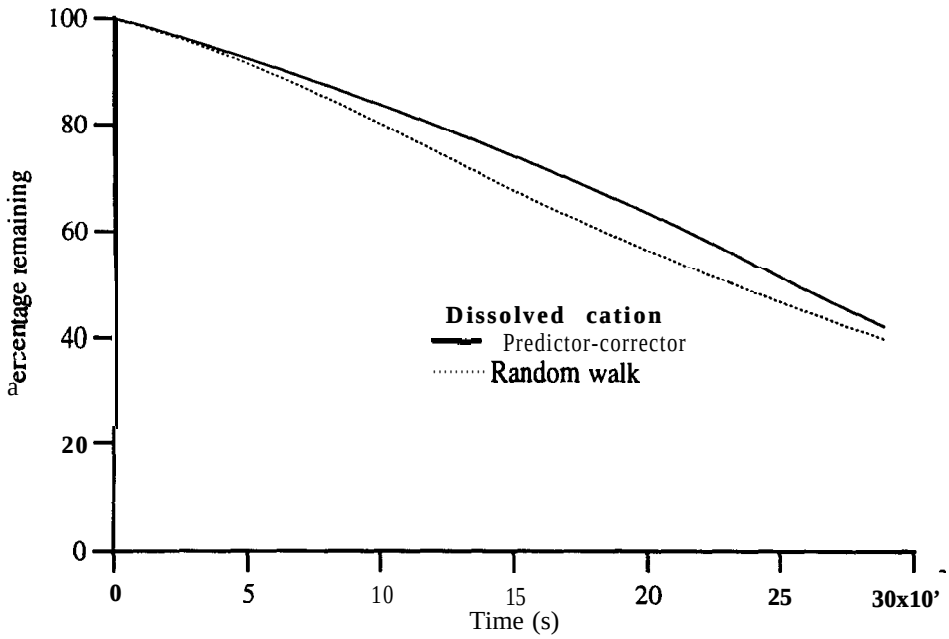

Figure 87 Variation in percentage dissolved sodium with time for ELK22

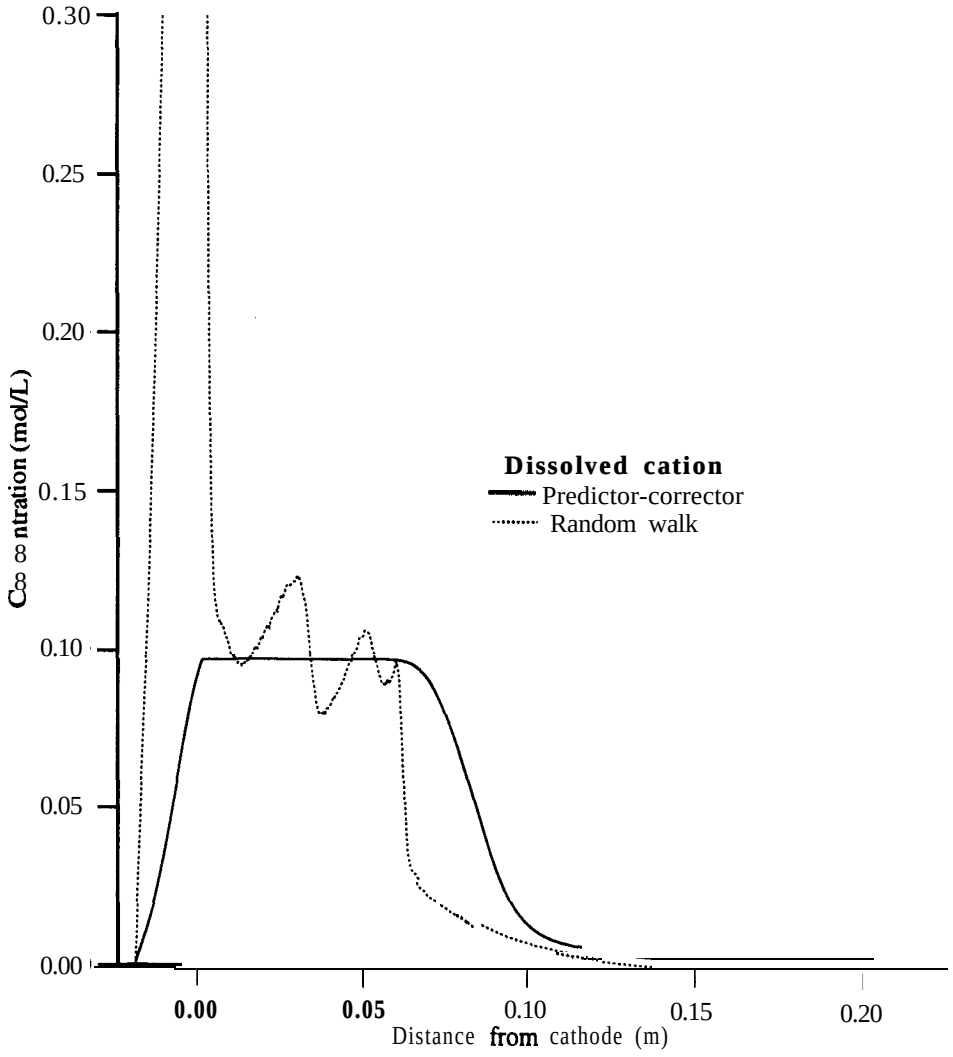

Figure 88 Final distribution of dissolved sodium for ELK22

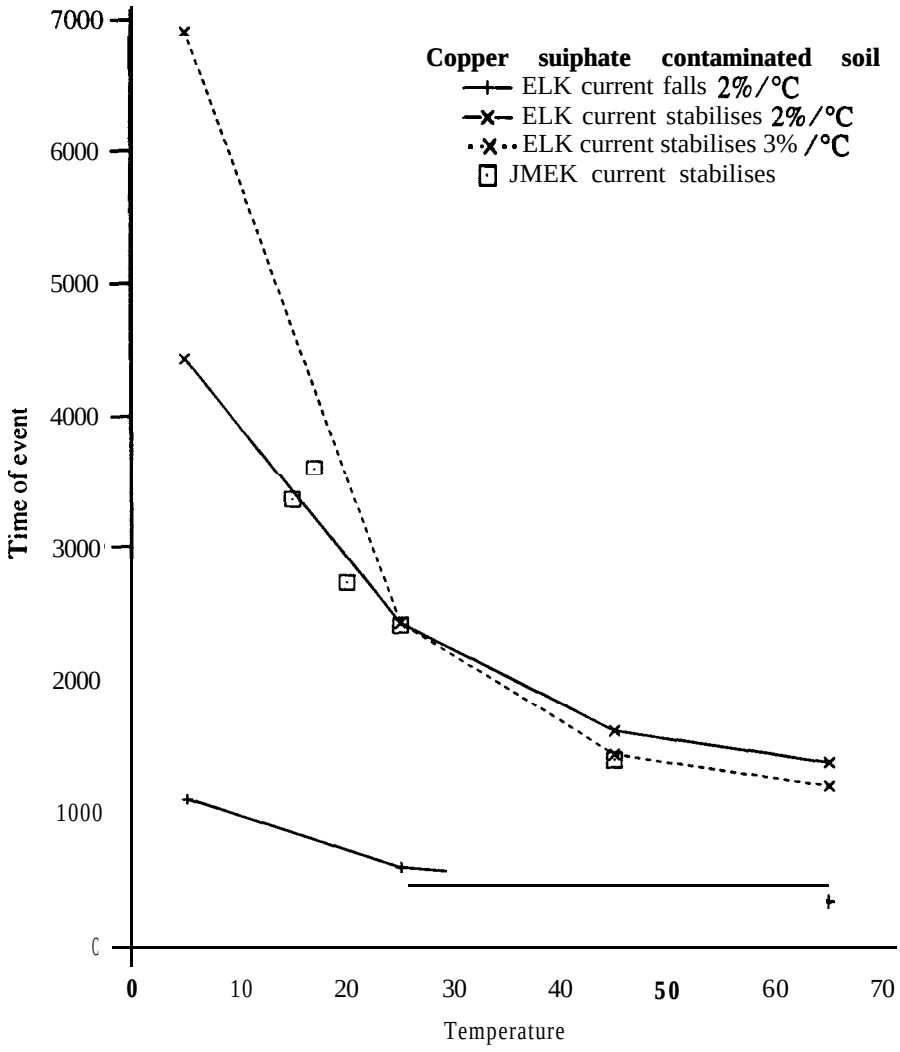

Figure 89 Transition times for electric current for versus temperature

APPENDIX A — ELECTROPHORETIC COUPLING, ELECTRONEUTRALITY AND PH DURING IONIC DIFFUSION IN SOIL

Introduction

The classic equations for tracer electrolyte diffusion into soil predict the development of an electric charge separation, since the cations and anions generally have different diffusion coefficients, and therefore different migration speeds. Simple calculations indicate that the resulting electric field would be extremely large. No such charge separations are observed.

Ions, being charged, tend to migrate in electric fields. In a simple, two-ion system the electric field generated by the difference in migration speeds will tend to slow down the fast moving ion and speed up the slow moving ion. The dynamic equilibrium state where the electrophoretic effect exactly compensates for the difference in intrinsic diffusion rates is attained in the Debye relaxation time, effectively instantaneously [Robinson and Stokes, 1959], at which point the ions diffuse together at a rate characterised by the coupled diffusion coefficient D_{cc} . A charge separation still exists, causing the concentration cell junction potential, but this is small [Robinson and Stokes, 1959] and the solution is effectively electrically neutral everywhere.

The Nernst-Hartley relationship for D_{cc} reduces to:

$$D_{cc} = \frac{2D_+D_-}{D_+ + D_-} \tag{A.1}$$

for a univalent-univalent electrolyte at infinite dilution, where D_+ is the intrinsic diffusion coefficient of the cation and D_- that of the anion [Robinson and Stokes, 1959].

It is an experimentally observed fact that ions migrate together in simple electrolyte solutions, with diffusion coefficients given by the Nemst-Hartley relationship [Harned and Nuttall, 1947, 1949; Turq *et al.* 1977]. It has also been observed that ions do not migrate together in the more complex environment of soils and rocks [Crooks and Quigley 1984; Kim *et al.* 1993; Maloszewski and Zuber 1993], whether natural or laboratory.

This note presents an analysis of electrophoretic coupling during ionic diffusion in soil. It deals strictly with the diffusive migration of non-reacting species in inactive soils, but the issues raised are relevant to studies of transport processes where chemical reactions take place, in active soils, or where migration results from an imposed electric field. In this last case cations and anions are observed to move in opposite directions [Yeung and Mitchell, 1993] and proper consideration of electroneutrality is particularly important.

Problem conceptualisation

The chosen scenario is the one-dimensional semi-infinite diffusion cell of figure A. 1, made up of two blocks of saturated soil. The soil grains are uncharged and inert. In one block the initial concentration of NaCl tracer in the pore water is c_0 , while in the other it is zero. As a result, both sodium and chloride ions will diffuse across the interface. The concentration

distribution and the concentration imbalance at some later time for independent diffusion is shown in figure A.2. The concentration imbalance generates an internal electric field coupling the two ions together.

From Yeung and Mitchell [1993] the governing equation for one-dimensional transport of species i at concentration c_i having valency z_i in an electric field of strength E with stationary pore water is:

$$\frac{\partial c_i}{\partial t} = D_i^* \frac{\partial^2 c_i}{\partial x^2} + \frac{u_i^* z_i}{|z_i|} \frac{\partial \{E c_i\}}{\partial x} \tag{A.2}$$

where x is distance. In equation (A.2) D_i^* is the effective diffusion coefficient and u_i^* is the effective ionic mobility, the speed of migration clown a unit concentration gradient and the speed of migration in an electric field of unit strength, respectively.

The effective transport properties D_i^* and u_i^* are related to the aqueous diffusion coefficient D_i and the aqueous ionic mobility u_i by:

$$D_i^* = \omega D_i \tag{A.3}$$

and

$$u_i^* = \omega u_i \tag{A.4}$$

respectively, where tortuosity ω indicates how much more difficult it is for the ion to move because of the need to travel around the soil grains.

For a pore solution containing two species, a cation of valency z_+ at concentration c_+ mol L^{-1} and an anion of valency z_- at concentration c_- mol L^{-1}, the charge density σ in C m^{-3} of soil is:

$$\sigma = 1\,000 n (z_+ c_+ + z_- c_-) F \tag{A.5}$$

where n is the porosity and F = 9.6485 x 10^4 mol L^{-1} is the Faraday constant. If the soil is uniform and can be characterised by some average relative permittivity ε_r Gauss's Law relating the charge density and the electric field strength E gives:

$$E = \frac{1}{\varepsilon_r \varepsilon_0} \int \sigma \partial x \tag{A.6}$$

where ε_0 = 8.85419 x 10^{-12} F m^{-1} is the permittivity of free space [Halliday and Resnick, 1974].

Relative permittivity is frequency dependent. The low frequency relative permittivity of water at 25°C is 78 [Atkins, 1994] but that for saturated clays can range up to 10^4 or more [Arulanandan and Mitchell 1968], possibly due to bound ion polarisation effects. This note is concerned with the rate and effects of the dissipation of a small perturbation from electroneutrality within the pore space, so it is appropriate to use ε_r for water; it is assumed that there is no interaction with the diffuse double layer of the soil grains during this process. Different values of ε_r, n and ω will lead to different estimates of the magnitude of the electric field strength and the rate at which it dissipates, but will not affect the final equilibrium state in

the model proposed. The concentration imbalance needed to generate large electric fields is minute: a 10"mol L^{-1} imbalance of a univalent-univalent electrolyte across 100 μm of pore space gives $E \approx 10^7 V\ m^{-1}$, which for a typical effective ionic mobility of 3 x $10^{-8}\ m^2\ s^{-1}\ V^{-1}$ gives a migration velocity of $0 \cdot 3 m\ s^{-1}$. The time taken for ions to migrate from the edges to the centre of the space is then $\approx 10^{-4} s$. If such a charge imbalance could build up the electrophoretic coupling effect would be large. The imbalance would dissipate too quickly for the soil to consolidate. There would be negligible electro-osmotic flow, although short lived excess pore pressures would exist.

Extension to include the effects of a background electrolyte at some uniform concentration c_s is straightforward: equation (AS) is rewritten to include all the ions in solution and equation (A.2) solved for each species, using the transport properties given by equations (A.3) and (A.4). Consideration of the hydronium and hydroxide ions resulting from water autoprotolysis in aqueous solution involves the dissociation reaction:

$$2H_2O\ (I) \leftrightarrow H_3O^+\ (aq) + OH^-\ (aq) \tag{A.7}$$

for which the equilibrium constant at standard state is:

$$K_w = [H_3O^+][OH^-] = 10^{-14} \tag{A.8}$$

where the terms in brackets are the activities of the respective ions; for dilute solutions activity and molar concentration are equivalent. The reversible reaction (A.7) reaches equilibrium extremely rapidly, and it is normal to assume that equation (A.8) applies at all times.

Numerical solution

A truly satisfactory numerical analysis of the effect of electrophoretic coupling on ionic diffusion would require a mass-conservative, highly accurate method. The mixed hyperbolic parabolic non-linear nature of equation (A.2) makes this extremely difficult. Moreover, the time discretisation would have to be finer than the Debye relaxation time, making conventional solution methods impractical for migration times greater than a few minutes. Instead, a two period operator splitting approach is adopted: the ions are first allowed to diffuse independently for a period t_D, creating a charge imbalance, and the electrophoretic effect is included over a second period. This second period is taken sufficiently short for diffusion to be negligible, so that ion migration continues until the electric field strength is everywhere zero. The distribution at the end of the first period is [Freeze and Cherry, 1979]:

$$c_i = \frac{c_0}{2} erfc\left(\frac{x}{2\sqrt{D_i^* t_D}}\right) \tag{A.9}$$

taking $x = 0$ at the interface, where c_0 is the source concentration.

Discarding the diffusion term, equation (A.2) becomes a first order hyperbolic equation, solvable using an explicit method-of-characteristics technique and a Lagrangian co-ordinate system, illustrated in figure A.3. The soil is discretised using a grid of moving nodes $j = 1.. .n_j$

with node spacing Ax. Over the time increment At each node displaces by $\pm u_i^* E\Delta t$, where E is the field strength at the nodal position at the start of the increment, since $\pm u_i^* E$ is the speed of the ions at node j at the start of the increment.

If the concentration and field strength distributions are *sufficiently* smooth within the intervals and At is sufficiently small then ions within the interval will not overtake the ions represented by the moving nodes. The amount of material within each interval is therefore constant over the increment, so the estimated concentration at the centre of each interval is this amount divided by the interval's current thickness. The concentration at each initial co-ordinate is calculated by linear interpolation between the central values. Having solved for all species, E at the initial co-ordinates is found by numerical integration of equation (A.6) using the trapezium rule, and then at the Lagrangian co-ordinates by linear interpolation.

Autoprotolysis is handled using a separate operator splitting approach: the H_3O^+ and OH^- concentrations are calculated as before and reaction (A.7) then driven to equilibrium. If m mol L^{-1} recombine then $H_3O^+ \rightarrow H_3O^+ - m$ and $OH^- \rightarrow OH^- - m$, so substitution into (A.8) gives:

$$m \approx \frac{[H_3O^+][OH^-] - 10^{-14}}{[H_3O^+] + [OH^-]} \qquad \text{(A. 10)}$$

for small m. Iterating equation (A. 10) establishes the equilibrium state.

Five sets of analyses were done, each having the initial NaCl distribution given above: the transient relaxation of the two ions; the effect of a background electrolyte of potassium iodide on the equilibrium state; the effect of initial pH on the equilibrium state where the pH has been adjusted with either sodium hydroxide or hydrochloric acid but no further water dissociation occurs during relaxation; the effect of initial pH as before but including water dissociation during relaxation; the combined effect of a background electrolyte and initial pH including water dissociation during relaxation. All but the transient set were allowed to relax for 1μs.

The activity coefficients are taken equal to one for every species, the values of D_i and u_i at 25°C used, and $\omega = 0 \cdot 5$, $n = 0 \cdot 5$ and ε_r = 78 used throughout. Other reasonable values would not change the results significantly. The transport properties of the species considered are shown in table A. 1. Scenario parameters t_D = 10hours and c_0 = 0 · 001mol L^{-1} give the curves in figure A.2. Other parameters were At = 10^{-10}s, Δx = lmm and n_j = 101.

For each analysis the apparent diffusion coefficient D_{ac} was calculated for both tracer ions from the concentration distributions. That is, D_{ac} is the ionic diffusion coefficient back-calculated from the concentration distribution as if transport were a purely diffusive process. For the transient analyses this was done by non-linear regression for D_i using equations (A.9) and (A.3), and separately by finding x for c_i = 0 · 05c_0, 0 · 1c_0, 0 · 2c_0, 0. 3c_0, 0. 7c_0, 0 · 8c_0, 0 · 9c_0 and 0 · 95c_0, inverting equation (A.9) for D_i and averaging the results. For the remaining analyses the second method only was used.

Results

Figure A.4 shows the variation in D_{ac} with time as the two-ion system relaxes towards equilibrium, with D_i for each ion and D_{cc} from equation (A.l) also shown. The two methods for estimating D_{ac} yield indistinguishable results. As the ions rearrange the D_{ac} values tend towards D_{cc} , and equilibrium is reached after $\approx 1\mu s$.

Figure A.5 shows the variation in final D_{ac} with background electrolyte concentration for the four-ion system, while figure A.6 shows the final KI distribution for $c_s = 1 \cdot 0$. For $c_s < 0 \cdot 1c_0$ $D_{ac} = D_{cc}$ while for $c_s > 10c_0$ $D_{ac} \approx D_i$, with a smooth transition in the range $0 \cdot 1c_0 < c_s < 10c_0$. When $c_s = c_0$ D_{ac} is approximately halfway between the two extreme values. Comparing figures A.2 and A.6 shows that for high c_s electroneutrality is attained by rearranging the background electrolyte's ions.

Figure A.7 shows the variation in final D_{ac} with initial pH, where the dotted lines represent analyses without autoprotolysis during relaxation and markers represent those with autoprotolysis. The pattern is similar to that for the four-ion system, with $D_{ac} \approx D_{cc}$ at near neutral pH, where the NaCl provides most of the ions, and $D_{ac} \approx D_i$ where other ions dominate. At initial pH = 3 · 0 and I 1 ·0 the respective hydronium and hydroxy ion concentrations equal c_0, and $D_{ac} \approx D_i$. The results with and without autoprotolysis during relaxation are indistinguishable.

Figure A.8 shows the variation in final D_{ac} with background electrolyte concentration for initial pH values of 3·0, 4·0, 5·0 and 7·0, representing very acid through neutral soils, while figures A.9 and A.10 show the final pH distribution and the final potassium distribution respectively, for different initial conditions, in the four-ion systems with autoprotolysis during relaxation. Only when the initial pH is near neutral and the background electrolyte's concentration is much less than c_0 does $D_{ac} \approx D_{cc}$. That is, equilibrium is reached by rearrangement of the predominant ionic species in the system, and $D_{ac} \approx D_{cc}$ where the NaCl provides most of the ions and $D_{ac} \approx D_i$ otherwise.

Discussion

The initial perturbation imposed here is large, but smaller perturbations should dissipate in the same manner. If so, the simulations approximate the dynamic equilibrium state and the nature and degree of ionic interaction during tracer diffusion.

The results indicate that the charge imbalance dissipates by rearrangement of the predominant ion species. In clean solutions the tracer ions dominate, and the migration is coupled. In soil water many species may be present: in clean, fine-grained laboratory soils this could be due to the soil's pH buffering capacity; in natural soils due also to ion accumulation. In inactive soils the diffusing ions should migrate independently if in trace concentrations, with electroneutrality maintained by movement of other ions. Crooks and Quigley [1984] claimed that this explained the apparent charge imbalance in measurements of salt migration beneath a domestic landfill,

although they did not consider movement of water dissociation products. In active soils, the behaviour will depend on whether the interaction is by ion exchange or by chemisorption involving changes in surface charge.

The insignificant effect of the water dissociation reaction (A.7) during the relaxation process is explained by considering the change in thickness of the Lagrangian intervals for H_3O^+ and OH-. If that for H_3O^+ grows by an amount AZ in the increment At then that for OH- will shrink by a similar though smaller amount. The product $[H_3O^+][OH^-]$ in equation (A.8) will change only slightly, and reaction (A.7) stays near equilibrium. However, the dissociation products do have an effect when present in concentrations comparable to or higher than the tracer, and the degree of coupling between the tracer ions is less than for a background electrolyte at the same concentration because H_3O^+ and OH- are about four times more mobile than other ions. As a result, the tracer migration is effectively uncoupled when either the H_3O^+ concentration or the OH- concentration exceeds that of the tracer.

Conclusions

The classic equations for tracer electrolyte diffusion into soil predict the development of an electric charge separation, but ignore the effect of electrophoretic coupling between the moving ions. Electroneutrality is reached practically instantaneously by rearrangement of the predominant ion species, with the tracer ions diffusing independently where there is a background electrolyte concentration $c_s > 10c_0$ or the initial pH is such that either $[H_3O^+] > c_0$ or [OH-] > c_0. Multi-ion transport geochemical models should ensure that electroneutrality is enforced, particularly if chemical speciation is to be considered. The applicability of laboratory diffusion rates measured using high tracer concentrations to field situations where the tracer is not the predominant ion species must be carefully considered.

Ion	Transport property	
	D_i $10^{-9}\,m^2\,s^{-1}$	u_i $10^{-8}\,m^2\,s^{-1}\,V^{-1}$
Na'	1.33	5·19
Cl^-	2.03	7.91
K^+	1.96	7.62
I^-	2·05	7.96
H^+	9·31	36.23
OH^-	5·30	20.64

Table A.1 Ionic transport properties

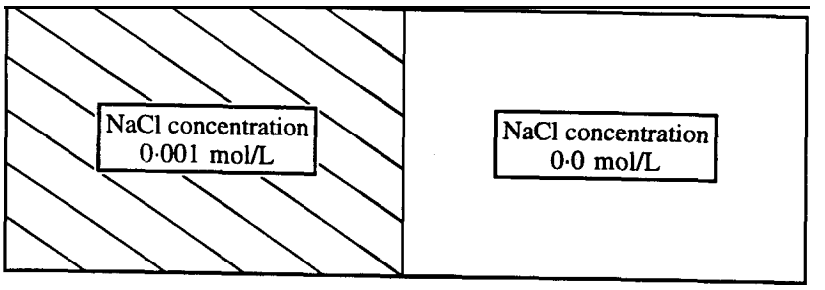

Figure A.1 Initial condition

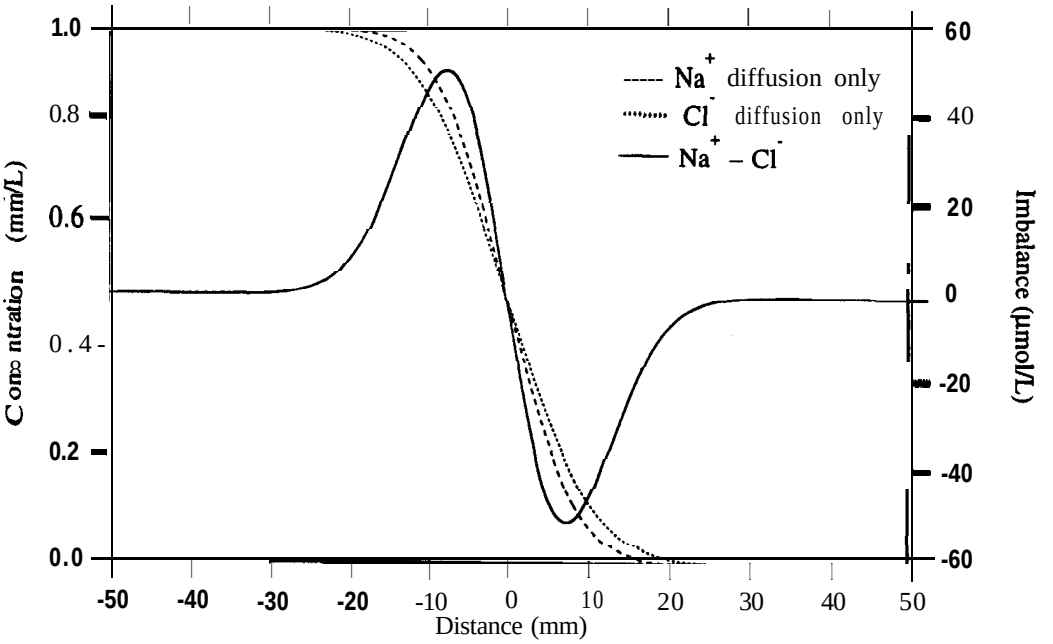

Figure A.2 Ion distributions for independent diffusion

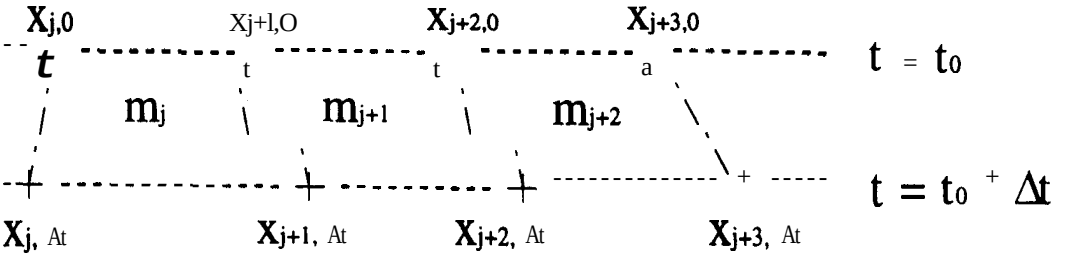

Figure A.3 Displacement of Lagrangian nodes

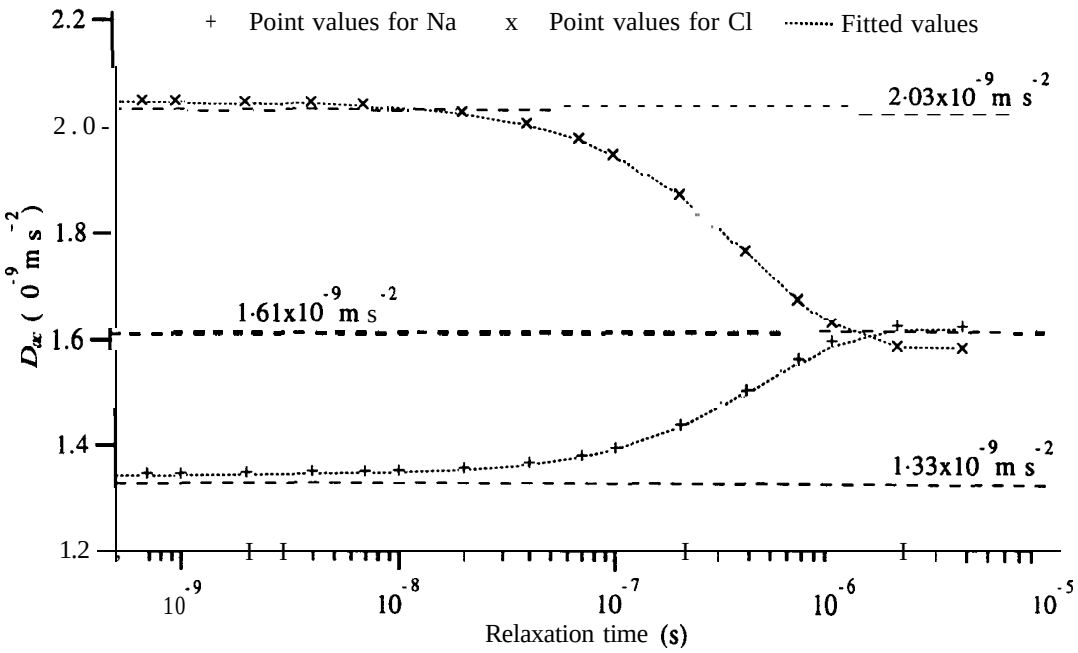

Figure A.4 Variation in D_{ac} during relaxation for **two-ion system**

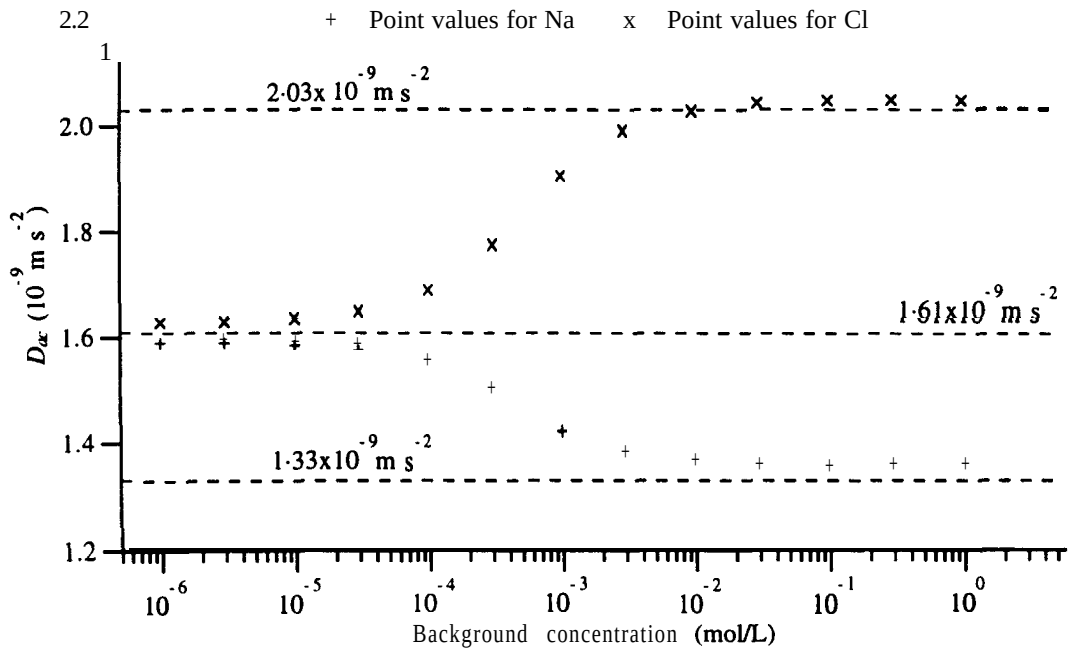

Figure A.5 Variation in D_{ac} with c_s for four-ion system

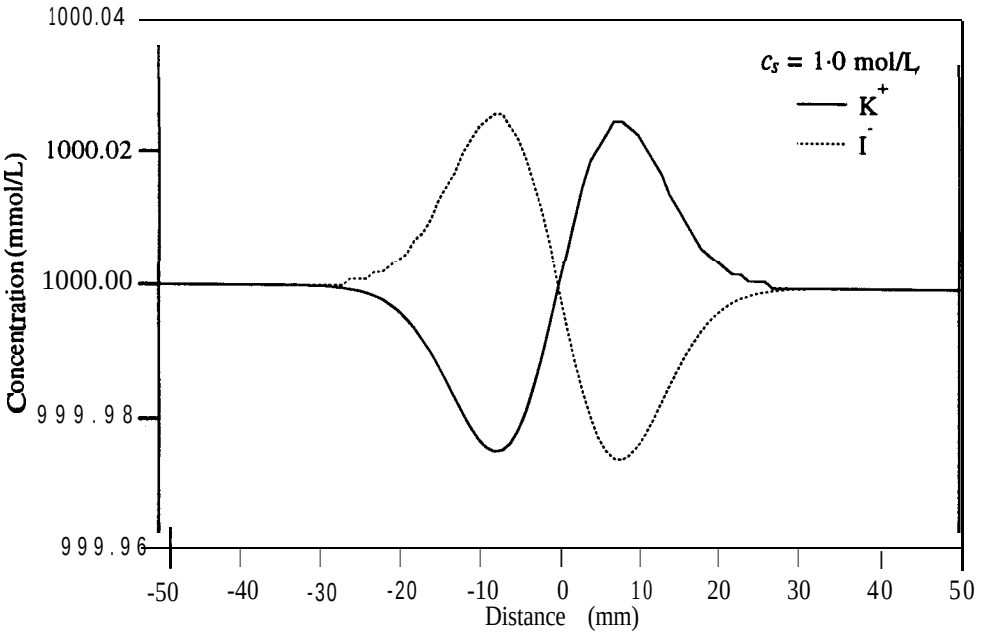

Figure A.6 Final KI distribution for four-ion system, $c_s = 1 \cdot 0$

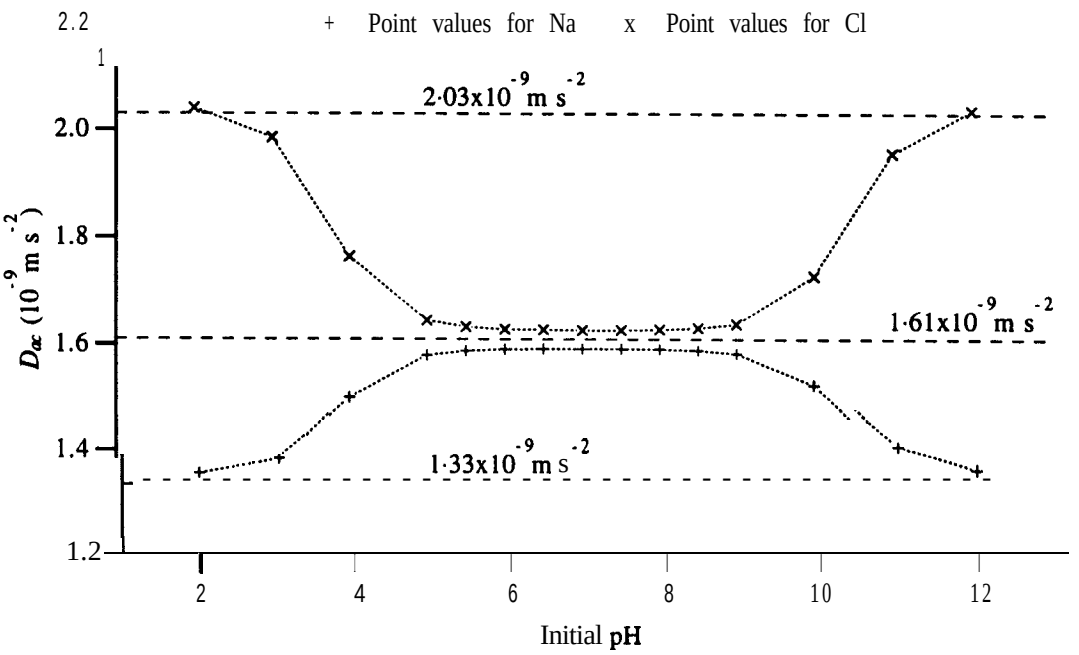

Figure A.7 Variation in D_{ac} with initial pH for two-ion aqueous system

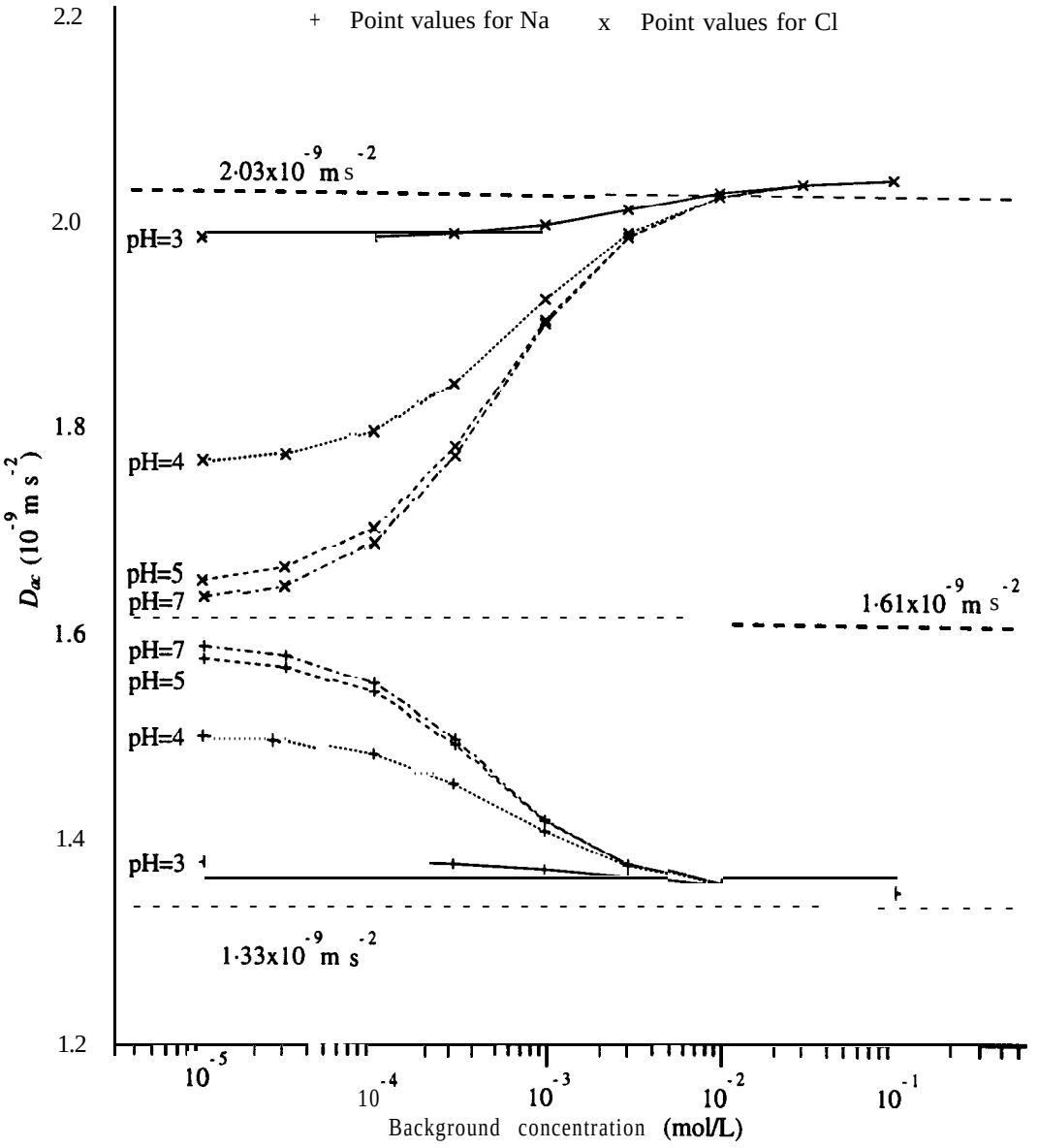

Figure A.8 Variation in D_{ac} with c_s for four-ion aqueous system

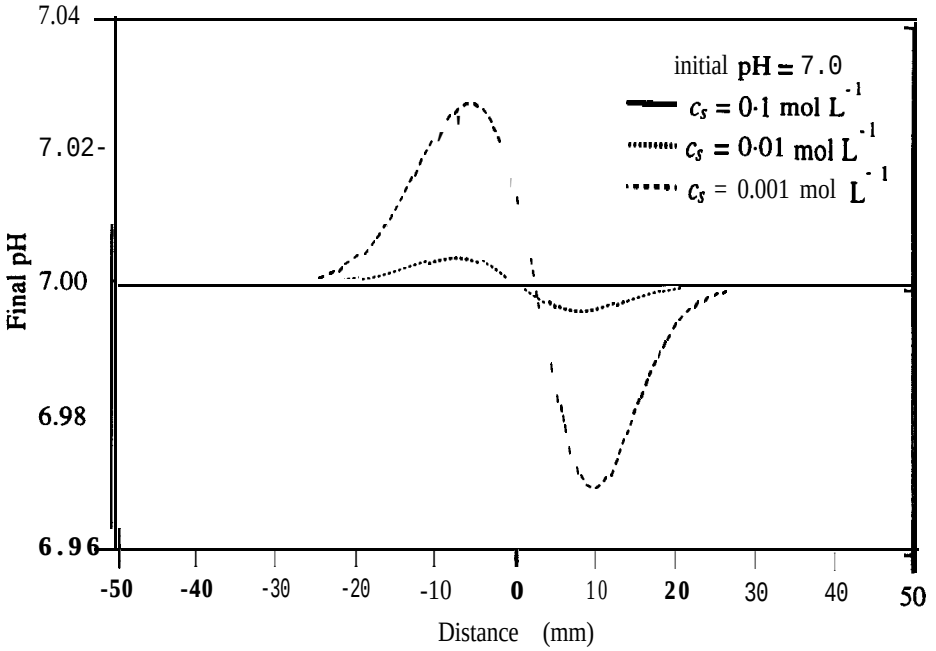

Figure A.9 Final pH distribution for four-ion aqueous system

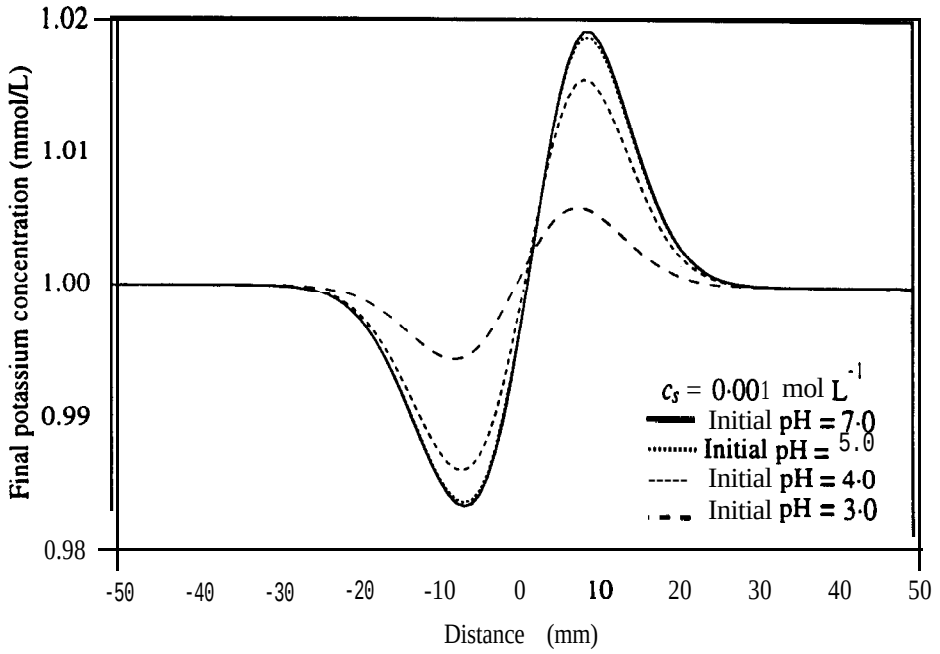

Figure A.10 Final potassium distribution for four-ion aqueous system

APPENDIX B - INPUT DATA FORMAT FOR ELK PROGRAMS

File format for ELK 1·2

The ELK 1·2 programs expect a data input file in the following space-delimited format:

L	Lfilter	A	EndT	Dei	Dh
Tabs	Tref	Tcorr			
Kh	Ke	Pors	Tors		
Disp_s	Disp_w				
zc	lc	cci	Rdc		
za	la	cai	Rda		
lH	cHi				
lO	cOi				
zsc	Isc	csci	Rdsc		
zsa	Isa	csai	Rdsa		
DcOa	ccOai				
DcOs	ccOsi				
Kw	KcOa	KcOs			
Feo	Flv	FtHO	Fts	FgK	Fic

where:

L	Sample length between the electrodes
Lfilter	Length of the filter between the electrodes and the soil
A	Sample cross-sectional area
EndT	Duration in the simulation
Dei	initial electric potential difference between the electrodes, leftmost electrode being the cathode
Dh	Hydraulic head difference between the electrodes
Tabs	Absolute temperature in simulation
Tref	Reference temperature at which ionic conductivities and diffusion coefficients are quoted
Tcorr	Correction factor for ionic conductivity (typically 0·02–0·03 / °C)
Kh	Hydraulic conductivity
Ke	Electra-osmotic permeability
Pors	Porosity
Tors	Tortuosity
Disp_s	Dispersivity in the soil
Disp_w	Dispersivity in the well
zc	Contaminant cation charge valency
lc	Limiting ionic conductivity of contaminant cation
cci	Initial concentration of contaminant cation
Rdc	Retardation factor for contaminant cation
za	Contaminant anion charge valency
la	Limiting ionic conductivity of contaminant anion
cai	Initial concentration of contaminant anion
Rda	Retardation factor for contaminant anion
lH	Limiting ionic conductivity of hydronium ion
cHi	Initial concentration of hydronium ion
lO	Limiting ionic conductivity of hydroxy ion
cOi	Initial concentration of hydroxy ion
zsc	Background electrolyte cation charge valency
Isc	Limiting ionic conductivity of background electrolyte cation
csci	initial concentration of background electrolyte cation
Rdsc	Retardation factor for background electrolyte cation
zsa	Background electrolyte anion charge valency

Isa	Limiting ionic conductivity of background electrolyte anion
csai	Initial concentration of background electrolyte anion
Rdsa	Retardation factor for background electrolyte anion
DcOa	Diffusion coefficient for aqueous contaminant cation hydroxide
ccoai	Initial concentration of aqueous contaminant cation hydroxide
DcOs	Diffusion coefficient for solid contaminant cation hydroxide
ccOsi	Initial concentration of solid contaminant cation hydroxide
Kw	Equilibrium constant for water autoprotolysis
KcOa	Equilibrium constant for aqueous contaminant cation hydroxide formation, K_c
KcOs	Equilibrium constant for solid contaminant cation hydroxide formation, K_{sp}
Feo	Flag for electro-osmosis calculated from minimum voltage gradient; set to 1 for yes, 0 for no
Flv	Flag for assuming a linear voltage variation between the electrodes;set to 1 for yes, 0 for no
FtHO	Flag for solving for the migration of the hydronium and hydroxy ions; set to 1 for yes, 0 for no
Fts	Flag for solving for the migration of the background electrolyte ions: set to 1 for yes, 0 for no
FgK	Flag for accounting for ionic strength in ionic equilibrium calculation: set to 1 for yes, 0 for no
Fic	Flag for maintaining the current at the initial value throughout; set to 1 for yes, 0 for no

Input file for test ELK01

```
0·2       0.002     4·418E-3  28800.0  40        0
298.15    298.15    0.02
4·0E-9    1·0E-9    0·5       0·5
1·0E-6    1·0E-5
2·0       107·2E-4  0.09995   1·0
2·0       160·0E-4  0·1       1·0
349·6E-4  1·0E-4
199·1E-4  1·0E-10
1·0       50·10E-4  0·0       1·0
1·0       76·35E-4  0·0       1·0
1·0E-9    6·326E-9
1·0E-9    0·0
1·0E-14   1·58E-13  3·09E-20
0         0         1         0         0         0
```

Notes on use of the ELK 1·2 programs

The ELK 1·2 programs sub-divide the space between the electrodes into 499 intervals, so that there are 500 equally spaced nodes from cathode to the anode. The filter thickness is rounded to the nearest whole number of intervals, and each well region is taken as being fifty intervals long. The predictor-corrector and random walk versions of ELK differ only in the routines which solve the transport equation for each species. The six ionic species (contaminant cation, contaminant anion, hydronium ion, hydroxy ion, background cation and background anion) must be distinct. Both aqueous and solid contaminant cation hydroxides are taken to be completely mobile.

The transport coefficients Ic, la, IH, IOH, Isc, lsa, DcOa and DcOs are multiplied by the factor $\{1+(T_{abs}-T_{ref})\times T_{corr}\}$ to derive transport coefficients at temperature T_{abs} from the input values at temperature T_{ref}. This therefore affects the ionic mobility and diffusion coefficients calculated from these transport coefficients. The filters are taken as having the same hydraulic conductivity, porosity and tortuosity as the soil, but have zero electro-osmotic permeability and

a retardation factor of 1·0 for all species. The limiting ionic conductivity is the product of the charge valency and the ionic conductivity of one equivalent of the ion species; the latter is what is listed in some references. At the start of the simulation, the contaminant ions are present at the input concentrations at every node within the soil and the filters, the background electrolyte ions are present at the specified concentration at every node in the model, and the hydronium and hydroxy ions are present at the specified concentration at every node within the soil and the filters and at concentrations giving neutral pH at the nodes in the wells.

Electroneutrality and chemical equilibrium is enforced before the first time increment, and after every time increment. It is therefore advisable that the input concentrations represent an equilibrium and electrically neutral state for the pore water in the soil, since otherwise the starting condition may not be the one intended. Activity coefficients are calculated for each ion species as part of the chemical equilbrium calculation.

In general, it is recommended on physical grounds that flags Feo and Flv both be set to 0 and flag FtHO be set to 1. Flags Fts and FgK currently have no effect but must be set in the input data file. It is recommended that they both be set to 0, since the output for a given input file will then be unchanged once they are implemented.

The calculation loop performed by ELK 1·2 for each time increment is as follows:

1. calculate the electrical conductivity at each node;
2. calculate the current density, and adjust applied voltage for constant current case;
3. calculate the electrical potential distribution;
4. calculate the specific discharge;
5. solve the transport equation for the contaminant cation;
6. solve the transport equation for the contaminant anion;
7. solve the transport equation for the aqueous contaminant cation hydroxide;
8. solve the transport equation for the solid contaminant cation hydroxide;
9. solve the transport equation for the hydronium ion;
10. solve the transport equation for the hydroxy ion;
11. correct for electroneutrality at each node;
12. calculate and enforce the chemical equilibrium state at each node;
13. calculate the activity coefficients for each ion at each node;
14. calculate the pH at each node;
15. output selected results for the increment.

File format for ELK 2·0

The ELK 2·0 program expects a data input file in the following space-delimited format:

dx	A					
nElec1	nSoil1	nSoil2	nElec2	nDim		
Tabs	Tref	Tcorr				
Kh	Ke	Pors	Tors			
Disp_s	Disp_w	Dl_well				
zc	lc	cci	Rdc			
za	la	cai	Rda			
lH	cHi					
10	cOi					
zsc	lsc	csci	Rdsc			
zsa	lsa	csai	Rdsa			
DcOa	ccoai					
DcOs	ccOsi					
Kw	KcOa	KcOs				
Feo	Flv	FtHO	Fts	FtOs	FgK	Fic
Dh	VorI	dt	nTsteps	nTskip	nd	

where:

dx	Spacing between nodes
A	Sample cross-sectional area
nElec1	Node number for left hand electrode
nSoil1	Node number for left hand end of soil sample
nSoi12	Node number for right hand end of soil sample
nElec2	Node number for right hand electrode
nDim	Node number for right hand end of simulation domain
Tabs	Absolute temperature in simulation
Tref	Reference temperature at which ionic conductivities and diffusion coefficients are quoted
Tcorr	Correction factor for ionic conductivity (typically 0·02–0·03 / °C)
Kh	Hydraulic conductivity
Ke	Electra-osmotic permeability
Pors	Porosity
Tors	Tortuosity
Disp_s	Dispersivity in the soil
Disp_w	Dispersivity in the well
Dl_well	Dispersion coefficient in the well, in addition to that from the dispersivity
zc	Contaminant cation charge valency
lc	Limiting ionic conductivity of contaminant cation
cci	Initial concentration of contaminant cation
Rdc	Retardation factor for contaminant cation
za	Contaminant anion charge valency
la	Limiting ionic conductivity of contaminant anion
cai	Initial concentration of contaminant anion
Rda	Retardation factor for contaminant anion
lH	Limiting ionic conductivity of hydronium ion
cHi	Initial concentration of hydronium ion
10	Limiting ionic conductivity of hydroxy ion
cOi	Initial concentration of hydroxy ion
zsc	Background electrolyte cation charge valency
Isc	Limiting ionic conductivity of background electrolyte cation
csci	Initial concentration of background electrolyte cation
Rdsc	Retardation factor for background electrolyte cation

zsa	Background electrolyte anion charge valency
Isa	Limiting ionic conductivity of background electrolyte anion
csai	Initial concentration of background electrolyte anion
Rdsa	Retardation factor for background electrolyte anion
DcOa	Diffusion coefficient for aqueous contaminant cation hydroxide
ccOai	Initial concentration of aqueous contaminant cation hydroxide
DcOs	Diffusion coefficient for solid contaminant cation hydroxide
ccOsi	Initial concentration of solid contaminant cation hydroxide
Kw	Equilibrium constant for water autoprotolysis
KcOa	Equilibrium constant for aqueous contaminant cation hydroxide formation, K_c
KcOs	Equilibrium constant for solid contaminant cation hydroxide formation, K_{sp}
Feo	Flag for electro-osmosis calculated from minimum voltage gradient; set to 1 for yes, 0 for no
Flv	Flag for assuming a linear voltage variation between the electrodes;set to 1 for yes, 0 for no
FtHO	Flag for solving for the migration of the hydronium and hydroxy ions; set to 1 for yes, 0 for no
Fts	Flag for solving for the migration of the background electrolyte ions; set to 1 for yes, 0 for no
FtOs	Flag for solving for the migration of the solid contaminant cation hydroxide; set to 1 for migration in whole domain, 0 for migration in the wells only
FgK	Flag for accounting for ionic strength in ionic equilibrium calculation; set to 1 for yes, 0 for no
Fic	Flag for constant current conditions; set to 1 for constant current, 0 for constant voltage
Dh	Hydraulic head difference between the electrodes
VorI	Electrical current (if Fic=1) or electrical potential difference (if Fic=0) between the electrodes
dt	Time increment between steps
nTsteps	Number of time steps in the run
nTskip	Number of time steps between each reporting of the time step results
nd	Discretisation parameter in the particle method (typically set to 4 or more)

Notes on use of the ELK 2·0 program

The ELK 2·0 program is a modification of the ELK 1·2 programs described and used in this report. It uses a mass conservative, deterministic particle method based on a discretisation of the local Green's function solution of the advection dispersion equation. The simulation domain is divided into five regions: nodes 0 and nElec1 bound the left hand well; nodes nElec1 and ngoi11 bound the left hand filter region; nodes nSoil1 and nSoil2 bound the soil sample; nodes nSoil2 and nElec2 bound the right hand filter region; and nodes nElec2 and nDim bound the right hand well. Flag FgK currently has no effect but must be set in the input data file, and it is recommended that FgK be set to 0, since the output for a given input file will then be unchanged once it is implemented. In all other respects, the notes for Elk 1·2 apply.

The calculation loop performed by ELK 2·0 for each time increment is as follows:

1. calculate the electrical conductivity at each node;
2. calculate the current density and applied voltage;
3. calculate the electrical potential distribution;
4. calculate the specific discharge;
5. solve the transport equation for the contaminant cation;
6. solve the transport equation for the contaminant anion;
7. solve the transport equation for the aqueous contaminant cation hydroxide;

8. if FtOs then solve the transport equation for the solid contaminant cation hydroxide for in whole simulation domain, otherwise solve the transport equation for the solid contaminant cation hydroxide in the wells only;
9. if FtHO then solve the transport equation for the hydronium ion;
10. if FtHO then solve the transport equation for the hydroxy ion;
11. if Fts then solve the transport equation for the background cation;
12. if Fts then solve the transport equation for the background anion;
13. correct for electroneutrality at each node;
14. calculate and enforce the chemical equilibrium state at each node;
15. calculate the activity coefficients for each ion at each node;
16. calculate the pH at each node;
17. output selected results for the increment.

APPENDIX C - DEPENDENCY OF PORE FLUID VELOCITY ON OVERALL HYDRAULIC AND ELECTRICAL GRADIENTS

Consider a one-dimensional soil sample divided into N slices such that the nodal coordinates are $x_0 \ldots x_N$ and the spacing between consecutive nodes is constant; the corresponding nodal hydraulic potential heads are $h_0 \ldots h_N$ and the corresponding nodal electrical potentials are $\Phi_0 \ldots \Phi_N$. Assuming that both the hydraulic head and the electric potential varies linearly within each slice the specific discharge through slice i is:

$$v_i = -\left(k_h\big|_{i-1,i} \frac{h_i - h_{i-1}}{x_i - x_{i-1}} + k_e\Big|_{i-1,i} \frac{\Phi_i - \Phi_{i-1}}{x_i - x_{i-1}} \right) \tag{C.1}$$

from equation (25), where $k_h\big|_{i-1,i}$ is the electro-osmotic permeability for the soil between nodes $i-1$ and i, and $k_e\big|_{i-1,i}$ is the electro-osmotic permeability for the soil between nodes $i-1$ and i For a non-deforming soil matrix, the specific discharge through each slice must be the same, so v_i is constant. Summing across all slices gives:

$$Nv = -\frac{1}{\Delta x}\left(\sum_{i=1}^{N} k_h\big|_{i-1,i}(h_i - h_{i-1}) + \sum_{i=1}^{N} k_e\big|_{i-1,i}(\Phi_i - \Phi_{i-1}) \right) \tag{C.2}$$

where Ax is the node spacing. Alternatively, equation (C.l) can be written:

$$\frac{v\Delta x}{k_h\big|_{i-1,i}} = -(h_i - h_{i-1}) - \frac{k_e\big|_{i-1,i}}{k_h\big|_{i-1,i}}(\Phi_i - \Phi_{i-1}) \tag{C.3}$$

which again can be summed across all slices to give:

$$v\Delta x \sum_{i=1}^{N}\left\{ \frac{1}{k_h\big|_{i-1,i}} \right\} = -(h_N - h_0) - \sum_{i=1}^{N}\left\{ \frac{k_e\big|_{i-1,i}}{k_h\big|_{i-1,i}}(\Phi_i - \Phi_{i-1}) \right\} \tag{C.4}$$

since the terms $h_1, h_2, \ldots, h_{N-1}$ cancel. Hence:

$$v = -\frac{N}{L\sum_{i=1}^{N}\left\{ \frac{1}{k_h\big|_{i-1,i}} \right\}}\left(h_N - h_0 + \sum_{i=1}^{N}\left\{ \frac{k_e\big|_{i-1,i}}{k_h\big|_{i-1,i}}(\Phi_i - \Phi_{i-1}) \right\} \right) \tag{C.5}$$

because the total sample length $L = N\Delta x$. Equation (C.5) can be used to calculate the specific discharge through a non-deforming soil knowing the distribution of k_h, of k_e and of Φ, and the value of h imposed at the ends of the sample; it is not necessary to calculate the distribution of h.

If both k_e and k_h are constant then equations (C.2) and (C.5) both reduce to:

$$v = -\left(k_h \frac{h_N - h_0}{L} + k_e \frac{\Phi_N - \Phi_0}{L} \right) \tag{C.6}$$

noting that $L = N\Delta x$. Comparison with equation (25) shows that the specific discharge is determined by the overall electrical potential gradient $(\Phi_N - \Phi_0)/L$ and the overall hydraulic potential gradient $(h_N - h_0)/L$ if both k_e and k_h are constant.

In general, for a non-deforming sample, local variations in the gradient of Φ must be compensated for by changes in the local hydraulic potential heads such that the specific discharge is the same through all slices. If the hydraulic conductivity and the electro-osmostic permeability are constant then the specific discharge can be calculated quite simply knowing the boundary values for the hydraulic potential head and the electrical potential. The effect is illustrated in figure C. 1 for the case where a zone of low electrical conductivity develops close to the cathode, and for the case where one develops near the centre of the sample: in the former case the hydraulic potential head decreases close to the cathode, in the latter it increases on the cathode side and decreases on the anode side of the low electrical conductivity zone. The stress boundary conditions will determine the effect of this change in h: if the sample is free to deform at constant total stress then the change in mean effective stress p' will be opposite to that of h. As a result, if a zone of low electrical conductivity develops close to the cathode then the soil at the point where there is a break in slope in the electrical conductivity will compact, and if a zone of low electrical conductivity develops near the centre of the sample then the soil on the cathode side of this zone will expand and that on the anode side will compact.

If k_h is constant but k_e varies, then two interesting special cases can be examined: that where the electrical conductivity is constant; and that where there is a very narrow zone of relatively much lower electrical conductivity. Firstly, if the electrical conductivity is constant then the electrical potential distribution is linear and $\Phi_i - \Phi_{i-1} = (\Phi_N - \Phi_0)/N$, so equation (C.5) gives:

$$v = -\left(k_h \frac{h_N - h_0}{L} + \left(\frac{1}{N}\sum_{i=1}^{N} k_e\big|_{i-1,i}\right)\frac{\Phi_N - \Phi_0}{L}\right) \qquad \text{(C.7)}$$

Comparing equation (C.6) and equation (C.7) shows that if the hydraulic conductivity is constant and the electrical potential distribution is linear then the specific discharge is dependent on the mean electro-osmotic permeability.

Secondly, if there is a very narrow zone of relatively much lower electrical conductivity, the smallest such zone that can be represented by nodal values is one in which the electrical conductivity at a single node, node j say, is much lower than that at the other nodes. The electrical conductivity is dependent on the ionic composition of the pore water, as is k_e in general [Gray and Mitchell, 1967; Eykholt and Daniel, 1994], so k_e is also likely to vary across the soil sample. The hydraulic conductivity may also vary as a result of the change in pore water chemistry, but the effect on k_h should normally be smaller than the effect on k_e and is ignored in this simplified analysis.

In the limit as the electrical conductivity contrast increases the applied electrical potential will be dropped linearly across the interval between nodes $j-1$ and $j+1$, and v will be:

$$v = -\left(k_h \frac{h_N - h_0}{L} + \left(\frac{k_e\big|_{j-1,i} + k_e\big|_{j,j+1}}{2} \right) \frac{\Phi_N - \Phi_0}{L} \right) \tag{C.8}$$

that is, the specific discharge is dependent on the mean electro-osmotic permeability around the node with the much lower electrical conductivity. The effect indicated by equation (C.5) is that the electro-osmotic flow rate is determined mainly by the electro-osmotic permeability at the positions where the electric potential gradient is greatest; equations (C.6), (C.7) and (C.8) are special cases of this observation.

The hydraulic potential head and therefore the pore water pressure distribution predicted by this analysis is in equilibrium with the electrical potential gradient distribution, and will be set up instantaneously in an ideal, rigid soil. In reality, some consolidation of the soil matrix will occur, and the variation in electrical potential gradient can be treated as equivalent to an overburden pressure on the soil [Esrig, 1968]. It is possible therefore to perform a coupled analysis for both consolidation of the soil and the electrokinetic transport, which is likely to become necessary for simulations of long duration tests in compressible soils where non-linear electrical potential distributions develop or one of the electrodes is closed to prevent fluid movement. This has not been done here. If assuming full consolidation is one extreme condition, as here, the other is to assume that there is no consolidation and therefore no pore pressure development, in which case the local specific discharge will be determined by the local electrical potential gradient according to equation (25) and there will be a discontinuity in the mean pore fluid velocity.

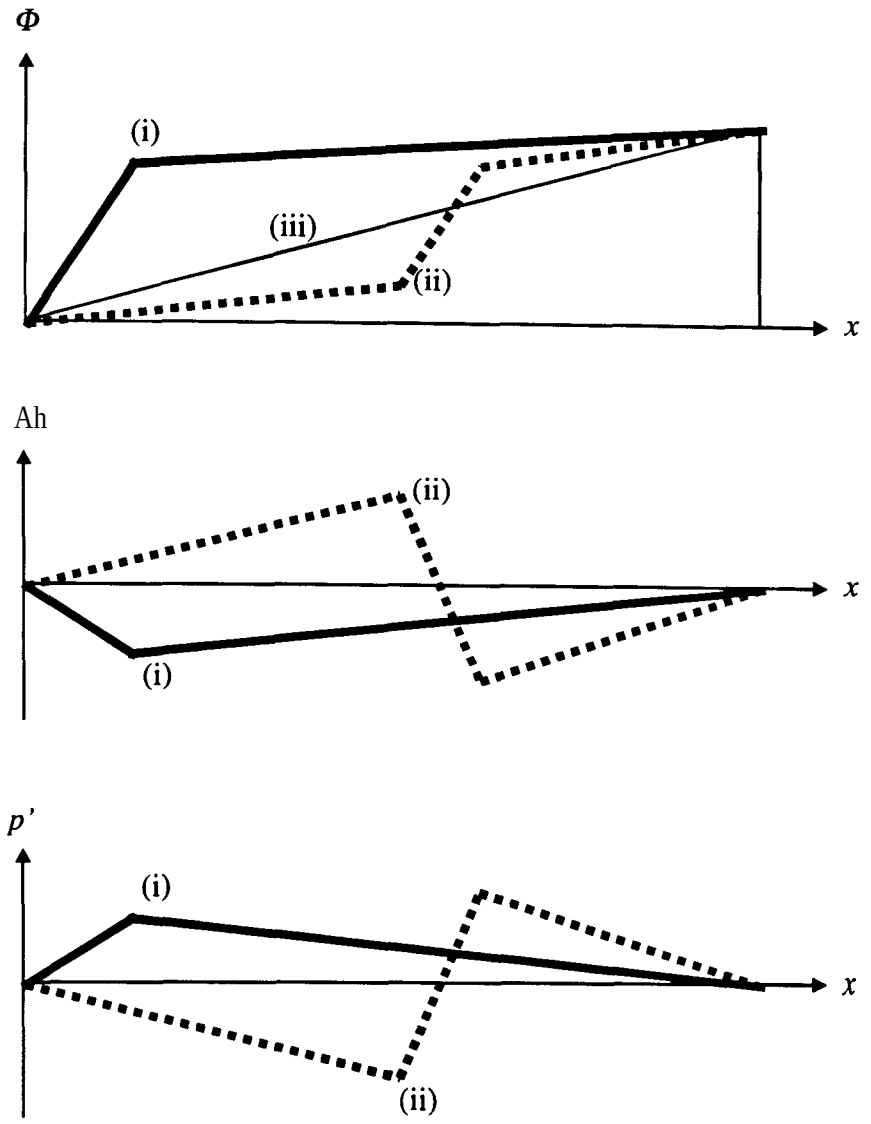

Figure C.l Effect of low electrical conductivity zone in a soil with constant properties: a. variation in electrical potential; b. change in hydraulic head; and c. change in mean effective stress for constant total stress conditions. Curve (i) is for a low electrical conductivity zone close to the cathode, curve (ii) for one near the centre of the sample, and curve (iii) is the constant electrical conductivity case

APPENDIX D - GRID PECLET NUMBER LIMIT IN THE MODELLING OF ELECTROKINETIC TRANSPORT

Consider a one-dimensional soil sample divided into N slices such that the nodal coordinates are $x_0 \ldots x_N$ and the spacing between consecutive nodes is constant; the corresponding nodal electrical potentials are $\Phi_0 \ldots \Phi_N$. An important parameter relating to the stability of numerical solutions of the classic one-dimensional advection-dispersion equation:

$$\frac{\partial c}{\partial t} = \frac{\partial}{\partial x}\left\{D_L \frac{\partial c}{\partial x}\right\} - \frac{\partial}{\partial x}\{\bar{v}c\} \tag{C.2}$$

is the grid Peclet number $Pe = \bar{v}\Delta x/D_L$, where Δx is the grid spacing. Comparing equations (C.2) and (23) indicates that the relevant grid Peclet number for electrokinetic transport is:

$$Pe = \frac{\Delta x}{D_L}\left|\bar{v} - u_i^* \frac{z_i}{|z_i|}\frac{\partial \Phi}{\partial x}\right| \tag{D.1}$$

and will vary with position and time if a non-linear voltage gradient develops as a result of variations in electrical conductivity.

The worst case would be if a very narrow zone of relatively much lower electrical conductivity develops. The smallest such zone that can be represented by nodal values is one in which the electrical conductivity at a single node, node j say, is much lower than that at the other nodes, and in the limit as the electrical conductivity contrast increases the applied electrical potential will be dropped linearly across the interval between nodes j − 1 and j + 1. At node j therefore:

$$\frac{\partial \Phi}{\partial x} \approx \frac{\Phi_N - \Phi_0}{2\Delta x} \tag{D.2}$$

where $\Phi_N - \Phi_0$ is the total applied electrical potential difference. Ignoring the pore fluid velocity term in equation (D. 1) and approximating the dispersion coefficient by:

$$D_L \approx D_i^* = \frac{u_i^* RT}{|z_i| F} \tag{D.3}$$

using the Einstein relationship between ionic mobility and diffusion coefficient [Crow, 1994] gives:

$$Pe = \frac{u_i^*}{D_i^*}\frac{\Phi_N - \Phi_0}{2\Delta x}\Delta x = \frac{|z_i| F}{2RT}(\Phi_N - \Phi_0) \approx 19 \cdot 5|z_i|(\Phi_N - \Phi_0) \tag{D.4}$$

at 25°C. Equation (D.3) again assumes that the pore fluid velocity is negligible. On the same basis the maximum grid Courant number $Cr = \bar{v}\Delta t/\Delta x$, modified to account for transport due to the electrical potential gradient, will be:

$$Cr = \frac{u_i^*}{2}\frac{z_i}{|z_i|}\frac{\Delta t}{(\Delta x)^2}(\Phi_N - \Phi_0) \tag{D.5}$$

Zones of low electrical conductivity can only form where the concentration fronts due to the migration of the separate species overlap, and therefore at either the leading or trailing edges of the distribution for each species. In reality, the width of these zones would grow from zero and start to affect the transport of all species as soon as the zones form. In a numerical simulation, as indicated above, the smallest such zone that can be represented is one around a single node. However, if the time increment is larger than the time taken for a species to be transported across the space between nodes, that is, if the grid Courant number is larger than one, and the algorithm used to solve the advection-dispersion equation correctly models this, then the concentration front will jump over several nodes. A zone of low electrical conductivity wider than that considered above will result and the grid Peclet number will be correspondingly smaller. This will only occur in algorithms which correctly handle large grid Courant numbers: the random walk particle is one such algorithm, but simple finite difference solutions such as the predictor-corrector method cannot transport material further than from one node to an adjacent node in a single increment of time.

Equation (D.4) indicates that the grid Peclet number which results from the formation of a zone of low electrical conductivity is independent of the grid spacing and is potentially much greater than one: $|z_i|$ is typically one or two, and $\Phi_N - \Phi_0$ may be of the order of 40–50V, giving a maximum $Pe \approx 2000$. The usual tactic for algorithms which do not model large Peclet number problems well, that of reducing the grid spacing, will be ineffective in this problem. Moreover, because of the $(\Delta x)^2$ term in equation (D.5) this tactic would result in a disproportionate increase in either the grid Courant number for constant At, or the computation time for constant grid Courant number.

APPENDIX E — NOTATION

a_i	activity of species i in pore water
A	sample cross-sectional area
A	deterministic forcing term in random walk particle method
B	deterministic scaling term in random walk particle method
c_i	concentration of species i in pore water
c_s	background electrolyte concentration
c_0, C_0	initial concentration of contaminant in pore water
c_-	concentration of anion in pore water
c_+	concentration of cation in pore water
Cr	grid Courant number
D_{ac}	apparent electrophoretically coupled diffusion coefficient
D_{cc}	electrophoretically coupled diffusion coefficient
D_i	free diffusion coefficient of species i
D_i^*	effective diffusion coefficient of species i
D_L	coefficient of longitudinal hydrodynamic dispersion
D_-	intrinsic diffusion coefficient of the anion
D_+	intrinsic diffusion coefficient of the cation
E	electric field strength
f	pH dependent error term in metal hydroxide formation calculation
f	particle number density in random walk particle method
F	Faraday constant
G_i	source and sink term in transport equation for species i
h	pore water head
i, j	indices
I	electric current through sample
I_s	ionic strength of pore water
k_e	electro-osmotic permeability
k_h	hydraulic conductivity
K_c	equilibrium constant for aqueous metal hydroxide dissociation
K_{sp}	solubility product for solid metal hydroxide
K_w	equilibrium constant for water autoprotolysis
l_a	migration distance of cations away from anode in simple analysis
l_c	migration distance of anions away from cathode in simple analysis
L	sample length
m	number of moles per litre of water formed by ion association
m_i	molality of species i in pore water

n	porosity
N	number of slices into which sample is divided
P'	mean effective stress
Pe	grid **Peclet** number
R	gas constant
R_i	retardation factor for species i
R_s	total electrical resistance of sample
t	time
t_D	initial diffusion time during which electrophoretic effects ignored
T	absolute temperature
T	time for acid and alkali fronts to meet in simple analysis
u_i	ionic mobility of species i
u^*	mean effective ionic mobility
u_i^*	effective ionic mobility of species i
u_-^*	effective ionic mobility of anion
u_+^*	effective ionic mobility of cation
v	specific discharge
$\bar{v}$	mean pore fluid velocity
w	approximated value for concentration
x, X	spatial coordinate
z_i	charge valency of species i
z_-	charge valency of anion
z_+	charge valency of cation
Z	random number with mean zero and unit variance
α_L	dispersivity
γ_i	activity coefficient of species i in pore water
ε	permittivity of the pore fluid
ε_r	relative permittivity
ε_0	permittivity of free space
ζ	zeta potential
η	viscosity of the pore fluid
κ	electrical conductivity of pore water
κ^*	equivalent bulk electrical conductivity
κ_0^*	equivalent bulk electrical conductivity of central zone in simple analysis
κ_a^*	equivalent bulk electrical conductivity of anode zone in simple analysis
κ_c^*	equivalent bulk electrical conductivity of cathode zone in simple analysis
λ_i	molar conductivity in water of species i

λ_i^0	limiting ionic conductivity in water of species i
λ_i^*	effective molar conductivity in soil of species i
σ	charge density
Φ	electrical potential
ω	tortuosity
ω_i	tortuosity for species i
A	difference operator

APPENDIX F — REFERENCES

1. Acar, Y.B. and Gale, R.J. (1992): *Electrochemical decontamination of soils or slurries,* United States Patent 5 137608, .
2. Acar, Y.B., Li, H., and Gale, R.J. (1992): 'Phenol removal from kaolinite by electrokinetics'; ASCE Journal of Geotechnical Engineering vol. 118, no. 11, pp. 1837-1852.
3. Acar, Y.B., Hamed, J.T., Alshawabkeh, A.N., and Gale, R.J. (1994): 'Removal of cadmium (II) from saturated kaolinite by application of electrical current'; Géotechnique vol. 44, no. 2, pp. 239-254.
4. Alshawabkeh, A.A. and Acar, Y.B. (1992): 'Removal of contaminants from soils by electrokinetics: a theoretical treatise'; Journal of Environmental Science and Health Part A vol. 97, no. 7, pp. 1835-1861.
5. Arulanandan, K. and Mitchell, J.K. (1968): 'Low frequency dielectric dispersion of clay-water-electrolyte systems'; Clays and Clay Minerals vol. 16, pp. 337-35 1.
6. Atkins, P.W. (1994): *Physical chemistry;* Oxford University Press, 5th ed. edition.
7. Bagtzoglou, A.C., Tompson, A.F.B., and Dougherty, D.E. (1992): 'Projection functions for particle-grid methods'; Numerical Methods for Partial Differential Equations vol. 8, no. 4, pp. 325-340.
8. Bear, J. (1969): 'Hydrodynamic Dispersion'; *Flow through porous media;* Acadenic Press, de Wiest, R.J.M. (Ed), ch. 4, pp. 109-199.
9. Bear, J. (1988): *Dynamics of fluids in porous media;* Dover Publications Inc..
10. Campanella, R.G., Davies, M.P., Boyd, T.J., and Everard, J.L. (1994): 'Geoenvironmental subsurface site characterization using in-situ soil testing methods'; *Proceedings of the first international congress on environmental geotechnics,* pp. 153-159, Carrier, III, W.D. (Ed), BiTech Publishers Ltd..
11. Casagrande, L. (1949): 'Electra-osmosis in soils'; Gtotechnique vol. 1, no. 3, pp. 159-177.
12. Compos, F.F. and Rollett, J.S. (1995): 'The exponents method for calculating equilibrium concentrations of complex species in solution'; Journal of Computational Chemistry vol. 16, no. 5, pp. 534-544.
13. Cox, R.A. and Nishikawa, T. (1991): 'A new total variation diminishing scheme for the solution of advective-dominant solute transport'; Water Resources Research vol. 27, no. 10, pp. 2645-2650.
14. Crooks, V.E. and Quigley, R.M. (1984): 'Saline leachate migration through clay: a comparative laboratory and field investigation'; Canadian Geotechnical Journal vol. 21, no. 2, pp. 349-362.
15. Crow, DR. (1994): *Principles and applications of electrochemistry;* Blackie Academic and Professional, 4th ed. edition.

16. Datla, S. and Yeung, A.T. (1994): 'Subsurface migration of contaminants under the coupled influences of hydraulic, electrical and chemical gradients'; *Proceedings of the eighth international conference of the International Association for Computer Methods and Advances in Geomechanics,* vol. 2, pp. 1043-1048, Siriwardane, H.J. and Zaman, M.M. (Eds), A. A. Balkema.

17. Davies, C.W. (1962): *Ion association;* Butterworths.

18. Elnawawy, O., Valocchi, A.J., and Ougouag, A.M. (1990): 'The cell analytical-numerical method for solution of the advection-dispersion equation: two dimensions'; Water Resources Research vol. 26, no. 11, pp. 2705-2716.

19. Esrig, M.I. (1968): 'Pore pressures, consolidation, and electrokinetics'; ASCE Journal of the Soil Mechanics and Foundations Division vol. 94, no. SM4, pp. 899-921.

20. Eykholt, G.R. and Daniel, D.E. (1994): 'Impact of system chemistry on electro-osmosis in contaminated soil'; ASCE Journal of Geotechnical Engineering vol. 120, no. 5, pp. 797-815.

21. Freeze, R.A. and Cherry, J.A. (1979): *Groundwater;* Prentice Hall.

22. Gray, D.H. and Mitchell, J.K. (1967): 'Fundamental aspects of electro-osmosis in soils'; ASCE Journal of the Soil Mechanics and Foundations Division vol. 93, no. SM6, pp. 209-236.

23. Groenevelt, P.H. and Elrick, D.E. (1976): 'Coupling phenomena in saturated homo-ionic Montmorillonite: II. Theoretical'; Soil Science Society of America Journal vol. 40, no. 6, pp. 820-823.

24. Grosse, C. and Foster, K.R. (1987): 'Permittivity of a suspension of charged spherical particles in electrolyte solution'; Journal of Physical Chemistry vol. 91, no. 11, pp. 3073-3076.

25. Halliday, D. and Resnick, R. (1974): *Fundamentals of physics;* John Wiley & Sons, Inc., revised printing.

26. Hamed, J., Acar, Y.B., and Gale, R.J. (1991): 'Pb(II) removal from kaolinite by electrokinetics'; ASCE Journal of Geotechnical Engineering vol. 117, no. 2, pp. 241-271.

27. Harned, H.S. and Nuttall, R.L. (1947): 'The diffusion coefficient of potassium chloride in dilute aqueous solution': Journal of the American Chemical Society vol. 69, pp. 736-740.

28. Harned, H.S. and Nuttall, R.L. (1949): 'The differential diffusion coefficient of potassium chloride in aqueous solutions'; Journal of the American Chemical Society vol. 71, pp. 1460-1463.

29. Healy, R.W. and Russell, T.F. (1993): 'A finite-volume Eulerian-Lagrangian localized adjoint method for solution of the advection-dispersion equation'; Water Resources Research vol. 29, no. 7, pp. 2399-2413.

30. Hellawell, E.E. (1994): ***Modelling transport processes in soil due to hydraulic, density and electrical gradients;*** PhD thesis, University of Cambridge.

31. Herrington, J.M., Clarke, A.Q., and Watts, J.C. (1992): 'The surface charge of kaolin'; Colloids and Surfaces vol. 62, no. 3, pp. 161-169.

32. Hibbert, D.B. ***(1993): Introduction to electrochemistry;*** Macmillan Physical Science.

33. Kim, H.T., Suk, T.W., Park, S.H., and Lee, C.S. (1993): 'Diffusivities for ions through compacted Na-bentonite with varying dry bulk densities'; Waste Management vol. 13, no. 4, pp. 303-308.

34. Kinzelbach, W. (1988): 'The random walk method in pollutant transport simulation'; ***Groundwater flow and quality modelling***; D. Reidel Publishing Company, Custodio, E., Gurgui, A., and Ferreira, J.P.L. (Eds), pp. 227-245.

35. Lageman, R., Pool, W., and Seffinga, G. (1989): 'Electra-reclamation: theory and practice'; Chemistry and Industry, pp. 585-590.

36. Maloszewski, P. and Zuber, A. (1993): 'Tracer experiments in fractured rocks: matrix diffusion and the validity of models'; Water Resources Research vol. 29, no. 8, pp. 2723-2735.

37. Martell, A.E. and Smith, R.M. (1974): ***Critical stability constants;*** Plenum Press.

38. McBride, M.B. (1978): 'Copper (II) interactions with kaolinite: factors controlling adsorption'; Clay and clay minerals vol. 26, no. 2, pp. 101-106.

39. McBride, G.B. (1985): 'Incorporation of point sources in numerical transport schemes'; Water Resources Research vol. 21, no. 11, pp. 1791-1795.

40. Mitchell, J.K. (1991): 'Conduction phenomena: from theory to geotechnical practice'; Géotechnique vol. 41, no. 3, pp. 299-340, The 1991 Rankine Lecture.

41. Noorishad, J., Tsang, C.F., Perrochet, P., and Musy, A. (1992): 'A perspective on the numerical solution of convection dominated transport problems: a price to pay for the easy way out'; Water Resources Research vol. 28, no. 2, pp. 551-561.

42. Press, W.H., Flannery, B.P., Teukolsky, S.A., and Vetterling, W.T. (1989): ***Numerical recipes in pascal***; Cambridge University Press.

43. Robinson, R.A. and Stokes, R.H. *(1959): Electrolyte* ***solutions;*** Butterworth & Co. Ltd., 2nd ed. edition.

44. Shackelford, C.D. and Redmond, P.L. (1995): 'Solute breakthrough curves for processed kaolin at low flow rates'; ASCE Journal of Geotechnical Engineering vol. 121, no. 1, pp. 17-32.

45. de Stefano, C., Princi, P., Rigano, C., and Sammartano, S. (1989): 'The calculation of equilibrium concentrations ES4EC1: a FORTRAN program for computing distribution diagrams and titration curves'; Computers and Chemistry vol. 13, no. 4, pp. 343-359.

46. Tagamets, T. and Sternberg, Y.M. (1974): 'A predictor-corrector method for solving the convection-dispersion equation for adsorption in porous media'; Water Resources Research vol. 10, no. 5, pp. 1003-1011.

47. Thevanayagam, S. and Wang, J. (1994): 'Flow behaviour during electrokinetic decontamination'; ***Proceedings of the first international congress on environmental geotechnics,*** pp. 379-385, Carrier, III, W.D. (Ed), BiTech Publishers Ltd..

48. Tompson, A.F.B. and Dougherty, D.E. (1988): 'On the use of particle tracking methods for solute transport in porous media'; ***Computational methods in water resources: Volume 2. Numerical methods for transport and hydrologic processes,*** pp. 227-232, Celia, M.A., Ferrand, L.A., Brebbia, C.A., Gray, W .G., and Pinder, G.F. (Eds), Elsevier.

49. Tompson, A.F.B. and Gelhar, L.W. (1990): 'Numerical simulation of solute transport in three-dimensional randomly heterogeneous porous media'; Water Resources Research vol. 26, no. 10, pp. 2541-2562.

50. Tompson, A.F.B. (1993): 'Numerical simulation of chemical migration in physically and chemically heterogeneous porous media'; Water Resources Research vol. 29, no. 11, pp. 3709-3726.

51. Turq, P., Chemla, M., Latrous, H., and M'halla, J. (1977): 'Coupling between tracer and mutual diffusion in electrolyte solutions'; Journal of Physical Chemistry vol. 81, no. 5, pp. 485-491.

52. Uffink, G.J.M. (1988): 'Modelling of solute transport with the random walk method'; ***Groundwater flow and quality modelling;*** D. Reidel Publishing Company, Custodio, E., Gurgui, A., and Ferreira, J.P.L. (Eds), pp. 247-265.

53. Valocchi, A.J. and Malmstead, M. (1992): 'Accuracy of operator splitting for advection-dispersion-reaction problems'; Water Resources Research vol. 28, no. 5, pp. 1471-1476.

54. Yeh, G.T., Chang, J.R., and Short, T.E. (1992): 'An exact peak-capturing and oscillation-free scheme to solve advection-dispersion transport equations'; Water Resources Research vol. 28, no. 11, pp. 2937-2951.

55. Yeung, AT. and Mitchell, J.K. (1993): 'Coupled fluid, electrical and chemical flows in soil'; Géotechnique vol. 43, no. 1, pp. 121-134.

56. Yeung, A.T. and Datla, S. (1995): 'Fundamental formulation of electrokinetic extraction of contaminants from soil'; Canadian Geotechnical Journal vol. 32, no. 4, pp. 569-583.